



# Certification

**We** certify that this thesis entitled "**Computer-Aided-Design of Focused Ion Beam for a Lithography System**" is prepared by *Mr. Fadhil Abdulabaas Ali* under our supervision at the College of Science of Al-Nahrain University in partial fulfillment of the requirements for the degree of **Doctor of Philosophy in Physics**.

Supervisor: *Prof.Dr.SabahM.Juma*

Date: // 2006

Supervisor: *Dr.Ahmad K.Ahmad*


Date: // 2006

In view of recommendation, I present this thesis for debated by the examining committee.

**Dr.Ahmad K.Ahmad**

Head of Physics Department

Date: // 2006



# Examining Committee Certification

**We** certify that we have read this thesis entitled "**Computer – Aided - Design of Focused Ion Beam for a Lithography System**", and as an examining committee, we examined the student **Mr. Fadhil Abdulabaas Ali** on its contents, and that in our opinion it is adequate for the partial fulfillment of the requirements for the degree of **Doctor of Philosophy in Physics**.

Signature:  
Name: **Dr.Inaa'm Sami Hamdi**  
Title: ***Professor***  
(Chairman)  
Date: // 2006

Signature:  
Name: **Dr.Khalil M. Al-bayati**  
Title: ***Professor***  
(Member)  
Date: // 2006

Signature:  
Name: **Dr.Ayad A. Al -Ani**  
Title: ***Assistant Professor***  
(Member)  
Date: // 2006

Signature:  
Name: **Dr.Samir Khdir Yassin Al -Ani**  
Title: ***Assistant Professor***  
(Member)  
Date: // 2006

Signature:  
Name: **Dr.Ali H.H. Al-Batat**  
Title: ***Assistant Professor***  
(Member)  
Date: // 2006

Signature:  
Name: **Dr.Ahmad K.Ahmad**  
Title: ***Assistant Professor***  
(Member)  
Date: // 2006

Signature:  
Name: **Dr.Laith A. Al -Ani**  
Title: ***Assistant Professor***  
Dean of the College of Science  
Date: // 2006

# Synopsis

A complete computer aided design (CAD) by using optimization methods for the ion optical systems have been developed, by mixing the dynamic programming procedure and artificial intelligence technique. The relative spherical and chromatic aberrations coefficients were obtained according to figure of merit for the following optimized optical systems:

- a. Single-lens design (electrostatic and magnetic).
- b. Two-lens system consists of two electrostatic lenses.
- c. Three-lens system consists of three electrostatic lenses.
- d. Multi-lens system (electrostatic and magnetic).

Four types of electrostatic lenses and a magnetic lens model were designed as small as possible of optical properties (i.e. the first and third optical properties), and reconstructions of electrodes and pole pieces were plotted in two and three dimensions graphics by using SIMION 7.0 simulator depending on the stored database (i.e. knowledge base). These lenses are as follows:

- Unipotential lens 1 (operated in deceleration mode).
- Unipotential lens 2 (operated in acceleration mode).
- Immersion lens.
- Diaphragm lens.
- Magnetic lens.

Present software has been designed and written in Java expert system shell (JESS) and Visual Basic 6 (VB6) for optimizing and analyzing full calculation processes, it has called CADION package.

The optimized axial potential distributions for both electrostatic and magnetic fields according to the constraints have been used in the optical column setup, which are two-lens system, three-lens system and multi-lens system. Spot size measurements were calculated in nano scales, which have values closed to (3.0) nm applicable in nano technology applications used in lithographic systems.

Also, the present work has been suggested definitions and abbreviations in charged particle optics to be consider some of the results, as a verification of the uncertainty principle relationship like.

# Commemoration



*In a memory of our IEO father*  
*Prof. Dr. Sabah M. Juma*

# Acknowledgments

To my previous supervisor *Prof.Dr.Sabah M. Juma*, who was the father of *Ion and Electron Optics Group* in *Al-Nahrain University / Physics Department*, appreciate him for his scientific assistance and advice for the memory of his soul. To my recent supervisor *Dr.Ahmad Kamal*, who has always been my role-model, thank him for all his guidance, advice and encouragement. Also, his feedback and comments on my thesis and presentations were always very helpful, and I will continue to work hard in improving my skill in both.

I also want to deliver my special thanks to the *Dean of College of Science*, and for all the staff (present and past) of Al-Nahrian University, College of Science and Physics Department for providing me suitable scientific environments.

# *Table of Contents*

	<i>Page</i>
Dedication .....	
Synopsis .....	v
Commemoration .....	vii
Acknowledgement .....	viii
Table of Contents .....	ix
Nomenclature .....	xiii

## *Chapter One*

### Introduction

1.1 Introduction on Lithography .....	1
1.2 Electrostatic Lenses .....	4
1.2.1 Classification of electrostatic lenses .....	5
1.2.2 Properties of electrostatic lenses .....	6
1.3 Magnetic Lenses .....	7
1.3.1 Classification of magnetic lenses models .....	9
1.3.2 Properties of magnetic lenses .....	11
1.4 Historical Review .....	12
1.5 Optimization Method .....	17
1.6 Aims of the Project .....	18

# *Chapter Two*

## Theoretical Considerations

	<i>Page</i>
2.1 Motion of Charged Particles in rotationally symmetric Electrostatic and Magnetic fields .....	19
2.1.1 Paraxial-ray equation in electrostatic fields .....	20
2.1.2 Paraxial-ray equation in magnetic fields .....	21
2.1.3 Numerical determining field potentials .....	22
2.2 Light Optics Verses Ion Optics .....	27
2.3 Uncertainty Principle .....	28
2.4 Definitions of Some Optical Parameters .....	31
2.5 System of Lenses .....	34
2.6 Aberration Theorem in Ion Optics .....	35
2.6.1 Aberration Coefficients .....	37
2.6.2 Aberration of System of Lenses .....	44
2.7 Figures of Merit .....	47
2.8 Image Analysis by spot diagrams.....	48



# *Chapter Three*

## Computations and Analysis

	<i>Page</i>
3.1 Electrostatic and Magnetic spline lenses .....	51
3.2 Optimization by dynamic programming procedure (DPP) with the aid of artificial intelligence technique (AIT) .....	53
3.3 The Synthesis Procedure .....	56
3.4 Constraints and Optimization .....	60
3.5 Computational Grid .....	61
3.6 Simulation Software Description .....	66
3.6.1 Computer Aided Design for ION system (CADION) .....	66
3.6.2 ION and electron optics SIMulation package (SIMION).....	70
3.7 Reconstruction of Electrodes and Pole pieces .....	72
3.8 Spot Diagrams and Spot size .....	73

## *Chapter Four*

### Results and Discussion

	<i>Page</i>
4.1 Single-lens design .....	77
4.1.1 Electrostatic lenses .....	77
4.1.2 Electrode reconstruction .....	86
4.1.3 Magnetic lens design.....	93
4.1.4 Pole piece reconstruction .....	97
4.2 Two-lens system .....	101
4.3 Three-lens system .....	108
4.3.1 Column setup .....	108
4.3.2 Beam spot size measurement .....	111
4.4 Multi-lens system.....	114
4.5 A suggested estimations in charged particles optics.....	119

## *Chapter Five*

### Conclusions and Suggestions for Future Work

	<i>Page</i>
5.1 Conclusions .....	124
5.2 Suggestions for Future work .....	125

### Appendix

	<i>Page</i>
Appendix .....	126
References .....	128

## *Nomenclature*

AIT- artificial intelligence technique

$\mathbf{B}_z$  – Magnetic flux density (Tesla)

$\mathbf{B}_{\max}$  – Maximum magnetic flux density (Tesla)

c- Speed of light ( $\approx 3 \times 10^8$  m/s)

Cc – Chromatic aberration coefficient

Cco – Chromatic aberration coefficient at the object side

Cci – Chromatic aberration coefficient at the image side

Cs – Spherical aberration coefficient

Cso – Spherical aberration coefficient at the object side

Csi – Spherical aberration coefficient at the image side

Csco – Chromatic aberration coefficient of a system of lenses at the object position.

Csso – Spherical aberration coefficient of a system of lenses at the object position.

DPP-dynamic programming procedure

$d_c$  – Chromatic aberration disc diameter

$d_{ci}$  – Chromatic aberration disc diameter in the image plane

$d_s$  – Spherical aberration disc diameter

$d_{si}$  – Spherical aberration disc diameter in the image plane

$d_t$  – Total aberration disc diameter

d –magnetic flux density half width

$\mathbf{E}$  – Electrostatic field intensity (Volts / meter)

f – Focal length

$f_o$  – Object side focal length

$f_i$  – Image side focal length

$h$  – Planck's constant ( $=6.62377 \times 10^{-34}$  joule-sec)  
 $\mathbf{J}$  – Total current density (Ampere / meter<sup>2</sup>)  
 $L$  – Axial extension of the electrostatic lens (total length of the lens)  
 $L'$ -Geometrical Parameter  
 $M$ - Magnification  
 $M'$ - Ordinate dimension of the computational grid  
 $m_o$  – Particles rest mass  
 $n$  – Refractive index  
 $NI$ - magnetic excitation (Ampere-turns)  
 $NA$  – Numerical aperture  
 $q$  – Charge of the particles  
 $r$  – Radial component of the cylindrical coordinate system [ $r(z)$ ]  
 $r_i$  – Image height  
 $r_o$ - Object height  
 $r_i'$  – Slope of the trajectory at the image side  
 $r_o'$  - Slope of the trajectory at the object side  
 $u$  – Electrostatic potential function [ $U(r, z)$ ]  
 $u$  – Axial electrostatic potential distribution  $U(z)$   
 $u'$  – First derivative of the axial electrostatic field distribution  $U(z)$   
 $u''$  –Second derivative of the axial electrostatic field distribution  $U(z)$   
 $u_o$  – Object side potential distribution  
 $\Delta u$  – Energy spread  
 $v$ - Velocity of charged particles  
 $z_i$  – Image position  
 $z_o$  – Object position  
 $\alpha$ - Half acceptance angle  
 $\lambda$  – Charged particles wavelength

# *Chapter One*

## **Introduction**

### **1.1 Introduction on Lithography**

Lithography is the process of transferring patterns of geometric shapes in a mask to a thin layer of radiation – sensitive material (called resist) covering the surface of a semiconductor wafer. Figure 1.1 illustrates schematically the lithographic process employed in integrated circuit fabrication [Preuss 2002].

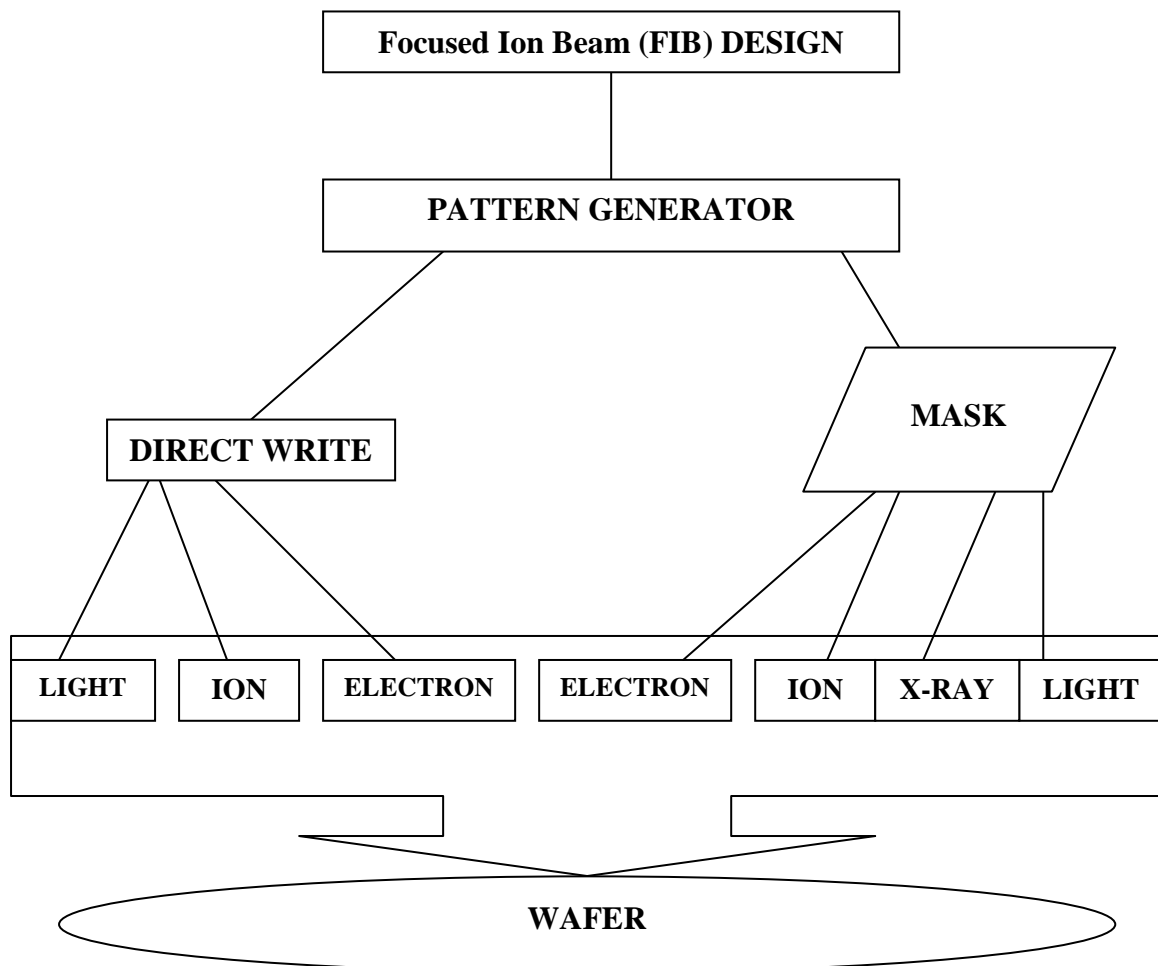


**Figure 1.1** shows lithographic process schemes [Preuss 2002].

Lithography advancements increased wafer size, and design innovation are three main constituents of the technology improvements that have kept the industry on this pace for more than 30 years [Harriott 2001]. Moore's Law states that the number of devices on a chip doubles every 18 months [Moore 1995]. Without the continuous improvements in lithographic process and equipment technology, personal computers, cell phones, and the Internet would not be in wide spread use today.

The resolution of an optical lithography system is usually expressed in terms of its wavelength  $\lambda$  and numerical aperture (NA) as follows [Huang et al 2001]:

$$\text{Resolution} = k_1 \lambda / NA \dots\dots\dots (1.1)$$

where  $k_1$  factor is the process-dependent coefficient of the resolution criterion for a diffraction limited lens. Ion lithography can achieve higher resolution than optical, x-ray, or electron beam lithographic techniques because ions undergo no diffraction and scatter much less than electrons [Harriott 2001].

Recent investigations have demonstrated that devices can be scaled down to sub-20 nm and smaller; therefore much shorter wavelength radiation needs to be considered for patterning such small features. The electron beam or ion beam lithography tools are limited by the aberration of the optical design. Theoretically, they can be used as lithography tools at 30 nm mode and beyond [Kedzierski et al 2000, Choi et al 2001].

Efforts have been devoted for developing ion projection lithography (IPL) in Europe and the United States of America. Figure 1.2 shows that IPL uses the same principles as optical steppers with mask patterns being printed to resist coated wafer substrates. Multi-electrode electrostatic ion optics is implemented to generate a broad ion beam illuminating the reticule and to project the image of the stencil mask patterns to the wafer substrate [Kaesmaier and Loschner 2000].

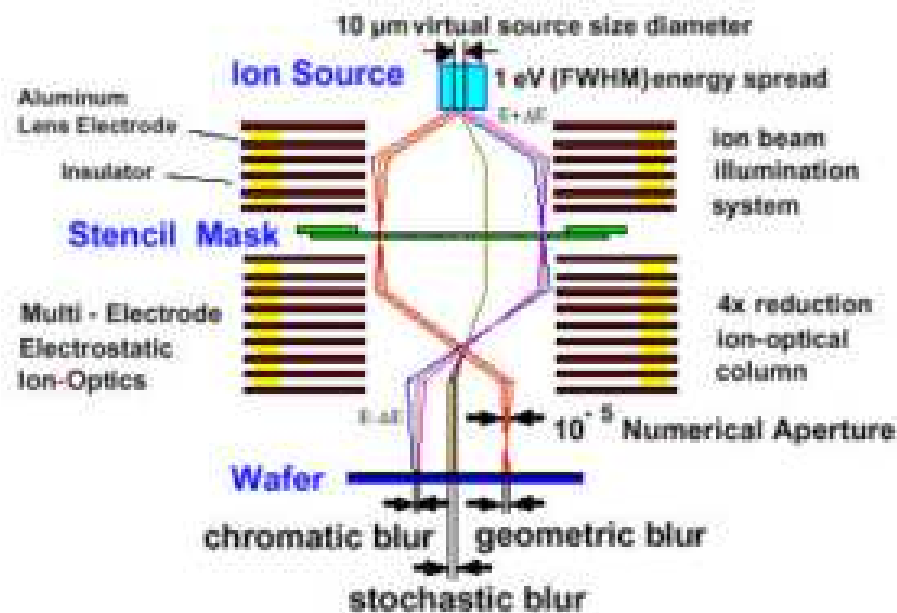


**Figure 1.2** represents European (Ion Projection Lithography )  
[Kaesmaier and Loschner 2000]

Ions are much heavier than electrons; the wavelength of ions can be two orders of magnitude shorter than electrons at the same energy. Ion beam resolution higher than electron beam may be achieved.

The actual beam size achieved by an ion projector is governed by ion source parameters (e.g. virtual source size, and energy spread of the extracted ions) and errors of the electrostatic lens system. Another advantage of using ions over electrons is that ions experience much reduced backscattering and proximity effect. All electrostatic lenses are often used to focus massive particles such as ions because round magnetic lenses have rather weak focusing properties for ion [Melngailis et al 1998].

In a conventional focused ion beam (FIB) system, a liquid-metal ion source (LMIS) is used to deliver current in the range of a few hundred pA into a spot size of approximately 50 nm [Melngailis1987]. But those days high-resolution FIB have been applied in a number of technologically important ways [Orloff 1993]: maskless implantation into semiconducting materials; lithographic mask repair for visible light and x rays; micromachining to create micrometer structures; deposition of materials from the vapor phase by ion-induced decomposition; modification of integrated circuits; failure analysis as part of the integrated circuit manufacturing process; and surface analysis. The present investigation will be focused on the first part of a lithographic system (FIB) only.

## 1.2 Electrostatic Lenses

A conventional optical system consists of several rotationally symmetric (round) lenses which enable light to be focused and imaged. Ion optical imaging systems also consist of several rotationally symmetric ion lenses that enable the ions to be focused and imaged. Similar to a light optical imaging system, the action of the ion optical system is to transfer the ion image from the object plane to the image plane. Electrostatic lenses are finding increased



applications in so many areas of technology, with the aid of electrostatic lenses ion probes are employed in ion implantation to change the local properties of semiconductors. Furthermore, lenses show great promise in modern optoelectronics and lithographic processes [Lencova 1997].

### 1.2.1 Classification of electrostatic lenses

The axial symmetric electrostatic field (rotational symmetry) acts upon charged particle beam moving in the near axis region the same way a light optical lens acts on a light beam.

Generally speaking, any electrostatic charged particle lens is any region of an axially symmetrical electrostatic field in which there taken place the inequality  $U''(z) \neq 0$ , where  $U(z)$  is the axial potential distribution and  $U''(z)$  is the second derivative of  $U(z)$  with respect to  $z$ . Therefore, depending on the electrode shape, voltages and the distribution of the electrostatic field in front and beyond the lens (i.e. the object and image region), such as one can classify several kinds of electrostatic lenses.

According to the charged particle optics, electrostatic lenses are classified into groups depend on the relationships between their electrode potentials. Such main groups are [Szilagyi 1988]:

- a. The immersion lens: It has two different constant potentials at its sides; it can be accelerated or retarded the particles while the beam focused and may consist of as few as two electrodes.
- b. The cathode lens: It can be called immersion objective lens with a field abruptly terminated on the object side by the source of the charged particles.

- c. The unipotential (**Einzel**) lens: This kind of lens has the same constant potential at both sides (the object and image sides). Therefore, the energy of charged particles remains unchanged.
- d. The diaphragm (single aperture) lens: This kind of lens has a homogeneous field on at least one side. Thus, the potential on one side or on both is not constant but increases or decreases linearly.
- e. The foil lens: It consists of thin metal films transparent to the particles and possessing discontinuous field distributions.

Apart from the classification of lenses according to the potential distribution one may distinguish one, two and multi electrode lenses. Furthermore, can distinguish between strong and weak charged particle lenses.

### 1.2.2 Properties of electrostatic lenses

Some of main properties of electrostatic lenses and their important features can be summarized as [**Hawkes 1989**]:

- a) In most non-relative cases the focusing properties as well as the aberrations are independent of the quotient of charge to mass ( $q/m$ ) of the particles. Therefore, the electrostatic lenses maybe used for any system focusing various ions.
- b) Electrostatic lenses are characterized by their simple electrodes fabrication, alignment and small size. The major problem of manufacturing is due to electric breakdown and accumulation of charges on the insulating surfaces.
- c) The potential ratios have influence on their properties. Therefore, if particles of the opposite sign have to be focused, so that the signs of all electrode potential must be reversed to arrive at the same properties.

- d) The most problem with electrostatic lenses is the difficulty of evaluation of their properties, because of the large number of characteristic parameters.

Thus, any comparison of the properties of different lenses is very difficult, where the lens properties are deployed in the form of tables and graphs. Unlike magnetic lenses, no universal design curves are available for the electrostatic lenses. Therefore, to select the best lens, a suitable dimensionless figure of merit may be constructed for the problem and then to choose the lens with the smallest acceptable value of this figure of merit. One common requirement of all applications is to reduce the aberration to as small as possible [**Hawkes 1989**].

### 1.3 Magnetic Lenses

Any axially symmetric magnetic field produced by current carrying coils with or without ferromagnetic materials or by permanent magnets is called a magnetic lens. Manufacturing of magnetic lenses is usually more complicated than that of electrostatic lenses. The action of a magnetic lens can be understood on the basis of the **Lorentz** force. Owing to the interaction of the radial velocity component of the particle with the longitudinal component of the magnetic flux density the velocity acquires an azimuthal component, which in turn interacts with the longitudinal component resulting in a radial focusing component, as shown in Figure (1.3) [**Lencova and Wisselink 2001**].

Ferromagnetic materials do not cause any difficulty if the magnetic scalar potential can be considered constant on the surfaces of the materials. Since the potential field is uniquely determined by Laplace's equation and by the potential distribution on the boundaries and there is no difference between

the calculations of the magnetic field and that of the corresponding electrostatic field [Szilagyi 1988].

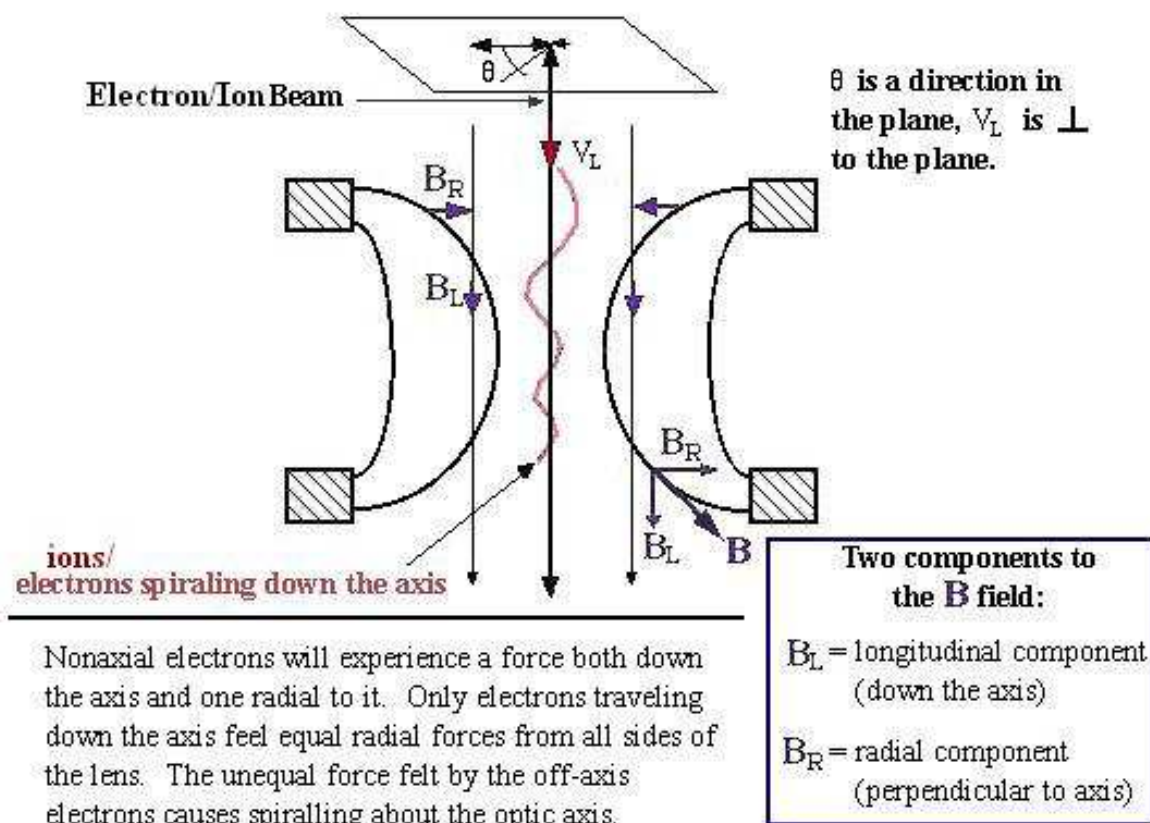


**Figure 1.3** represents schematic diagrams of the forces in a cylindrical magnetic lens [Lencova and Wisselink 2001]

There are three main types of magnetic lenses in any FIB system as shown in figure (1.4) [Rollett and Garmestani 2003]:

- (a) A multi-layer coil: i.e. an air-core solenoid coil. (Iron free lens)
- (b) A coil enclosed by soft iron plates (containing a gap).
- (c) A coil enclosed by soft iron plates containing a gap and internal soft iron pole pieces.

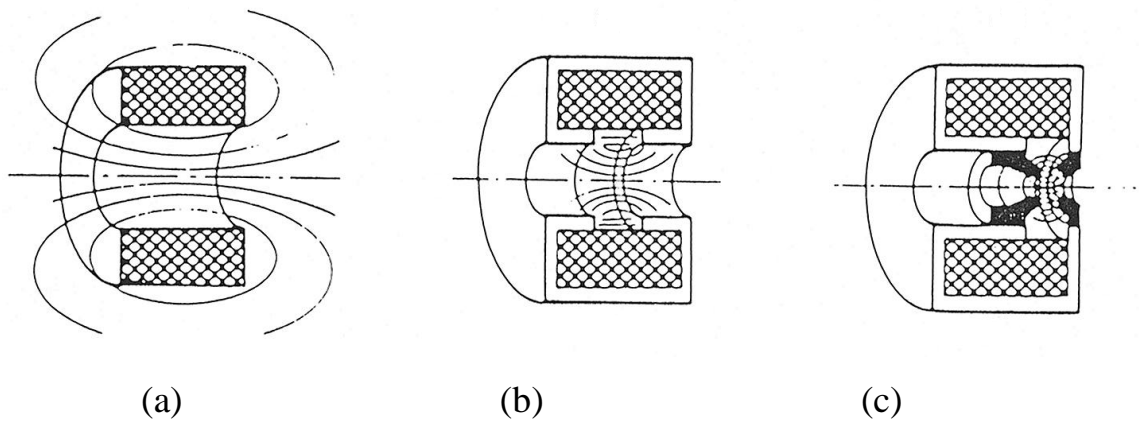


**Figure 1.4** shows schematic diagrams of the three types of magnetic lenses (a)A multi-layer coil , (b)A coil enclosed by soft iron plates and (c)A coil enclosed by soft iron plates containing a gap [Rollelt and Garmestani 2003].

### 1.3.1 Classification of magnetic lenses models

It is often desirable to perform a rapid approximate evaluation of lens properties without carrying out a detailed analysis. This can be accomplished if we have a simple mathematical model for the lens. Magnetic lenses can be classified into two basic categories: long lenses with distributed fields and short lenses with highly concentrated fields. Several good analytical models exist to classify magnetic lenses [Hawkes 1989]:

- a. **The rectangular model:** The simplest possible magnetic lens model is that of the equivalent solenoid. The idea is to replace the actual lens with a homogeneous field of finite length, which is; of course, practically unrealizable but it is very convenient mathematical model.
- b. **The step function model:** The axial flux density distribution can be approximated by a piecewise homogeneous distribution, i.e. by a series

of uniform fields of different strengths. The flux density distribution is divided into a number of segments and in each segment the flux density is assumed to have a constant value. This model is not very accurate but its great advantage is its extreme simplicity combined with flexibility.

- c. **The piecewise linear model:** The accuracy of approximation can be increased by using a model based on the replacement of the actual flux density distribution with a series of linear segments. The whole analysis of the given magnetic lens can be carried out with high accuracy by linking together the subsequent trajectory segments continuously. This model was successfully used for the synthesis of magnetic lenses.
- d. **The spline model:** This model has used a quadratic function for each segment of the flux density distribution which is equivalent to a piecewise cubic approximation of the magnetic scalar potential.
- e. **Glaser's Bell-Shaped and Grivet-Lenz models:** The axial flux density distribution of a typical symmetric short magnetic lens is a bell-shaped curve. In practice ferromagnetic materials are used to concentrate the field to a small region, the following function has proposed by W.Glaser closely approximates the axial flux density distribution of such a lens if it is close to saturation.

$$B(z) = B_{\max} / 1 + (z/d)^2 \dots\dots\dots (1.2a)$$

where  $B_{\max}$  is the maximum flux density distribution,  $d$  is determined by the shape of the pole piece and the degree of saturation. The model curve is very satisfactory at the center of the lens but decreases very slowly at its two edges. Nevertheless Grivet-Lenz model proposed the following field model which is satisfactory at the edges, and it represents the unsaturated lenses.

$$B(z) = B_{\max} / \cosh(z/b) \dots\dots\dots (1.2b)$$

where  $B_{\max}$  is the maximum flux density distribution,  $b$  is determined by the the field half-width.

### 1.3.2 Properties of magnetic lenses

The lens properties can be determined once the real lens field is replaced by an ideal rectangular field of length **L**. Physically this ideal field is that of a solenoid of length **S** and diameter  $\frac{2}{3} \mathbf{D}$  carrying the same ampere – turns **NI( excitation)** (i.e. number of turns  $\times$  D.C.current). The diagonal **L** of the solenoid is related to the real lens geometry by [Lencova 1997]:

$$\mathbf{L} = \sqrt{\mathbf{S}^2 + (\frac{2}{3}\mathbf{D})^2} \dots\dots\dots (1.3)$$

Under non – saturation conditions and according to Ampere's law, the maximum magnetic flux density **B<sub>max</sub>** becomes [Lencova and Wisselink 2001]:

$$\mathbf{B}_{\max} = (\mu_0 \times \mathbf{NI}) / \mathbf{L} \dots\dots\dots (1.4)$$

where **L** is geometrical parameter,  $\mu_0 = 4\pi \times 10^{-7}$  **Henry/meter** is the permeability of free space. Therefore, the magnetic field generated by a magnetic lens depends on its shape and excitation **NI**.

The distinctive feature of magnetic lenses is that their optical properties are dependent on the charge to mass ratio of the particles. Stationary magnetic fields cannot accelerate charged particles, therefore in the absence of electrostatic fields magnetic lenses leave their energy unaltered. So that in magnetic lenses the particle trajectories depend on the particles mass, where heavy particles are less focused than light ones. The boundaries of long lenses are difficult to define, but even in the case of short lenses the object or the image or both can be immersed in the field, therefore real properties become important in this case. Magnetic lenses are used for forming electron probes or highly magnified images of small objects; they can also be utilized for energy analysis. The effect of the magnetic field in any magnetic lens on a

paraxial beam of charged particles is similar to that of a convex glass lens on a beam of light rays [**Hawkes 1989**].

## 1.4 Historical Review

Many researchers attempted the design and optimization of electron lenses and systems with minimum aberrations from the early days of charged particle optics. **Scherzer** in 1936 found the best axial potential distribution for a weak electrostatic unipotential lens to become as [**Septier 1966**] ;

$$U(z) = U_0 [1 + C \exp(-S z^2)] \dots\dots\dots (1.3)$$

where  $z$  is the optical axis,  $U_0$  is the constant potential at both sides of the lens, and  $C$  and  $S$  are constants to be determined from some predefined values. In 1937, **Rebsch and Schneider** found the best potential distribution for a weak immersion lens to be [**Szilagyi 1988**];

$$U(z) = C_1 \exp(-S_1 z^2) \dots\dots\dots (1.4)$$

where  $C_1$  and  $S_1$  are constants to be determined from some predefined values.

After few years, **Plass** in 1942 attempted to discover what the shape of the electrodes is, in order to produce the potential distribution given by equation (1.3) in a reasonably simple way [**Septier 1966**]. He calculated the potential distribution near the axis using the power series expansion;

$$U(r, z) = U(z) - (1/4) r^2 (d^2 U(z)/dz^2) + (1/64) r^4 (d^4 U(z)/dz^4) - \dots\dots\dots (1.5)$$

In 1948, **Rüdenberg** drew the attention to the properties of the hyperbolic lenses [**Septier 1966**]. These lenses are the ideal symmetrical einzel lenses where the equation of potential distribution was;



$$U(r, z) = C_2 (z^2 - 0.5 r^2) + S_2 \dots\dots\dots (1.6)$$

where  $C_2$  and  $S_2$  are constants to be determined from some predefined values.

The first serious attempt to synthesis thick lenses was made by **Kasyankov** in 1952. He derived a set of high order nonlinear differential equations, the solution of which would minimize certain aberration integrals. On the other hand, **Burfoot** in 1953 attempted to calculate the electrodes shape of a lens with quadrupole – octupole symmetry, free of spherical aberration [**Hawkes 1973**].

**Tretner** used in 1959 the technique of calculus of variation to find the minimum spherical and chromatic aberrations that could be obtained with round magnetic and electrostatic lenses. He used several different constraints on the fields to represent the construction resources available. In 1968 **Crewe et al** designed a field emission electron gun under the assumption that the axial potential  $U(z)$  in the space between the first and the second anode can be represented by a cubic polynomial, the coefficients of which were the optimization parameter .Later on, **Munro** in 1973 showed that this design does not represent a true optimum [**Munro 1975**].

**Moses** [1970, 1971, 1973 and 1974] also used the calculus of variation in his work to minimize the values of the spherical and chromatic aberration coefficients  $C_s$  and  $C_c$  respectively; his work was concentrated on magnetic lenses only. More recently, **Szilagyi** [1977, 1978] introduced the dynamic programming approach. The integration interval  $z_0 \leq z \leq z_i$  between object and image is dissected into a set of small subintervals .Then starting from the object coordinate  $z_0$  , the integrand of an aberration integral , for instance that  $C_s$  is minimized under given constraints in each of these subintervals. The

result was a piecewise analytic axial field distribution, which is then assumed to be the best field [**Hawkes and Kasper 1989**].

Furthermore, systematic investigations of a large number of practically feasible axial potential distributions were carried out by [**Szilagyi 1983, 1984 and 1985**] with a subsequent reconstruction of the electrode systems producing such distribution. In this approach different curve fitting techniques and parameterized analytical function are used to find many potential distributions with both small spherical and chromatic aberrations. [**Martinez and Sancho 1983**] introduced a new version of the charged density method applicable to the analysis of the potential distribution in multi-element electrostatic lenses used for focusing charged particles and study of the optical properties of four cylinders lens has been carried out. Also, [**Kurihara 1985**] achieved optimization of a focused ion beam system for submicron lithography. He employed a four electrode accelerating lens for the condenser lens and obtained guidelines for reducing the chromatic aberration coefficients by choosing the dominant design parameters and examining their relations to the coefficients.

In 1987, **Tang and Sheng** made an analysis of the combined electrostatic focusing and deflection system using moving object lens concept. They developed a practical electrostatic system to give good overall deflection aberration performances [**Tang and Sheng 1987**]. But, [**Amos et al 1988**] introduced an analysis method in the optimization of the properties of micro focused ion beam system. Another approach for designing electrostatic lenses with given source parameters, first order properties and minimum aberrations is based on constrained nonlinear optimization techniques presented by [**Szilagyi and Szep 1988**]. However, **Tsumagari et al** in 1988 introduced a discussion presented on the optimization of the relative displacement in the

two lens system with an intermediate beam crossover. They showed that the design for crossover beam system was possible with almost the same performance as the collimated system in the same magnification conditions and short working distances [**Tsumagari et al 1988**].

[**Kiss 1989**] believed that systematic potential analysis will contribute to the development of the techniques of electrostatic lens design. He discussed a computerized investigation to find the axially symmetric electrostatic lens potential with acceptable first order properties and small spherical aberration.

[**Michiel van der Stam et al 1993**] showed that Optimization programs are becoming available to support the designing of complicated lens systems in charged particle optics. By exploring the consequences of design decisions automatically, they can increase the effectiveness of the designer. Adding that, [**Raymond 1993**] proved that Focused ion beam machines are becoming an accepted part of the semiconductor industry. They are used in the repair of photo masks and X-ray masks, for direct modification of devices, for failure analysis, and for process verification. As the scale of the lithography shrinks, the demands on the FIB tool increase accordingly, both in terms of its accuracy (for repair and modification) and its resolution (for imaging). One key factor that affects these parameters in the FIB column itself, in terms of its spot size performance. Many of today's applications demand spot sizes as low as 15 nm, at beam currents of 10 - 20 pA. Moreover, [**Steve et al 1993**] described a novel method of determining potentially successful starting designs by utilizing an expert systems algorithm which operates on a database of previously well-designed optical systems. Also, [**Xiaogang Chen et al 1993**] developed a small expert system used in lens design.

**Martinez and Sancho** in 1995 have used an accurate numerical method to calculate the geometric aberrations in electrostatic lenses (three cylinder einzel lens). They used an accurate version of the boundary element method to solve the Laplace's equation for the given lens geometry and potentials [**Martinez and Sancho 1995**].

Meanwhile, in 1997 **Martinez and Dymnikov** investigated the possibility of utilizing an electrostatic cylinder lens to focus the beam in microprobes. They used new analytical model of the axial potential distribution varying the parameters of this distribution and the size of the object aperture diaphragms to obtain the minimum spot size at the specimen for a given beam emitted, and finding by this way the optimal parameters of the axial potential distribution. They applied an accurate version of the integral equation method to solve Laplace's equation in order to obtain the parameters of the physical model which has the same axial potential distribution as the optimal analytical model [**Martinez and Dymnikov 1997**].

In recent years, most of researchers have interested in optimizing optical instruments and devices as a nano scale devices. In the Heisenberg microscope, the uncertainty principle has been used to determine the spatial position of a moving electron in the lateral direction. However, since charged particles follow the principle of Heisenberg, it is not possible to find solutions to the homogenous wave equation (paraxial ray equation) of electrodynamics that do not follow the behavior imposed by the uncertainty principle [**Stelzer 1999**]. Moreover, [**Sales 1998**] has recently shown that the axial lateral gain factors are related by a Heisenberg – like relationship. Also, [**Stelzer and Grill 2000**] have estimated the focal spot dimensions according to the same relationship. Adding that [**Ahmad et al 2002**] have introduced a computer aided design of an electrostatic FIB system consisting of three electrostatic

lenses approximated by the spline lens model. The present work have mixed the dynamic programming procedure and artificial intelligence technique optimization methods, in order to find FIB system consisting of three electrostatic lenses measuring the beam spot size.

## **1.5 Optimization Method**

The desire to produce electron and /or ion optical systems with prescribed first order properties and as small aberrations as possible is as old as electron/ion optics itself [Szilagyi 1988].

Optimization is the search for such electron and / or ion optical element that would provide the required optical properties with minimum aberrations. There are two approaches exist in optimization, namely analysis and synthesis. The method of analysis is based on trial and error, so that designer starts with certain elements and tries to improve their performance by analyzing the optical properties and varying the geometrical dimensions as well as the electric or magnetic parameters of the lens (system) until a satisfactory performance is achieved [Szilagyi 1985] .

However, many researchers attempted the design and optimization of electron lenses and systems according to the analysis method with the aid of computer programs. In recent years symbolic computing has become a promising aid in different kinds of decision making .Expert systems that have built in knowledge in the form of symbolically represented facts and rules .The design of optical elements and systems is based on the knowledge of simple facts and rules .An expert system for the design of electron/ion lenses could work in the following way. As a first step, a database must be established to provide efficient representation, storage, and retrieval of large

amounts of published information .A user interface would allow the selection of a specified set or a range of optical properties as well as some figure of merit. The system responds with a list of available lenses with the given properties indicating their order of preference based on the given figure of merit. Therefore, the system automatically performs the field calculations, and ray tracing .Also it determines the optical properties, adds the new configuration to the database, and evaluates it on the basis of the preferred figure of merit [Steve et al 1993].

## 1.6 Aims of the Project

In the present work, optimum and analyzed designs of a FIB system consists of single, two, three and multi lenses. It has consisted of both electrostatic and magnetic lenses which have investigated by adding the dynamic programming procedure (DPP) and artificial intelligence technique (AIT) in a nano scale measurements. Also, an optimization programming developed for getting a setup of optical column in two-lens, three-lens and multi-lens systems. Therefore, electrodes and pole pieces have designed and plotted in two and three dimensional viewing were simulated for the main lens systems. Also spot sizes measurements have been calculated and a suggestion of estimations in charged particles optics with mathematical manipulations has proposed to get a category based on uncertainty principle. Thus, synthesis procedures within the aid of analytical one under the following conditions have five main steps are taken place in this work, those are summarized as:

- ✚ Single-lens design: [electrostatic and magnetic lenses].
- ✚ Two-lens system: [electrostatic lenses].
- ✚ Three-lens system: [electrostatic lenses].
- ✚ Multi-lens system: [electrostatic and magnetic lenses].
- ✚ A suggestion of spot size calculations in terms of the uncertainty principle relationship.

# *Chapter Two*

## **Theoretical Considerations**

### **2.1 Motion of Charged Particles in rotationally symmetric Electrostatic and Magnetic fields**

In charged – particle optics , rotational symmetry (or axial symmetry as it is sometimes called) is of particular interest , since the most common charged-particle lenses are round , which means that they are built up from rotationally symmetric fields [**Hawkes and Kasper 1989**].

The motion of charged particles in such fields is similar to propagation of light through optical lenses. The most suitable coordinate system to fields with rotationally symmetry is the cylindrical polar coordinate system. The z-axis is the optical axis which represents the axis of symmetry. The value of the potential at any point can expressed in terms of the three coordinates r, z and  $\theta$  i.e. the potential  $u = u(z,r,\theta)$ . The condition for rotational symmetry in cylindrical coordinates can be expressed by  $u(r, z, \theta) = u(r, z)$ , where the values of r and z uniquely define the value of u, regardless of the angle of rotation. In rotationally symmetric space – charge – free fields, Laplace's equation is reduced to the following form [**Szilagyi 1985**]:

$$(1/r) \{ \partial / \partial r (r [\partial u / \partial r]) \} + \partial^2 u / \partial z^2 = 0 \quad \dots\dots\dots (2.1)$$

### 2.1.1 Paraxial-ray equation in electrostatic fields

The assumption that the trajectory of charged particles beam has small enough inclination angle with respect to the optical axis of the system, to allow replacing its tangent by its sine or its arc, greatly simplify the analysis of this system. Rays with these properties are referred to as paraxial rays, i.e. rays that are close to the axis [Hawkes and Kasper 1989].

In many designing lenses and deflectors, paraxial trajectories are dealt with, therefore **Gaussian dioptrics** is a theory of the behavior of paraxial rays is being considered. The paraxial ray equation is given by a linear homogenous second order differential equation, its solution gives the trajectory  $\mathbf{r}=\mathbf{r}(\mathbf{z})$ , for particles moving close to the optical axis in a rotationally symmetric electrostatic fields[Szilagyi 1988], as follows:

$$r'' + (u' / 2u) r' + (u''/4u) r = 0 \dots\dots\dots (2.2)$$

where  $u = u(z)$  is the electrostatic potential distribution in volts along the optical axis  $\mathbf{z}$ , the primes represent differentiation with respect to  $\mathbf{z}$ . For non – relativistic velocities and the absence of any azimuthal velocity components, the trajectory of charged particles (ions or electrons) can be treated in the  $\mathbf{rz}$  plane, where in cylindrical coordinates system;  $\mathbf{r}$  represents the radial component, and  $\mathbf{z}$  is the axial component of the trajectory along the optical axis of a lens.

The behavior of paraxial rays have two assumptions which are considered as [Szilagyi 1988]:

- a. In the power series expansion of the potential function  $u (r,z)$  , all terms containing powers of  $( r )$  higher than the first will be neglected .Then the potential distribution becomes ;



$$u(r, z) = u_0(z) - u_0''(z) (r^2/4) + u_0''''(z) (r^4/64) - \dots \dots \dots (2.3)$$

This assumption will be used only in the region where the field exists. Outside the field the trajectories are straight lines that may extend far away from the axis even if they are paraxial inside the field.

- b. The radial and azimuthal velocity components can be neglected in comparison with that of the axial one.

### 2.1.2 Paraxial-ray equation in magnetic fields

The paraxial ray equation in axially symmetric magnetic fields can be written as [Hawkes and Kasper 1989]:

$$r''(z) + k^2 r(z) = 0 \dots \dots \dots (2.4)$$

where  $k^2 = [q B_z^2 / 8 m V]$ ,  $B_z$  - is the axial component of the magnetic flux density,  $q$  - is the electric charge,  $V$  - is the accelerating voltage and  $m$  is the mass of charged particles accelerated through a magnetic field.

Unlike the behavior of paraxial rays in electrostatic fields, the paraxial rays in magnetic fields the distance  $r$  of the ion / electron path from the optical axis (compared to the total length of the beam path within the field region) should always be so small. Furthermore, the inclination of the beam path to the axis is required to be so small that second and higher powers of the inclination of the beam path can always be neglected with respect to the first power.

### 2.1.3 Numerical determining field potentials

The field equation to be solved will be Laplace's equation (2.1). The solution of Laplace's equation with specified boundary conditions make it possible to determine the potential  $u(r, z)$  as a function of coordinates, from which the components of the field intensity can be calculated. It is possible to obtain an analytic solution; the final expression is often too awkward and unsuitable for particular applications. Therefore, the uses of the numerical methods (approximate methods) are very useful in solving the charge particle optics problems [Ahmad 1993].

There exist a wide variety of approximate methods for solving the field equation (field potential); the most common are [Szilagy 1988]:

#### (a) Finite Element Method

The finite element method FEM was first used in electron optics by Munro 1970, who applied it to the computation of the magnetic field in round lenses. Since that time, it is of special interest in charged particle optics. In this method the system of algebraic equations reads as  $U_i = \sum_{j=1}^N A_{ij} U_j + B_i$ , the inhomogeneous terms arising from the boundary values of the potential are represented by  $U_i$  and  $B_i$ . The matrix  $A_{ij}$  depends on the node coordinates and on the partial differential equation (PDE).  $A_{ij}$  are derived from a variation principle –equivalent with the PDE to be solved. The functional is a volume integral as in the electrostatic case [Munro 1975]:

$$F = \iiint_{\text{total volume}} \frac{1}{2} \Delta U \cdot \Delta U dV \dots\dots\dots (2.5)$$

The above integral depends on the type of coordinates, the potential  $U$ , and its first derivatives with respect to the coordinates. The field is subdivided into triangles, each node being the common vertex of the adjacent triangles.

As shown in figure (2.1), within each triangle the potential is expressed by a lower order polynomial of the coordinates.

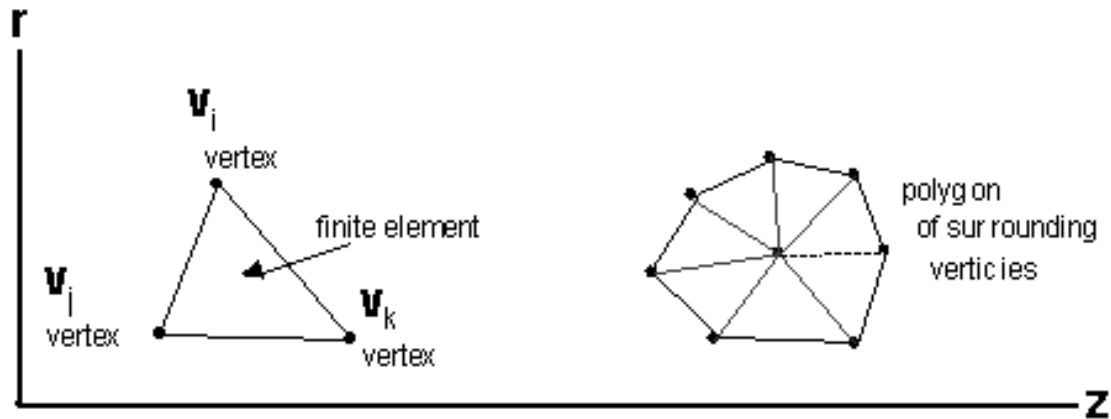


**Figure 2.1** represents mesh of the finite element method  
[Munro 1975]

With these approximations the potential through out each element is uniquely determined by potentials at its vertices. Hence the contribution for each element to the value of the functional can be expressed in terms of the vertex potential. Minimizing the functional, one yields a set of linear algebraic relations, relating the potentials at each vertex and its neighbours, where the  $A_{ij}$  depending on the coordinates of all vertices involved. This set of linear equations is solved to give the potential at each mesh point.

### (b) Finite Difference Method

The finite difference method was first introduced by **Liebmann** in 1918 and thus it is often called "Liebmann's method". The mathematical theory of this method is exhaustively studied in many researches. The basic concept of the procedure is to subdivide the space within the field under consideration

into finite squares or rectangular grids. The potential at each node is related to those at four or eight of its nearest neighbours as shown in figure (2.2).

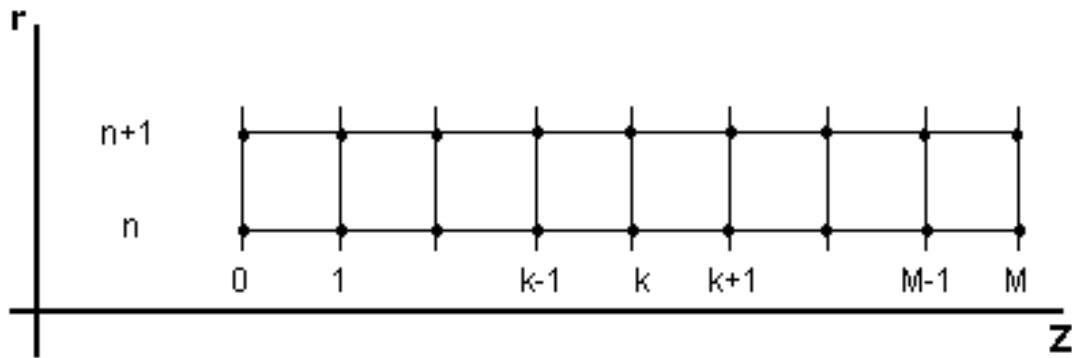


**Figure 2.2** represents the grid of the FDM in two dimensions  
[Hawkes and Kasper 1989]

There are essentially two different ways of deriving the finite difference formula that replaces Laplace's equation namely, the Taylor series method and the integral method. Further details on FDM are given in most of literatures like [Hawkes and Kasper 1989].

One of the simplest classes of parameterized analytical functions is the class of high degree polynomials whose coefficients are simple functions of the potential values at given locations. One can find excellent imaging field distributions even with a personal computer [Hawkes and Kasper 1989].

### (c) Artificial Intelligence Technique

In 1990's symbolic computing has become a promising aid in different kinds of decision making and building expert systems. These were the first attempts in this technique, programs are appearing that are able to deduce rules from a database without actually carrying out numerous amounts of numerical calculations [Friedman 2003, Menken 2002]. The design of optical elements and systems are based on the knowledge of simple facts and

rules, the initial data are laws of electron and/or ion optics and the knowledge about existing solutions [**Xiaogang et al 1993, Steve et al 1993**].

Present software (**CADION**)"which stand for computer aided design for ions" has adopted this technique with the aid of dynamic programming procedure, in order to maintain such smart database (i.e. expert system); the system contains database tables impeded inside the subroutines. The synthesis procedure of the dynamic programming has used with the aid of this technique to achieve such expert system.

#### **(d) Dynamic Programming**

Dynamic programming is a mathematical optimization technique used for making a series of interrelated decisions. It is start with a small portion of the problem and finds the optimal solution for this smaller problem. In contrast to other mathematical programming techniques, there is no standard formulation of the dynamic programming problem. This kind of programming is a general strategy for optimization rather than a specific set of rules. The dynamic programming procedure has been successfully applied to different problems of electron and ion optics [**Ahmad et al 2002, Orloff 1993, Chapra and Canale 1998, Amos et al 1988**].

A major distinction among dynamic programming problems is the nature of the decision variables. If the decision variable is restricted to integer values as in this investigation, the whole problem is to be **discrete**. If the decision variable can take on any real value, the problem is said to be continuous. Usually a multi stage decision process is transformed into a series of single stage decision processes. It is essentially a recursive optimization [**Kuester 1973**].

In the present work both the artificial intelligence technique and the dynamic programming procedure will be used. More details on the synthesis procedure will be given in chapter three.

### (e) Cubic spline function

A cubic spline function is a third order polynomial used for interpolation, curve fitting with continuous first and second derivative. The name is derived from the old drafting tool. It is a flexible thin piece of wood that was used to generate a smooth curve passing through specific points known by nodal points. The spline assumes that shape which minimizes its potential energy, and beam theory states that this energy is proportional to the integral with respect to the arc length of the square of the curvature, of the spline. If the spline is a function of coordinate  $z$  and if the slope is small, the second derivative approximates the curvature. Therefore, cubic spline function, its first and second derivative can be written as [Burden et al 1981]:

$$\left. \begin{aligned} F_k(z) &= A_k + B_k(z-z_{k-1}) + C_k(z-z_{k-1})^2 + D_k(z-z_{k-1})^3 \\ F'_k(z) &= B_k + 2C_k(z-z_{k-1}) + 3D_k(z-z_{k-1})^2 \\ F''_k(z) &= 2C_k + 6D_k(z-z_{k-1}) \end{aligned} \right\} \dots\dots\dots (2.6)$$

where  $z_{k-1}$  is the coordinates of the  $k$ -th interval's left end point ,  $k=1,2,3,\dots,n$  is the number of intervals ,  $A,B,C$  and  $D$  are the coefficients of the spline function which are for each region.  $F_k(z)$  may approximate the axial potential distribution  $U(z)$  for both rotationally symmetric electrostatic and magnetic lenses.

The continuity conditions for the spline function, its first and second derivatives can be rewritten as:

$$\left. \begin{aligned} F_{k+1}(z_k) &= F_k(z_k) \\ F'_{k+1}(z_k) &= F'_k(z_k) \\ F''_{k+1}(z_k) &= F''_k(z_k) \end{aligned} \right\} \dots\dots\dots (2.7)$$

## 2.2 Light Optics Verses Ion Optics

There are significant differences between light and ion optics, such as [Steve et al 1993]:

- **Radius of Refraction**

Light optics makes use of sharp transitions of light velocity (e.g. lens edges) to refract light. These are very sharp and well defined (by lens shape) transitions. The radius of refraction is infinite everywhere (*straight lines*) except at transition boundaries where it approaches zero (*sharp bends*).

Ion optics make use of electric field intensity and charged particle motion in magnetic fields to refract ion trajectories. This is a distributed effect resulting in gradual changes in the radius of refraction. Desired electrostatic/magnetic field shapes are much harder to determine and create since they result from complex interactions of electrode/pole shapes, spacing, and potentials and can be modified significantly by space charge.

- **Energy (Chromatic) Spreads**

Visible light varies in energy by less than a factor of two. Ions can vary in initial relative energies (or momentum for magnetic) by orders of magnitude. This is why strong initial accelerations are often applied to ions to reduce the relative energy spread.

- **Physical Modeling**

Light optics can be modeled using physical optics benches (interior beam shapes can be seen with smoke, screens, or sensors).

Ion optics hardware is generally internally inaccessible and must normally be evaluated via end to end measurements. Numerical simulation programs allow the user to create a virtual ion optics bench and look inside much like physical light optics benches.

## 2.3 Uncertainty Principle

The motion of charged particles at non relativistic velocities is governed by the laws of classical mechanics. Naturally, the wave nature of particles is an important limitation for dimensions comparable with the following **de Broglie** wavelength [Yariv 1982]:

$$\lambda = h/mv \dots\dots\dots (2.8)$$

where  $h = 6.62 \times 10^{-34}$  Js is Planck's constant,  $m$  and  $v$  are the mass and velocity of the accelerated particle respectively. In classical mechanics it is possible to measure both the velocity and the coordinate of a particle at some time without disturbing it. However quantum mechanically the act of measurements interferes with the system and modifies it. The resulting perturbation is negligible in "large" (classical) systems, but assumes major importance in small systems such as atoms, electrons and nucleons. It is a basic result of electromagnetic theory (specifically, of the theory of diffraction) that the spatial limit of resolution is approximately equal to the wavelength of electromagnetic radiation used [Szilagy 1988].

Therefore, momentum and position of a charged particle cannot be measured simultaneously with arbitrary accuracy. This was due to the fact that the uncertainty principle works. The uncertainty relationships are often referred to in order to illustrate the constraints on propagating quantum mechanical



wave functions. Since position and momentum are the key factors characterizing a particle in classical mechanics, it is important to know that the corresponding quantum mechanical operators do not commute for a known function. Quantum mechanically the position  $\mathbf{r}$  and momentum  $\mathbf{p}$  are represented by the following expression [Yariv 1982]:

$$[\mathbf{r}_i, \mathbf{p}_j] = i\hbar \delta_{ij} \dots\dots\dots (2.9)$$

where  $\mathbf{r}_{i=x,y,z} = x, y$  or  $z$ , and  $\mathbf{p}_{j=x,y,z} = p_x, p_y$  or  $p_z$  and so on. Thus find that the position and momentum as operators of a charge particle do not commute.

In principle the quantity  $\Delta z$  can be used as a measure of the uncertainty (fuzziness) in position (along optical path), and  $\Delta p$  is a measure of the momentum spread; both are related by [Yariv 1982]:

$$\Delta p \Delta z \geq \hbar / 2 \dots\dots\dots (2.10)$$

where  $\hbar = h/2\pi$ , and all particles are considered under the non-relativistic case. Equation (2.10) holds for any physical system.

Consequently, most of present work results were calculated in a nano scale or less of accuracy. To distinguish the final idea and discuss it for more precise factors, the aspects have been adopted in this investigation are the whole dramatic notions of the uncertainty principle hypothesis.

Therefore, to select the best lens, a suitable dimensionless figure of merit may be constructed for the problem and then to choose the lens with smallest acceptable value of an optimized factors. One common requirement

of all applications is to reduce the spherical and chromatic aberrations to as small as possible.

It seems then that the absolute figure of merit of any optical system is the size of its total aberration disc diameter ( $\mathbf{d_t}$ ). Adding that the beam spread angle  $\alpha$  can be ascribed to the fact that the charged particles (electrons or ions) are confined initially to a distance, which it is corresponding to the total aberration disc diameter. Therefore, the transverse momentum spread is  $\Delta \mathbf{p} \sim \hbar / \text{total aberration disc diameter } (\mathbf{d_t})$ , then the spread angle  $\alpha$  has taken as [Yariv 1982]:

$$\alpha \sim \Delta \mathbf{p} / \mathbf{p} \sim \hbar / (\mathbf{d_t}) (2 \pi \hbar / \lambda) = \lambda / 2 \pi \mathbf{d_t} \dots\dots\dots (2.11)$$

where  $\mathbf{p} = 2 \pi \hbar / \lambda$ ,  $\lambda$  is the wavelength of the charge particles wave.

This is a well-known formula, it is approached as a problem in electromagnetic theory .Equation (2.11) reflects the Fourier transform relationship that exists between the field distribution in the lens plane and the far-field distribution of the image spot size .This Fourier transform relationship is also the basis for the uncertainty relations in quantum mechanics[Shannon and Weaver 1949].

## 2.4 Definitions of Some Optical Parameters

Figure (2.3) shows some of the optical parameters, such as object plane  $z_o$ , the image plane  $z_i$ , the principal planes and points, the focal points and the focal planes. There are so many definitions of such parameters and properties. The following steps are summarized some of them [Szilagyi 1988];

- ❖ Object side: the side of the lens at which the charged particles enter.
- ❖ Image side: the side of the lens at which the charged particles leave.
- ❖ The object plane  $z_o$ : The plane at which the physical object is placed or a real image is formed from a previous lens, on the object side.
- ❖ The image plane  $z_i$ : The plane at which a real image of the object plane  $z_o$  is formed, on the image side.
- ❖ The principal points: The planes passing through the intersections and perpendicular to the axis are called principal planes. The intersections of the principal planes with the optical axis are called principal points.
- ❖ The focal points: A focal point is the image of a bundle of rays incident on a lens parallel to the axis. If these rays arrive at the lens from the object side, then these rays are collected at the image focal point  $f_i$ . If these parallel rays are incident from the image side, they will be collected by the lens at the object focal point  $f_o$ . The plane perpendicular to the optical axis and passing through either  $f_o$  or  $f_i$  is known as the object or the image focal plane respectively.

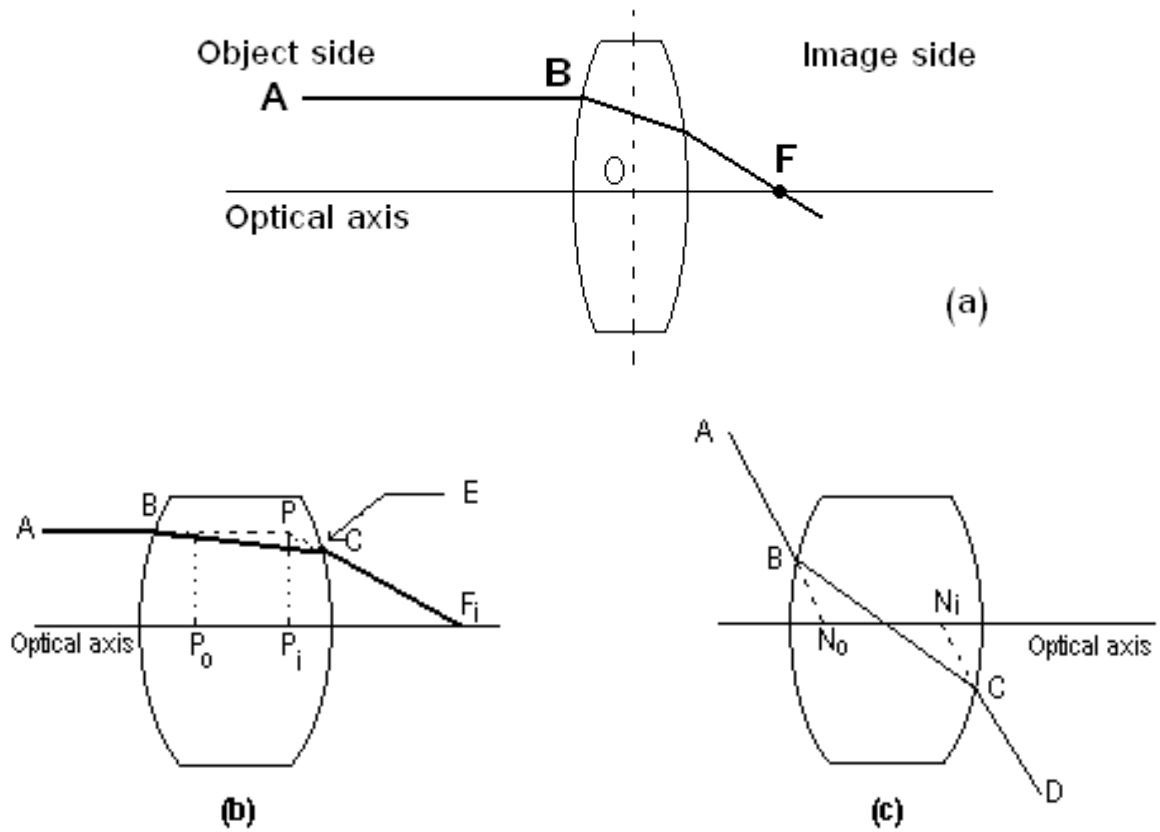


**Figure 2.3** represents the Cardinal Elements (Optical Parameters) of an axially symmetric lens (a) Definition of focal point, (b) Definition of principal points and (c) Definition of nodal points.

- ❖ The objective and projector properties : In many cases the charged particle beam trajectory crosses the optical axis inside the lens ( strong lens ) .It cannot be assumed that the path of the trajectory will be rectilinear after crossing the optical axis , because it can still be modified by the field until it emerges from the lens. This is illustrated in figure (2.4), where the trajectory crosses the axis at the objective focal point  $f_{obj}$ . The objective focal point, the objective midfocal length, and the objective principal point are denoted by  $f_{obj}$ ,  $Of_{obj}$ , and  $P_{obj}$  respectively. The projective focal point  $f_{proj}$  , the projective principal point  $P_{proj}$ , and the projective mid focal length  $Of_{proj}$  are also shown in

the figure (2.4).For weak lenses , where the intersection of the beam with the optical axis occur outside the lens field , the objective and projective cardinal points coincide [ **El-Kareh and El-Kareh 1970**].

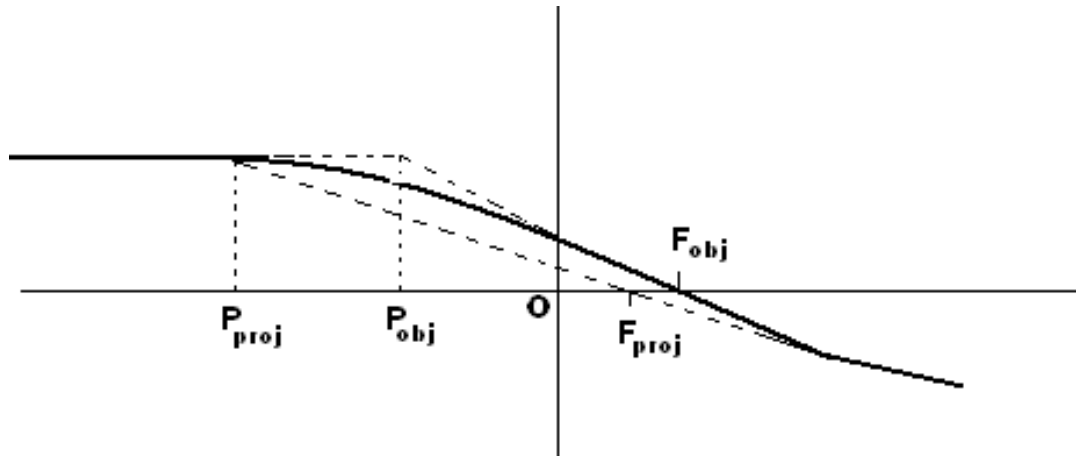


**Figure 2.4** shows the definition of Objective Cardinal Points in a Strong Lens

There are three magnification conditions under which a lens can be operated, namely zero, infinite and finite magnification .Figure (2.5) shows the three conditions, thus magnification in any optical system is the ratio between the transverse dimension of the final image and the corresponding dimension of the original object, i.e. the magnification (M) as[**Munro 1975**]:

$$M = r_i / r_o = \text{image height} / \text{object height} \dots\dots\dots (2.12)$$

As shown in the figure (2.5) these conditions are summarized as [**Hawkes 1989**]:

- a) Zero magnification condition : In this case the operating conditions is  $z_o = -\infty$ , as an example , the final probe forming lens in a scanning electron microscope (SEM) is usually operated in this condition.
- b) Infinite magnification condition: The operating condition is  $z_i = +\infty$  , as an example, the objective lens in a transmission electron microscope (TEM) is usually operated in this condition.
- c) Finite magnification condition: The operating condition in which  $z_o$  and  $z_i$  is at finite distances, as an example, the electrostatic lens in field emission gun is usually operated in this condition.

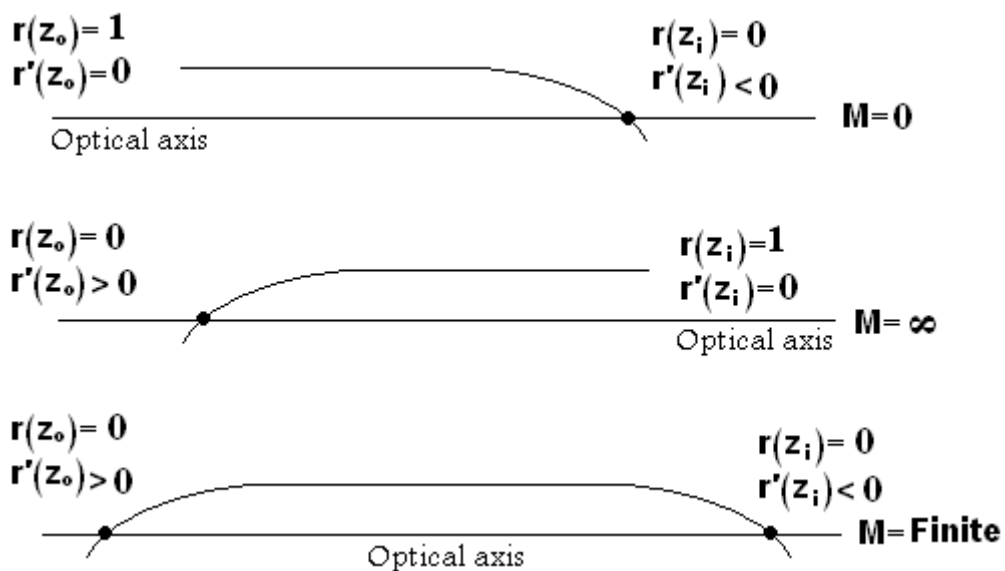


**Figure 2.5** shows the magnification conditions

## 2.5 System of Lenses

A system of lenses is a combination of several lenses arranged in the axial direction and forming an intermediate image of an object in the field free regions between them. If the fields of any two consecutive lenses overlap,

they must be considered as one single lens. The two most important practical reasons to employ a system of lenses are [Szilagyí 1988]:

- i. To allow variations of the magnification over a wide range by changing the lens excitations when the object and lenses are all situated at fixed locations.
- ii. To provide the possibility of achieving very high or very low magnifications.

To construct the final image of the object, the intermediate image produced by the  $N$ th lens will be the object for the  $(N+1)$ th lens, where  $N$  is the ordinal number of the lens in the system. This number is usually small in most equipment such as the electron microscopes, and the micro fabrication devices, and no more than three lenses are used. In some applications, like in particle accelerators, the number of successive focusing elements may be very large. So that the fewer the number of lenses is the shorter is the optical column, which is equivalent to a much easier practical realization (better mechanical stability, not so complicated alignment, smaller number of power supplies, etc.). In the present investigation, different combinations were used as a focusing portion of the system.

## 2.6 Aberration Theorem in Ion Optics

Microscopes and other optical instruments are commonly plagued by lens errors that distort the image by a variety of mechanisms associated with defects (commonly referred to as aberrations) resulting from the spherical geometry of lens surfaces. There are three primary sources of non-ideal lens action (errors) that are observed in any optical device.

Of the three major classes of lens errors, two are associated with the orientation of wave fronts and focal planes with respect to the optical axis. These include **on-axis** lens errors such as **chromatic** and **spherical** aberration, and the major **off-axis** errors manifested as **coma**, **astigmatism**, and **field curvature**. A third class of aberrations, commonly seen in stereomicroscopes that have zoom lens systems, is geometrical distortion, which includes both **barrel** distortion and **pincushion** distortion [Michiel et al 1993].

Rotationally symmetric electric fields may be generated by systems of metallic electrodes that are rotationally symmetrical in geometry and configuration and between which appropriate voltages are applied. In these electric fields, the equal-potential surfaces are rotationally symmetrical curved surfaces, which can be made to focus ion beams.

The study of aberrations is of great importance, since they cause limitations to the performance of various electron/ion optical elements and systems. It is as old as the electron microscope itself, for the first calculations of aberration coefficients were made in the early 1930s by **Scherzer** and **Glaser**. Hence, the operation of axially symmetric electron and ion lenses is based on the paraxial theory (first order) which is an approximation theory.

Similar to a light optical imaging system, the action of the ion optical system is to transfer the ion image from the object plane to the image plane. In the paraxial approximation the ion optical system can form an ideal and clear image known as the **Gaussian** image, but when aberration is present the image is distorted and unclear.



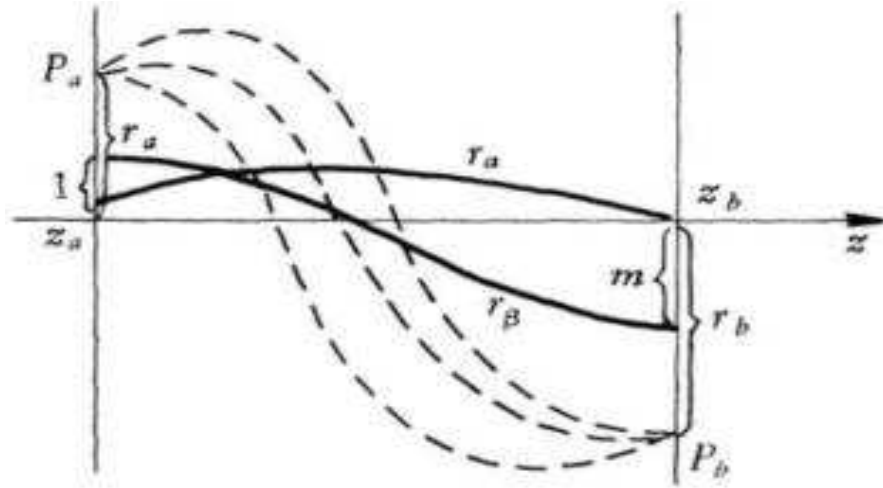


**Figure 2.6** shows the ideal imaging Gaussian trajectory

As shown in Figure (2.6), the object is at plane  $z=z_a$ , and its **Gaussian** image plane is located at  $z=z_b$ . Trajectories passing through the object point intersect at an image point are independent of their initial slope  $(x'_a, y'_a)$ . Thus all **Gaussian** trajectories emitted from an object point  $P_a (x_a, y_a)$  in the object plane, regardless of their slope, are focused at a point image  $P_b (x_b, y_b)$  in the image plane  $z=z_b$  [Lencova and Wisselink 2001] .

Unfortunately, aberration is not the only defect that the image suffers from. Other type of defects that due to the **fabrication of lenses**, such as mechanical imperfections and misalignment. The electrostatic repulsion forces between particles of the same charge causes a deviation in charged particles path. It is another defect, known as the **space charge effect**, and it is a case of charged particle optics alone, that cannot be found in light optics.

### 2.6.1 Aberration Coefficients

Aberrations are the problem of all image-forming systems. In general, they are defined as the departure from the ideal (paraxial) image formation.

Sometimes, they are called image defects or imperfections, because their presence causes deformation or complete damage to the image features [El-Kareh and El-Kareh 1970].

### **a. Spherical Aberration**

When the rays are monochromatic, which occur when the laws of refraction and reflection are applied to mathematically correct surfaces and which are not consequences of material inhomogeneity or fabrication errors are as follows [El-Kareh and El-Kareh 1970]:

1. Spherical aberration
2. Coma
3. Astigmatism
4. Field curvature
5. Distortion

Deformed image is not clear because of one of these aberrations, which are mostly taken place a mixture of them. This classification is arranged in a descending manner according to their extent of influence in the deformation of image features. They are called “geometrical aberrations” because each kind has a geometrical origin.

The calculation of the spherical aberration coefficient can be performed in two different ways. A straight forward approach is to retain the cubic terms in the paraxial ray equation (2.3) and evaluate the difference between the accurate ray equation, and the paraxial trajectory originating at the object point. The spherical aberration coefficient ( $C_s$ ) can be expressed in terms of integration involving knowledge of the paraxial trajectory and the value of the axial electrostatic potential. This procedure is commonly known as the trajectory method [Lawson 1977]. On the contrary, a general perturbation

theory may be developed, known as the **eiknal** method or method characteristic function [Hawkes and Kasper 1989]. The coefficient of spherical aberration referred to the object space **Cso** is represented by the following equation [Szilagyi 1985]:

$$\mathbf{Cso} = (1/16 \ r_o'^4 \ U_o^{1/2}) \int_{z_o}^{z_i} \{ [5/4(U''/U)^2 + 5/24(U'/U)^4] r^4 + 14/3(U'/U)^3 r r^3 - 3/2(U'/U)^2 r'^2 r^2 \} U^{1/2} dz \dots\dots\dots(2.13)$$

where **Cso** = spherical aberration coefficient in the object side,  $U = U(z)$ ,  $r = r(z)$  and  $U_o$  is the object side potential.

As shown in Figure (2.7), the focusing action of the fields in the region farther from the axis is stronger than that in the region nearer to the axis. The image position  $\mathbf{z}'_b$  for the marginal off-axis trajectories will be in front of the **Gaussian** focus and further from the **Gaussian** image plane than the position  $\mathbf{z}_b$  for paraxial trajectories. The minimum radius of the beam  $\delta_s$ , which is used to characterize spherical aberration, proportional to the third power of the angular aperture  $\alpha_a$  in the object plane. In electron or ion optical imaging devices, the ultimate resolution is limited mainly by the spherical aberration which is the only nonzero geometrical aberration at the axis and therefore the most harmful. It can be decreased by reduction of  $\alpha_a$  [El-Kareh and El-Kareh 1970].

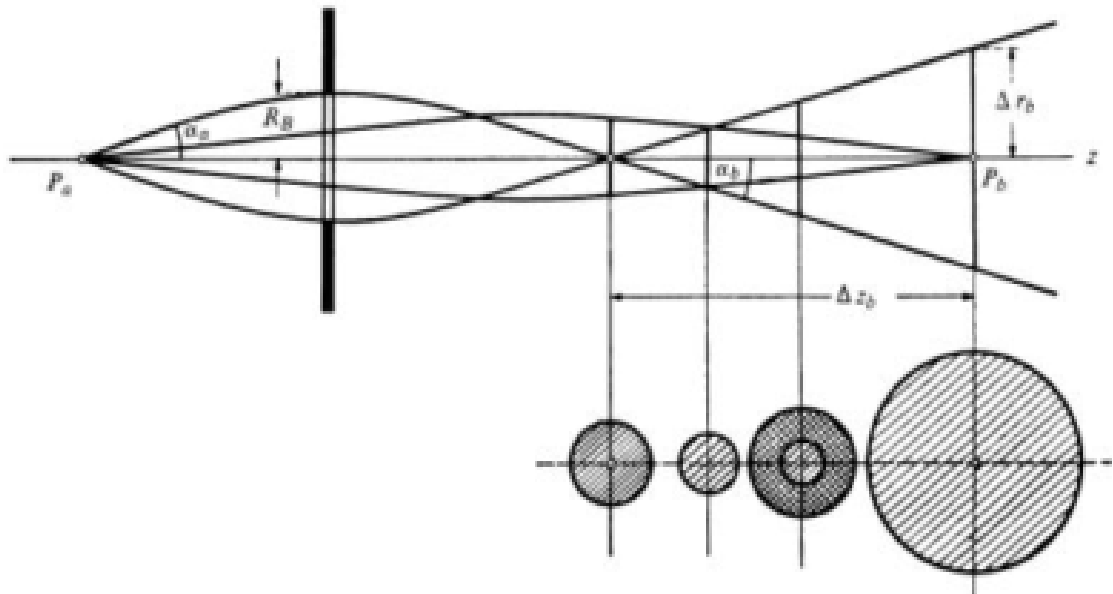


**Figure 2.7** represents the spherical aberration [El-Kareh and El-Kareh 1970]

As a result, in any charged – particle optics as well as in classical optics, the aperture aberration (spherical aberration or stop aperture) is by far the most important, because it limits the resolution of electron microscopes and the smallness of the probes of microanalysers. These aberrations are characterized by the values of the deviations  $\Delta \mathbf{x}$  and  $\Delta \mathbf{y}$  from the point of the image formed by the paraxial beam [Septier 1966].

The radius of the stop aperture ( $r_a$ ) is proportional to the tangent of the aperture angle  $\alpha$  (half acceptance angle). Since  $\alpha$  is very small (i.e.  $\tan(\alpha) = \alpha$  in radians). Thus, it would get the disc formula as [El-Kareh and El-Kareh 1970];

$$\mathbf{d_s} = \mathbf{Cs} \, \alpha^3 \dots\dots\dots (2.14)$$

where  $\mathbf{d_s}$ ,  $\mathbf{Cs}$  is the diameter of the spherical aberration disc and its coefficient respectively. As it has seen, the spherical aberration coefficient of the focusing device depends primarily on the diameter of the aperture.

On the other hand, the spherical aberration will cause blurring in the formed image if the angle  $\alpha$  is not very small. To evaluate the aberration disc for a very small angle  $\alpha$ , it makes the easiest way for getting such indications. Since, the aperture of the system ( electrical lenses ) have multi frames representations in the whole space [Michael 2005]. Mainly, the present work results have given this value the proper indication of uncertainty relationship.

## **b.Chromatic Aberration**

Chromatic aberration in light optics arises from the fact that light of different colors (wavelength  $\lambda$ ) is refracted with different strength. In ion optics, the ions passing through a lens with different energies will be refracted differently. First-order chromatic aberration is proportional to the fractional energy spread,  $\Delta U/U$ , at the image plane, and to the first power of  $\alpha$  or  $r$ . In rotationally symmetric electron lenses, chromatic aberration cannot be completely eliminated, but it can be reduced by increasing the acceleration voltage [Michael 2005].

In summary, geometrical aberrations have a functional dependence of the form  $\alpha^i r^j$ , where  $\alpha$  = beam half angle at the image plane,  $r$  = off-axis distance at the image plane, First-order chromatic aberration are proportional to the fractional energy spread,  $\Delta U/U$ , at the image plane, and to the first power of  $\alpha$  or  $r$ . As in the figure (2.8) a simple principals of the chromatic aberration defect in light optics is shown [El-Kareh and El-Kareh 1970].

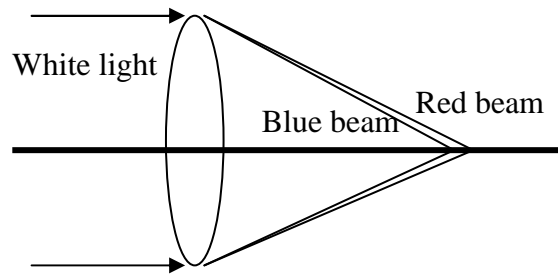


**Figure 2.8** represents the chromatic aberration

Since the charged particle wavelength  $\lambda$  is inversely proportional to the square root of the accelerating voltage  $U$ , the accelerating voltage must be very stable to have a narrow spread of wavelengths (i.e. energies). If  $\Delta U$  denotes the departure from the desired accelerating voltage, then  $\Delta U/U$  must not be greater than  $5 \times 10^{-5}$  in high resolution instruments [Hawkes 1972]. This ratio is known as a relative energy spread which is positive number, usually given as the characteristic parameter of the source. The chromatic aberration then can be reduced in two different ways; either by reducing the relative energy spread of the source or by reducing the aberration coefficient of the lens.

The chromatic aberration coefficient **Cco** is defined by the following equation [Szilagy 1985]:

$$\mathbf{Cco} = (U_o^{1/2} / r_o'^2) \int_{z_o}^{z_i} \{ (U'/2U) r'r + (U''/4U)r^2 \} U^{-1/2} \mathbf{dz} \dots\dots\dots (2.15)$$

where  $\mathbf{z_i}$  is the axial coordinate of the image space,  $\mathbf{z_o}$  is the axial coordinate of the object coordinate,  $r$  and  $r'$  are the solution of the paraxial ray equation and  $U$  is the electrostatic potential distribution along the optical axis .

The chromatic aberration results from the dependence of the optical parameters of the charged – particle lenses on the energy of the beam being focused. If the angle of convergence of the rays is  $\alpha$ , then the radius of least confusion  $d_c$  (i.e. diameter of chromatic aberration disc), is given by [Ahmad 1993]:

$$d_c = \alpha [\Delta f / \Delta p] \Delta p = \alpha f [p/f] [\Delta f / \Delta p] \Delta p/p \dots\dots\dots (2.16)$$

where  $p$  and  $\Delta p$  are the momentum and the change in momentum of the incident parallel beam of free charged particles respectively, and  $(f)$  is the focal length of a perfect lens .

But the coefficient of chromatic aberration  $C_c$  is given by [Lawson 1977] ;

$$C_c/f = (1/2) (p/f) (\Delta f / \Delta p) \dots\dots\dots (2.17)$$

Then the disc can be written as:

$$d_c = 2 C_c \alpha \Delta p/p \dots\dots\dots (2.18)$$

Since the present work deals with the non-relativistic case; the disc may get the new definition [Lawson 1977]:

$$d_c = C_c \alpha (\Delta U / U) \dots\dots\dots (2.19)$$

where  $U$  is the potential energy through which the charged – particles have been accelerated to reach the momentum  $p$ , and  $\Delta U$  refers to half the total energy spread in the beam. It can be seen from the above equation that  $d_c$  is proportional to the initial slope of the outermost ray and the relative energy spread  $(\Delta U / U)$ . From equations (2.14) and (2.19) one notes that at low values of the acceptance angle the performance of the optical system is limited by its chromatic aberration, where at larger apertures spherical aberration becomes

the dominant limiting factor. The total diameter of the aberration disc  $d_t$  is given by [Szilagyi and Szep 1988] :

$$d_t = \sqrt{d_s^2 + d_c^2} \dots\dots\dots (2.20)$$

## 2.6.2 Aberration of System of Lenses

According to the case of axial aberration (i.e. aberration due to paraxial approximation), the expression for any particular aberration coefficient of the lens system contains the corresponding coefficients of the individual lenses, and they do not depend on the off-axis aberration coefficients of the individual lenses [Szilagyi 1988].

The spherical aberration coefficients of the system referred to the object can be expressed as [Szilagyi 1988]:

$$\begin{aligned} C_{sso} &= C'_{so} + \{ [U(z_o) - U_o] / [U(z_m) - U_o] \}^{3/2} C''_{so} / M'^4 \\ &= C'_{so} + \{ [U(z_o) - U_o] / [U(z_i) - U_o] \}^{3/2} C''_{si} / M^4 \dots\dots\dots (2.21) \end{aligned}$$

where  $z_m$  is the coordinate of the intermediate image,  $M'$  is the magnification of the first lens in the system of two lenses,  $M$  is the total magnification.

It is clear that the first expression contains only coefficients referred to the object, while the overall magnification  $M$  appears in the second expression. In the case of two lenses with  $M'$  is infinitely large and  $M''$  (magnification of the second lens) is zero, only  $C'_{so}$  and  $C''_{si}$  are finite. Therefore, the second part of the above equation must be used, and the magnification of the system is given by [Szilagyi 1985-1988]:



$$M = - f''_1 / f'_2 = - (n_1 f''_2) / (n_2 f'_1) = - \sqrt{U_1 / U_2} \cdot (f''_2 / f'_1) \dots (2.22)$$

where  $f'_1$  and  $f''_1$  are the object side and image side focal lengths of the first lens in the system, and  $f'_2$  and  $f''_2$  are the object and image side focal lengths of the second lens in the system respectively. Hence,  $n_1$  and  $n_2$  are the refractive index of the lens. The spherical aberration for the system is thus given by the following equation:

$$C_{sso} = C'_{so} \infty - (f'_1 / f''_2) C''_{si (M=0)} / M \dots (2.23)$$

The spherical aberration coefficient will be smaller incase of infinite magnification .It is easy to generalize the above result for a chain of lenses by simply considering combinations of lens pairs as single lenses and using the procedure sequentially .By the same method , similar expression with some differences exist in determining the chromatic aberration coefficient . The chromatic aberration coefficients of the system referred to the object can be expressed by the following equation [Szilagyi 1988].

$$\begin{aligned} C_{sco} &= C'_{co} + \{ [U(z_o) - U_o] / [U(z_m) - U_o] \}^{3/2} C''_{co} / M'^4 \\ &= C'_{co} + \{ [U(z_o) - U_o] / [U(z_m) - U_o] \}^{3/2} C''_{ci} / M^4 \dots (2.24) \end{aligned}$$

where the coefficients  $C'_{co}$  and  $C''_{co}$  are functions of the magnifications  $M'$  and  $M''$ , respectively. The magnification  $M''$  on the other hand, depends on the separation of the two lenses from each other. Therefore, the chromatic aberration coefficient of the compound lens is a complicated function of the system parameters. For a system the chromatic aberration coefficients are given as follows:

$$C_{sco} = C'_{co} \infty - M (f'_1 / f''_2)^3 C''_{ci (M=0)} \dots (2.25)$$

The spherical aberration disc diameter in the image plane can be written in the following form:

$$d_{si} = M'' d_{si1} + d_{si2} \dots\dots\dots (2.26)$$

where,  $d_{si1} = M' C' \tan^3 (\alpha_1)$  is the spherical aberration disc diameter of the first lens and  $d_{si2} = M'' C' \tan^3 (\alpha_2)$  is the spherical aberration disc diameter of the second lens  $\alpha_1$  and  $\alpha_2$  are the acceptance half angle of the charged particles for the first and second lenses respectively .

The chromatic aberration disc diameter is given by:

$$d_{ci} = M'' d_{ci1} + d_{ci2} \dots\dots\dots (2.27)$$

where,  $d_{ci1} = M' C' \tan (\alpha_1) \Delta U_o / \{2[U(z_o)-U_o]\}$  is the chromatic aberration disc diameter of the first lens and  $d_{ci2} = M'' C' \tan (\alpha_2) \Delta U_o / \{2[U(z_m)-U_o]\}$  is the chromatic aberration disc diameter of the second lens.

The energy spread  $\Delta U_o$  expressed in electron volts, thus the above relationships indicate that the diameter of spherical (or chromatic) aberration disc of the system is the sum of the diameter of the spherical (or chromatic) aberration disc of the first lens magnified by the second lens and the diameter of the spherical (or chromatic) aberration disc of the second lens. The diameters of the spherical and chromatic aberration discs determine the diameter of the total aberration disc [Szilagyi 1988]:

$$d_{ti} = \sqrt{d_{si}^2 + d_{ci}^2} \dots\dots\dots (2.28)$$

## 2.7 Figures of Merit

There are many design problems (for different applications) in which the conditions (geometrical and electrical or magnetic parameters) can be varied to optimize the quality of this design (the final image). The number of these geometrical and electrical parameters may be quite high, where the requirement of different applications may be totally different [Ahmad 1993].

Therefore, to select the best lens, a suitable dimensionless figure of merit may be constructed for the problem and then to choose the lens with the smallest acceptable value of this figure of merit. One common requirement of all applications is to reduce the aberration to as small as possible. It seems then that the absolute figure of merit of an optical system is the size of its aberration disc. By using the known scaling laws (scaling down) one can make the aberration disc as small as possible. A reasonable suggestion has been made by relating the radius of aberration disc to another quantity that has the same dimension (dimension of length). Other factors can be used when selecting the figures of merit, for comparison of different lenses one may choose quantities like, the length of the lens field (field from  $z_o$  to  $z_i$ ), the object or the image –side focal length ( $f_o$  to  $f_i$  respectively), the probe radius etc. Important factors are the dependence of the size of the aberration disc on the magnification. Therefore, according to [Szilagyi 1988] the aberration coefficients of different lenses with equal refractive powers must be compared for the case of infinite magnification at equal maximum fields or potential ratios, or one can use for each problem its own individual: the figures of merit [Harting and Read 1976]. In this investigation the figures of merit taken into consideration are the relative spherical aberration coefficient  $C_s/f$  and the relative chromatic aberration coefficient  $C_c/f$  which give a dimensionless quantity.

## 2.8 Image Analysis by spot diagrams

A spot diagram is a collection of ray data resulting from tracing a large number of rays from a single object point through several aperture coordinates. The aperture coordinates are normally set up to form a square grid in the entrance pupil. Spot diagrams can be processed in a variety of ways to provide either geometrical or diffraction analyses of optical images. Although spot diagrams involve ray tracing, many aspects of spot diagram analysis involve considerations of statistics or numerical analysis that have little to do with the techniques used to trace rays. The image of a point by a lens that is not diffraction limited is often described by its geometrical spot size, defined to be the root mean square (i.e. rms) spot radius (not diameter). The rms spot size is defined as the square root of the variance of the distribution. This quantity does not indicate the fractional energy in the spot, it has an intuitive appeal and its square is widely used in optimization merit functions [**Forbes 1988**]. Calculating the spot size is thus a matter of considerable importance in present optical design software.

Rays should be spaced so that each ray represents an equal element of solid angle. Various patterns have been used, including circular patterns and square grids, neither of which is particularly accurate. In addition, the reference point on the image surface must be taken as the centroid of the distribution, not the intersection of the chief ray, so that asymmetries in the image are properly accounted for. The spot size to be defined by an integral equation that represents the limit that would be obtained if the number of rays traced approached infinity. Then, if the object point is located at a distance  $h$  from the axis, and the pupil intersection point is described using polar coordinates, one has the following expression for the mean square spot size as follows [**Sinclair & McLaughlin 1989**]:

$$\sigma^2(h) = \int_0^1 \int_0^{2\pi} [y(r, \theta, h) - \bar{y}(h)]^2 r d\theta dr \dots\dots\dots (2.29)$$

where  $\sigma^2(h)$  is the rms (i.e. root mean square) spot size and  $h$  is the distance from the axis of an object point. Figure (2.9) is shown the essential quantities included in spot size determination [Sinclair & McLaughlin 1989].

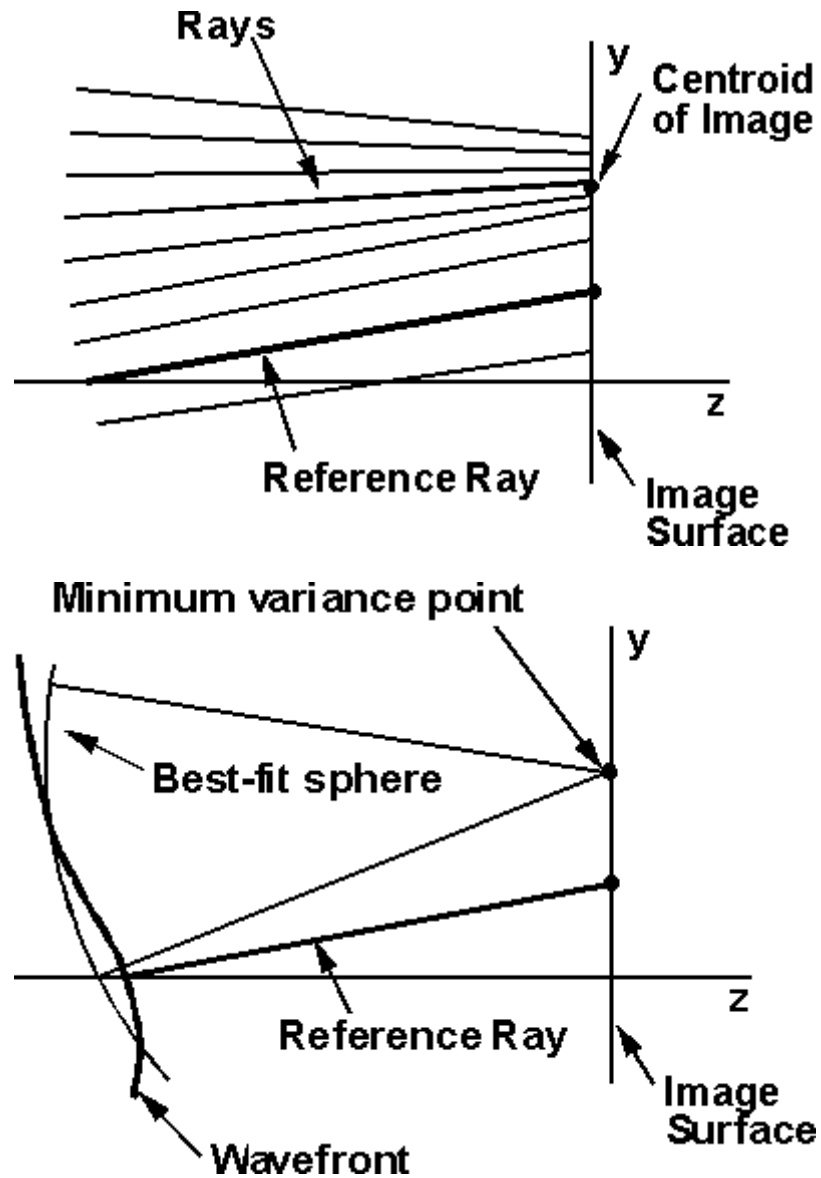


**Figure 2.9** shows the principal spot diagram parameters

The grid used to set up the aperture coordinates of rays in the spot diagram is determined by the value of the number of aperture divisions across the diameter of the entrance pupil. For systems that have a large numerical aperture on the object side, the grid cells are equally spaced in numerical aperture, not in entrance pupil coordinates. Figure (2.10) shows the grid pattern used in the present work for 10 aperture divisions. The number of aperture divisions is not restricted to integer values, but is a continuous parameter that determines the size of grid cells in the spot diagram [**Hawkes and Kasper 1989**].

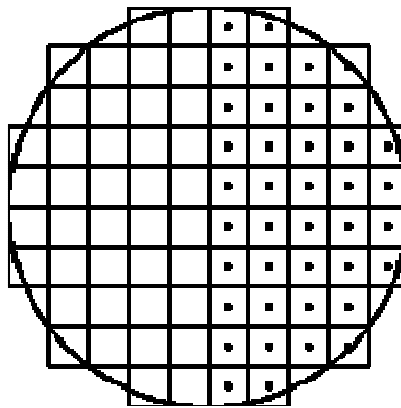


**Figure 2.10** represents the grid pattern

# *Chapter Three*

## **Computations and Analysis**

The following conditions have been used in the present work for both electric and magnetic lenses as follows:

- Non – relativistic velocities (low energy beams) are assumed for charged particles, and just paraxial trajectories are taken into account.
- The space charge effects are assumed negligible, that is satisfying exactly Laplace's equation.
- The aberrations due to the source of charged particles have been neglected.
- Machining inaccuracies and asymmetries in lens shape are neglected.
- The initial velocities of charged particles have been neglected.

And for magnetic lenses considerations only the following conditions:

- The influence of any currents is negligible.
- The relative permeability of the magnetic material can be considered infinite.

### **3.1 Electrostatic and Magnetic spline lenses**

The cubic spline model is the smoothest interpolating function, so that it is quite obvious to use it as a simple model for the representation of complicated axial potential distributions. The cubic spline is not the only possibility; fifth – or higher –order splines can also be used. The distribution along the length  $L$  is divided into  $N$  intervals by the following cubic polynomial:

$$\left. \begin{aligned} U_k(z) &= \mathbf{a}_k + \mathbf{b}_k(z-z_{k-1}) + \mathbf{c}_k(z-z_{k-1})^2 + \mathbf{d}_k(z-z_{k-1})^3 \\ U'_k(z) &= \mathbf{b}_k + 2\mathbf{c}_k(z-z_{k-1}) + 3\mathbf{d}_k(z-z_{k-1})^2 \\ U''_k(z) &= 2\mathbf{c}_k + 6\mathbf{d}_k(z-z_{k-1}) \end{aligned} \right\} \dots\dots\dots (3.1)$$

where  $U(z)$  represents the approximated potential distribution for either electrostatic or magnetic lens,  $U'_k(z)$  and  $U''_k(z)$  are the first and second derivatives with respect to  $z$  respectively. From the continuity conditions one may write equation (2.7) as follows [Szilagyi 1987, 1988]:

$$\left. \begin{aligned} U_{k+1}(z_k) &= U_k(z_k) \\ U'_{k+1}(z_k) &= U'_k(z_k) \\ U''_{k+1}(z_k) &= U''_k(z_k) \end{aligned} \right\} \dots\dots\dots (3.2)$$

Thus, the coefficients of the spline function can be interrelated by the following relationships:

$$\left. \begin{aligned} \mathbf{a}_{k+1} &= \mathbf{a}_k + \mathbf{b}_k h + \mathbf{c}_k h^2 + \mathbf{d}_k h^3 \\ \mathbf{b}_{k+1} &= \mathbf{b}_k + 2\mathbf{c}_k h + 3\mathbf{d}_k h^2 \\ \mathbf{c}_{k+1} &= 2\mathbf{c}_k + 6\mathbf{d}_k h \end{aligned} \right\} \dots\dots\dots (3.3)$$

where  $h = \mathbf{z}_k - \mathbf{z}_{k-1}$  is the length of each interval. It is important to remember that the discontinuity of the third derivative and the undefined higher derivatives do not cause any problem since one can calculate all the optical properties including the aberrations by using the first two derivatives only.



### 3.2 Optimization by dynamic programming procedure (DPP) with the aid of artificial intelligence technique (AIT)

It is aimed at finding the potential distribution that minimizes the aberration integral, at the same time satisfying the differential equation of the paraxial rays, and also the constraints imposed by practical requirements. By consider the rectangular computational grid as shown in the figure (3.1). It defines the domain of existence for the sought distribution function. It is limited by the maximum allowable value of the field strength or its derivatives. The axial extension is defined by the given length  $L$ , which is divided into  $N$  equal regions each of which is denoted by  $k$  and a length interval  $h = z_k - z_{k-1} = \text{constant}$ , so that [Ahmad et al 2002];

$$\Delta z = z_k - z_{k-1} = L/N = \text{const} \dots\dots\dots (3.4)$$

where  $k = 1, 2, 3 \dots N$  is the ordinal number of the given region.

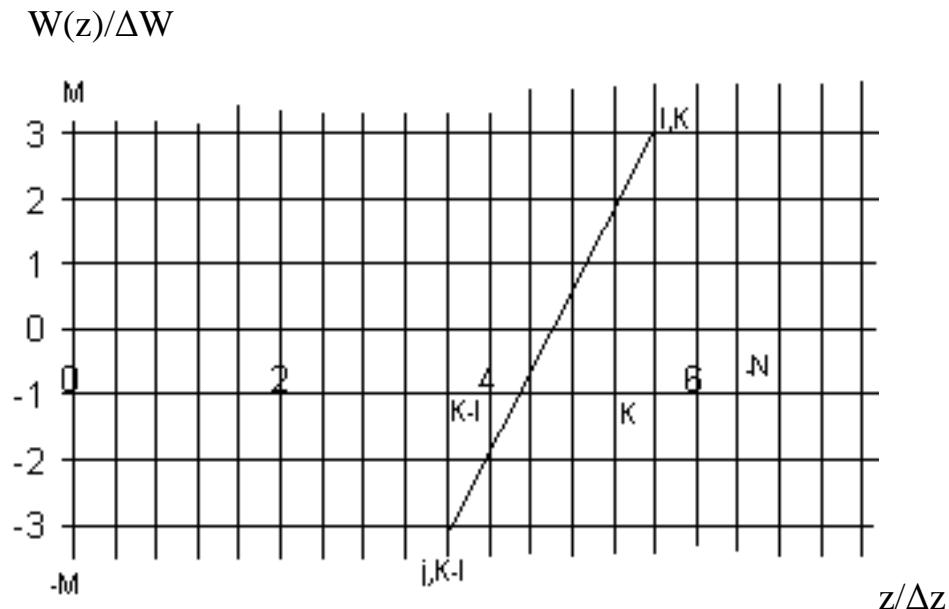


**Figure 3.1** computational grids for the dynamic programming procedure

This will lead to approximate the unknown distribution  $U(z)$  or one of its derivatives by a straight line in each region. If  $W(z)$  denotes the piecewise linear function, then for magnetic lenses one can assume that  $W(z) = B(z)$ , which is equivalent to the piecewise linear model, while electrostatic lenses can take  $W(z) = E_z(z)$ . But the effective approach may to use for the piecewise linear function  $W(z)$  the highest derivative that appears in the aberration integral. Also, assume further that  $W(z)$  can take only  $2|\mathbf{M}|+1$  different values at the boundaries of the regions, where  $\mathbf{M}$  represents the ordinate dimension of the computational grid. Thus this problem has been reduced to that to finding  $N \times (2|\mathbf{M}|+1)$  intersection points of the computational grid that will provide the linear segments for the optimized function  $U(z)$ . The present work seeks for a systematic investigation of lenses by varying the basic parameters of their potential distribution in the process of construction of the spline model. This procedure can be done according to either of the following two basic strategies [Szilagyi 1988]:

- 1) Considering a class of splines with a fixed number of intervals.
- 2) Approximating a certain class of potential distributions by different splines.

Consequently, the paraxial ray equation can be solved in each interval numerically. The continuity of the solution requires that the initial values for the particle trajectory and its first derivative for each region must be equal to their corresponding final values in the preceding region. The contribution of each region to the aberration integral can be calculated numerically using Simpson's rule. The ordinate dimension of the nodal points at the beginning and at the end of each interval is represented by  $j$  and  $i$  respectively. Then the initial and terminal values of the second derivative function in the  $k$ -th region are given by:

$$\left. \begin{array}{l} U''(z_{k-1}) = j \Delta U'' \\ U''(z_k) = i \Delta U'' \end{array} \right\} \dots\dots\dots (3.5)$$

where  $\Delta U''$  is the minimum amount of change of the second derivative, given by:

$$\Delta U'' = \delta / M, \quad \delta: \text{is a priori given number.} \quad \dots\dots\dots (3.6)$$

To ensure the continuity of the spline as well as of its first and second derivatives at each of the N-1 nodes, equation (3.3) must be satisfied for the coefficients where **h** is the equivalent as  $\Delta z$  in equation (3.4). Four coefficients of the spline function have to be calculated for each interval. The coefficients **c<sub>k</sub>** and **d<sub>k</sub>** are expressed in terms of i and j as follows [Ahmad et al 2002, Harriott2001]:

$$c_k = j \Delta U'' / 2, \quad d_k = (i-j) \Delta U'' / 6 \quad \dots\dots\dots (3.7)$$

While **a<sub>k</sub>** is the magnitude of the potential at the starting point, **b<sub>k</sub>** represents the magnitude of the first derivative of the potential function at the starting point of the k-th interval. For the first interval (i.e. k=1) the four coefficients were calculated from these definitions, and they were stored in one database to be reevaluated as a part of an expert system. While for the successive intervals **a**, **b** and **c** coefficients were calculated from the continuity conditions of the spline function and its first and second derivatives. The coefficient **d** is determined by varying the values of i and j. By using artificial intelligence technique, an expert system has been established with database list of the

entered coefficients to minimize the optical properties according to figures of merit.

Indeed the present investigation was trying to reconstruct exactly the same function that is the subject of our investigation, the spline function. . For  $N$  intervals there are  $4N$  coefficients , where  $3(N-1)$  of them are calculated from the continuity conditions and two of them kept fixed to determine the initial magnitude of the potential and to ensure the zero slope condition at the beginning of the first interval. Then the remaining  $N+1$  free coefficient are varied to search for sub-intervals of sets of coefficients that would be stored in unique database of the expert system, which it provides the best and optimum optical properties.

### 3.3 The Synthesis Procedure

Optimization by synthesis has always been one of the most ambitious goals of charged-particle optics. This approach is based on the fact that in any imaging field, it's first and third – order properties are totally determined by some axial functions [Ahmad 1993].

The axial electrostatic and magnetic scalar potential distribution  $U(z)$  is represented by a cubic spline function. That is, the solution will be in the form of a spline lens. The axial length  $L$  of the distribution is divided into  $N$  equal regions, each denoted by  $k$ , where  $k = 1, 2, 3 \dots, N$ . For each  $k$ -th interval, the potential distribution, and its first and second derivatives are expressed in the form of a cubic polynomial (equation 3.1). The constraints are formulated according to the pre-assigned requirements of the problem. Then the objective function that is to be minimized is selected. This function will be the coefficient of aberration, which is the most important rule into the present work rule-based system called a knowledge base of the expert system.

In the present procedure of our work, a database was established to provide storage and retrieval of calculated optical properties (i.e. spherical and chromatic aberration coefficients) and optimized potential distributions (i.e. electrostatic and magnetic) according to dynamic programming procedure. An expert system has been built according to artificial intelligence technique, which is called rule-based system [**Friedman 2003**]. It maintains a collection of knowledge nuggets called facts. This collection is known as the knowledge base, which is our relational database.

By using a Jess 6.1 (i.e. Java Expert System Shell-version 6.1) programming language and a class modules in VB 6 (i.e. visual basic studio - version 6) the present work expert system has been created and setting up the user interface. Jess is a tool for building a type of intelligent software called expert systems. An expert system is a set of rules that can be repeatedly applied to a collection of facts. It is spherically intended to model human expertise or knowledge [**Menken 2002**].

A specific set of optical properties (i.e. spherical and chromatic aberration coefficients) have been selected according to figures of merit and the spline functions (i.e. electrostatic and magnetic potential distributions) with their coefficient sets equation ((3.1) and (3.3)) were stored into our knowledge base. Our rule based expert system written in Jess is a data-driven program where the facts are the data stored in our knowledge base that stimulate execution via the inference engine. This engine decides which rules should be executed and when [**Menken 2002**]. Therefore, the present expert system automatically performs the field calculation and ray tracing, depending to the stored data base (i.e. jess knowledge base) and the following two factors:

1. The facts of the function to be analyzed (i.e. electrostatic and magnetic potential distribution).

2. The rule of dynamic programming procedure solutions, which obey the given constraints.

Thus, an important rule has been used in our procedure (i.e. jess rule based system) is the typical dynamic programming recursive formulation as [Kuester and Mize 1973]:

$$F_n(n, s, x) = g[R(n, s, x), F_{n-1}^*(s')] \dots\dots\dots (3.8)$$

where  $n$  is an integer denoting the stage of the problem,  $s$  is an integer denoting the state of the system at  $n$ ,  $s'$  is an integer denoting the state of the system at stage  $n-1$  resulting from the decision  $x$ ,  $x$  is the decision being evaluated at stage  $n$ ,  $R(n,s,x)$  is the immediate return associated with making decision  $x$  at stage  $n$  when the state of the system is  $s$ ,  $F_{n-1}^*(s')$  is the return associated with an optimal sequence of the decision at stage  $n-1$  when the state is  $s'$  and  $g$  is the minimal function.

In the present investigation, the function of  $F_{n-1}^*(s')$  will be added to  $R(n,s,x)$  but on the first stage (i.e.  $n = 1$ ) this term of the function will be omitted. At each stage, the results of the recursive formulation are calculated for all feasible values of  $x$ , and the optimal decisions are returned for subsequent use. Dynamic programming starts with a small portion of the problem and finds the optimal solution for this part. It then gradually enlarges the problem, finding the current optimal solutions from the preceding one, until the original problem is solved in its entirety. Considering the recursive relation expressed in equation (3.8), the objective function may take the following form [Ahmad et al 2002]:

$$G_{ik} = \min | F_{ijk} + G_{j(k-1)} | \dots\dots\dots (3.9)$$

where  $F_{ijk}$  is the contribution of the  $k$ -th region to the aberration integral,  $G_{ik}$  is the coefficient of aberration, and  $G_{j(k-1)}$  is the optimized intermediate value of the aberration integral.

The coefficients of the spline function are varied, and then the potential and its first and second derivatives are calculated. The paraxial ray equation is solved numerically using the fourth order **Runge – Kutta method** under pre-assigned initial conditions of  $r$  and  $r'$ , where  $r$  is the radial component of the ion trajectory and  $r'$  is its slope when the beam enters the lens field. After solving the paraxial ray equation, the constraints should be fulfilled, in order to determine the required optical properties (e.g. focal length, maximum electrostatic and magnetic potential and aberration coefficients). The aberration integrals can be solved numerically by using **Simpson rule** [Chapra and Canale 1998].

Among the different values of the coefficients, a minimum is selected according to the rules equation ((3.8) and (3.9)) of the knowledge base of our expert system. The database stored in the expert system searches over each  $k$ -th interval for a set of spline coefficients equation (3.3) that would lead to the axial distribution  $U(z)$  for both electrostatic and magnetic potentials, which gives a minimum aberration under the given constraints.

Our expert system in the present investigation which has responded to the SELECT statement is being used as one of the SQL (i.e. structure query language) statements in our programming, which is embedded in the **ANALYZER** program. Also, a search engine was created according to a given constraints, in order to get an optimum preference as the given figure of merit.

### 3.4 Constraints and Optimization

It is important that the magnitude of the potential, its first and second derivatives and the particles trajectory with its gradients along the optical axis, should be carefully taken into account in determining the optimum potential distribution. The present optimization procedure is carried out under these constraints, and results are determined after fulfilling the given conditions, that will limit the potential distribution and its derivatives as follows:

$$U_1 < U(z) < U_2 \dots\dots\dots (3.10)$$

$$|U'(z)| < U_1' \dots\dots\dots (3.11)$$

$$|U'(z)| < U_1'' \dots\dots\dots (3.12)$$

where  $U_1$  ,  $U_2$  ,  $U_1'$  and  $U_1''$  are selected values which stored in the database (i.e. jess - rule knowledge base system) as facts of our expert system to be evaluated. The potential distribution should be such that the beam trajectory would intersect the optical axis outside the effective lens field. Hence, this requirement can be formulated as follows:

$$r(z) > 0 \text{ where } 0 < z < L, \text{ where } \mathbf{L: the axial length} \dots\dots (3.13)$$

The problem of finding the constraints which can be easily fulfilled in the presence of other requirements such as maximum value of the potential function will be encountered. This problem is originated from the optimization procedure itself since the distribution is always brought back to the trivial case when one tries to give it a particular shape [**Ahmad et al 2002, Harriott 2001 and Amos et al 1988**].



### 3.5 Computational Grid

The rectangular grid is introduced to define the domain of existence of the solution for the distribution with the aid of dynamic programming and artificial intelligence techniques. Then two, out of four of the spline coefficients namely  $\mathbf{c}_k$  and  $\mathbf{d}_k$  are related with the variation of the ordinate position of the nodal points of the grid along the distribution at each interval. The variation of  $\mathbf{c}_k$  coefficients at the first interval (i.e.  $k=1$ ) and all the  $\mathbf{d}_k$  coefficients along the distribution are governed by the variations of  $i$  and  $j$  as in equation (3.7). These coefficients are restricted by the domain and the rate of change at which the magnitude of the second derivative function varies. Instead of testing an infinite number of coefficients for the spline function that may fulfill the given requirements,  $2|M|+1$  set of them for each nodal point at each interval is examined and the  $i_{th}$  fulfills the requirements were selected and stored in the database (i.e. jess knowledge base) of our expert system. The result is  $2|M|+1$  sets of coefficients for each of the  $N$  intervals.

Our procedure in the present work starts at  $k=1$  with the initial condition  $G_{j0} = 0$ , which expresses the simple fact that the contribution of the region beyond the object to the aberration integral is zero. Therefore, the search in the first region is reduced to comparing different  $F_{ij1}$  values (equation 3.9). The full procedure starts with determining the solution of the paraxial ray equation and the contribution to the aberration integral for each stored database pair  $(i, j)$  values. For each  $i$  the corresponding  $j$  value that minimizes  $F_{ij1}$  is selected and stored as unique database in the jess-knowledge base with the terminal values of the solution of the paraxial ray equation. After having done this for each of the  $2|M|+1$  possible values of  $i$  for the first interval, the procedure is repeated for the second interval keeping in knowledge base (i.e. rule-based expert system) that the recursion relation of

the minimized objective function equation (3.9) is not trivial anymore and what was  $i$  for the first interval becomes  $j$  for the second interval.

This procedure is performed from one interval to another recursively toward the image space until reaching the end of the computational grid ( $k=N$ ). It will give rise to a maximum of  $2|M|+1$  optimum distribution, and the one that fulfills the requirements is selected by using jess (i.e. java expert system shell) language compromised with SQL (i.e. structure query language) statements of our expert system.

Figures (3.2) and (3.3) are shown the computational grid for the dynamic programming procedure with the aid of artificial intelligence technique. They defined the domain of existence of the solution for the sought distribution function  $W(z)$  (i.e. the spline function equation (3.1) for both electrostatic and magnetic potential distributions). The abscissa of those figures represents the axial extension of the lens along which it's potential and field distribution exists. The ordinate shows the position of the nodal points where the axes of the grid intersect. These points control and fix the value of the spline function coefficients and consequently the potential and electric or magnetic field values, to be consistent with the given constraints.

The dynamic programming procedure examines each nodal point at the end of each sub-interval with all other points at the beginning of the same interval. By using artificial intelligence technique, the automatic search for the set of the spline coefficients that lead finally to the minimum value of the aberration integral. This procedure may inter-relate the two nodal points in particular that fulfill the aim of the search and discard the others. It may also occur that some of optimized solutions cut out due to the fact that last nodal point in the particular solution in the  $k_{th}$  interval either doesn't permit an

optimum solution in the next interval (i.e.  $(k+1)_{th}$  interval) or it cannot satisfy the given constraints. The optimum solution that was extracted from among similar ones is the solution that satisfies the design requirements (i.e. the jess rule knowledge base equations (3.8) and (3.9)) and all given constraints. It could choose a particular solution starting from the last nodal point which existed in the solution and tracing it back by using the jess rule knowledge base, until reaching the initial nodal point.

The computational grid has been taken and defined over twenty intervals only for the present work. This is one of the difficulties to incorporate one of synthesis procedure (i.e. dynamic programming procedure in our work) into our expert system. Basically, the knowledge base (i.e. database of our rule-based system) has limited capacity of memory stored in the personal computer hard drive. It may overcome this difficulty by using another type of jess as a programming language for determining the expert system. This may happen in future by take very sophisticated programming language called sweet jess [**Grosf et al 2002**].

Our expert system requirements are depending on three main steps: the speed in the processing unit (i.e. CPU speed 2.5 or more MHz), the capacity of the personal computer random accessing memory (i.e. RAM ~ 512 full caches) and operation system availability (i.e. windows XP (pack 2) or server2003).

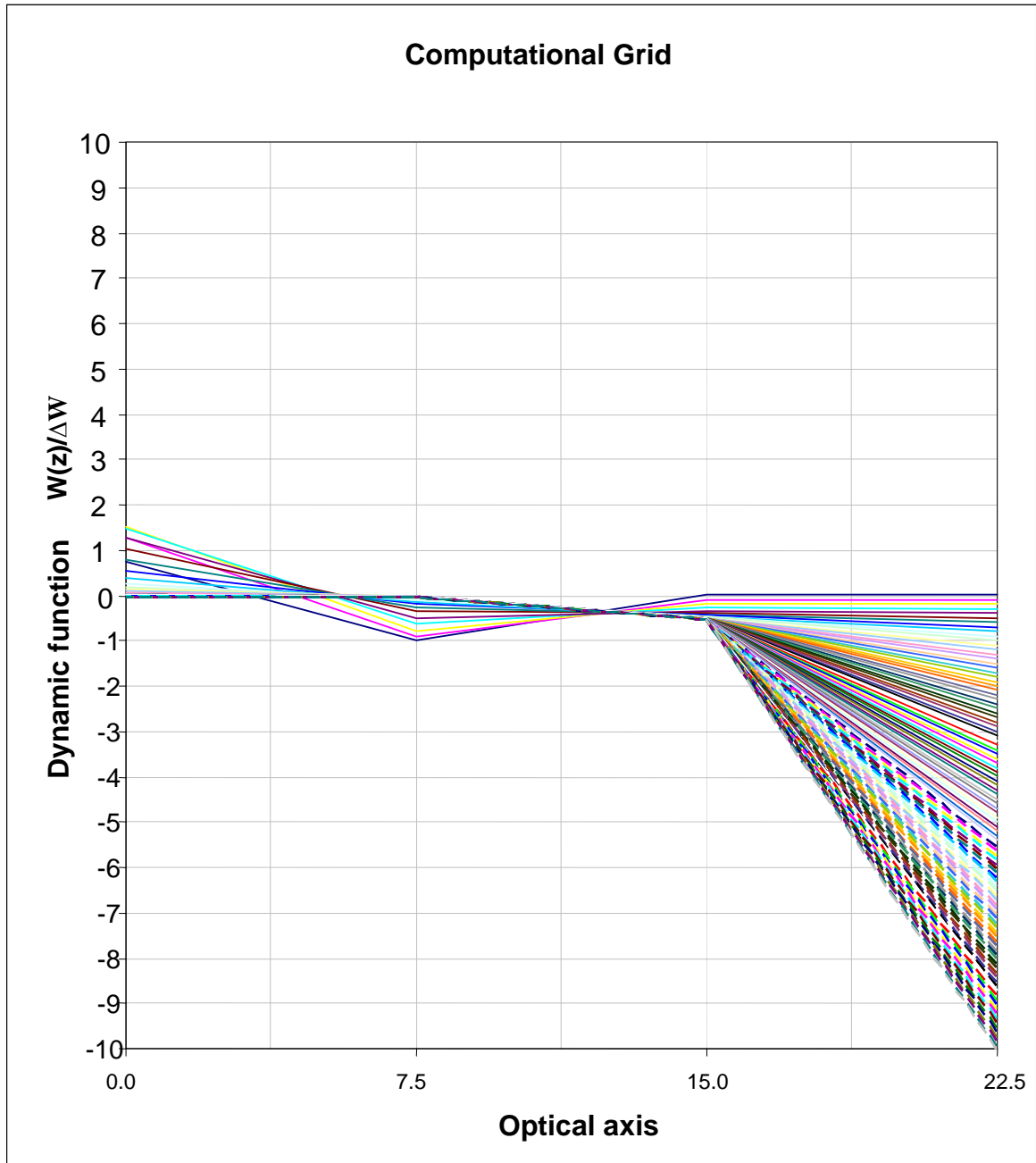


**Figure (3.2)** represents computational grid of the DPP with the aid of AIT for electrostatic lenses defined over twenty sub-intervals.

### Computational grid

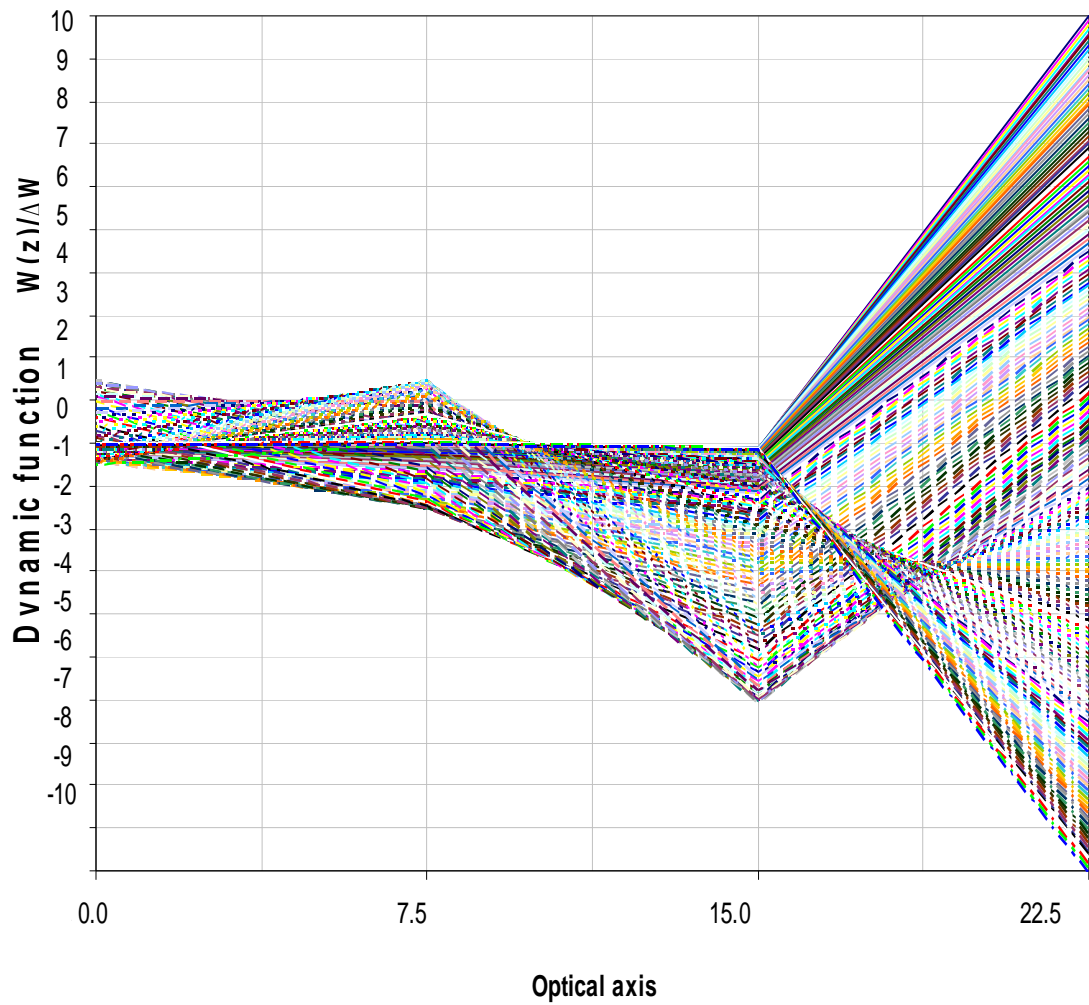


**Figure (3.3)** represents computational grid of the DPP with the aid of AIT for magnetic lenses defined over twenty sub-intervals.

### 3.6 Simulation Software Description

Two software packages have been used to design the focusing lenses that can be used in the ion beam lithography system. One is called CADION package, and the other is a SIMION simulator.

#### 3.6.1 Computer Aided Design for ION system (CADION)

The increasing demand for smaller structures for fundamental physics research as well as for faster and higher density electronic circuits pushed the fabrication technology in recent years to dimensions in the nanometer-scale region. For the fabrication of structures with extremely small details both pattern definition and pattern transfer play a crucial role. The ion-beam lithography system is widely used for the pattern definition [**Romijn and van der Drift 1988**]. As will be shown in the present work, a simulation and optimization procedure have used to design lenses with relatively large overall dimensions of the order of a few millimeters and of a medium resolution of the order of (30 – 100) nm.

The term optimization covers a wide range of methods of finding an optimal solution to a problem through the use of a computer. Optimization usually consists of two components:

1. A program as one package that produces an ultimate output given inputs such as data and parameters.
2. A measure of how good the solution is, that is termed as one of the following: objective function; criteria; goodness of fit.

Therefore, a computer programs have been written and used as a powerful techniques in the present work. These subroutines comprise one full package called (CADION) which is stand for (Computer Aided Design for ION system) .This package has been described as a class module program

written in visual basic-6 studio and designed as one simulator for getting a full simulation of whole processes. This program has been called (CADION Simulator package), which comprises many subroutines as follows:

- a- Accomplished program for the fourth order **Runge –Kutta** method, also this is used for computing trajectories when the initial conditions are given. The full details and outputs are given in a tabulated form (set of data) inside the PC stored as one database.
- b- Accomplished program to analyze all set of stored data, which can be given with many results. This program is called (**CADION ANALYZER**), it analyses all optimized field distributions (i.e. electrostatic and magnetic fields), and it has an ability to select the best formulae fitted to the optimization procedure (i.e. dynamic programming). This analyzer is involving both techniques i.e. artificial intelligence and dynamic programming. Also it is a search engine depending on the SQL database statements (i.e. SELECT statement). The programming language is classified into two categories: [JESS – java expert system shell and visual basic studio 6 as it to make the user interface], this program is a knowledge base with search and SQL server connector for the expert system used. (see section 3.3) and (see the appendix)
- c- Accomplished program for computing spherical and chromatic aberration coefficients, this is done by using **Simpson’s rule** integration method.
- d- Accomplished program to draw (2 and 3 Dimensions) all kind of inputs as optimized field distributions (both electrostatic and magnetic fields).
- e- Accomplished program to convert and read all outputs into another application, Visual Basic Application programs as an Excel sheets were used in this investigation [**Chapra and Canale 1998**]. This program has a search engine to facilitate work with multi formulae that could be stored in the **Analyzer** database.

f- Accomplished program to calculate and plot all outputs into another GUIs, aberration spot size diagrams were plotted and analyzed in this investigation.

The inputs of the programs processed and analyzed the values of the optimized potential distribution  $U(z)$  for both (the field  $E(z)$  and  $B(z)$  distributions). Otherwise, the outputs obtained the axial potential distributions and their first and second derivatives respectively.

Consequently, the above cases are clearly studied within more accurate investigations. These multi times iterations and testing examinations are composed in the present work, as well as the comparisons have been imposed in all results and outputs. This work may lead to get new estimations and predictions in the charged particle optics; also it may give a raise to consider most of the results as prospective aspect for entering the non classical technology – the nano technology.

The conditions associated with the required system are given at two different values of  $z$  ( i.e. boundary conditions  $z_0$  and  $z_i$ ) .Since the system is linear , the dynamic programming accompanied with artificial intelligence technique methods are the better choice to be taken .These methods are adopted in this work when the values of the axial potential are pre-specified at  $z_0$  and  $z_i$  .It is seem worthwhile to state that by the above procedures , one can determine the axial potential distributions required to produce a suitable trajectories. The **Runge-Kutta (RK)** method of the fourth order is used to solve the system equations which can be given the trajectories under the given constraints.



Once the tests have been completed and overwhelming the standard field distributions, the **CADION analyzer** has been used to give the best distributions within a specific parameters according to the initial conditions  $\mathbf{z}_0$  to  $\mathbf{z}_i$ ; the range of the optical axis was (-10 to 10) mm by an increment of (0.1) mm per each step.

Therefore, according to the aim of this work the investigations have been classified into two categories:-

- ✚ Electrostatic field distributions (the designing of electrostatic lenses )
- ✚ Magnetic field distributions ( the designing of a magnetic lens )

The spherical and chromatic aberration coefficients have been calculated within the CADION simulations, which gives the main indications of the best electrode design of each model .Four different cases in electrostatic lenses and two cases in magnetic lenses have been investigated in this work. Many factors and variables have to be calculated to make sure any of results among the others were corrected. Also, the dynamic program is used for those factors in optimizing process supported by artificial intelligence technique. So that, considerable amount of errors have obtained were neglected in the accumulation of data. Obviously, most of the formulae have taken the optimized results from the CADION simulator subroutines.

### 3.6.2 ION and electron optics SIMulation package (SIMION)

Instead of using Munro's programs [Munro 1975] for checking up the present work results and analyzed them into more accurate values, the well known and more updating simulator SIMION 7.0 package has been used, by which is the latest version for getting precise values and excellent optimized formulae. Present work results were imported into this simulator as a stored database; full computerized manipulation has been applied to get same precise results as in CADION package simulations, as well as plotting and configuring electrodes / pole - pieces in three dimensions graphs.

SIMION 3D version 7.0 is a Windows PC based ion optics simulation program designed to study and analyze ion optics in both two and three dimensional modes or views. Electrostatic and magnetic potential arrays can be studied with this software to determine their effect on ion trajectories. It incorporates an ion optics workbench strategy that allows you to size, orient , and position .The original version of SIMION was an electrostatic lens analysis and design program developed by **McGilvery** at Latrobe University Bundoora Victoria, Australia, 1977.

SIMION for the PC was developed at the Idaho National Engineering Laboratory.SIMION utilizes potential arrays to define electrostatic and magnetic fields. These arrays can be either electrostatic or magnetic. Also it is an array of points organized so that the points form equally-spaced square (2D-two dimensions) or cubic (3D-three dimensions) grids. Equally-spaced means that all points are equal distances from their nearest neighbor points. To summarize the present work plan as a brief flow chart, describing the optimization procedures with all input and outputs, figure (3.3) shows the flow chart of the optimization steps for the present investigation.

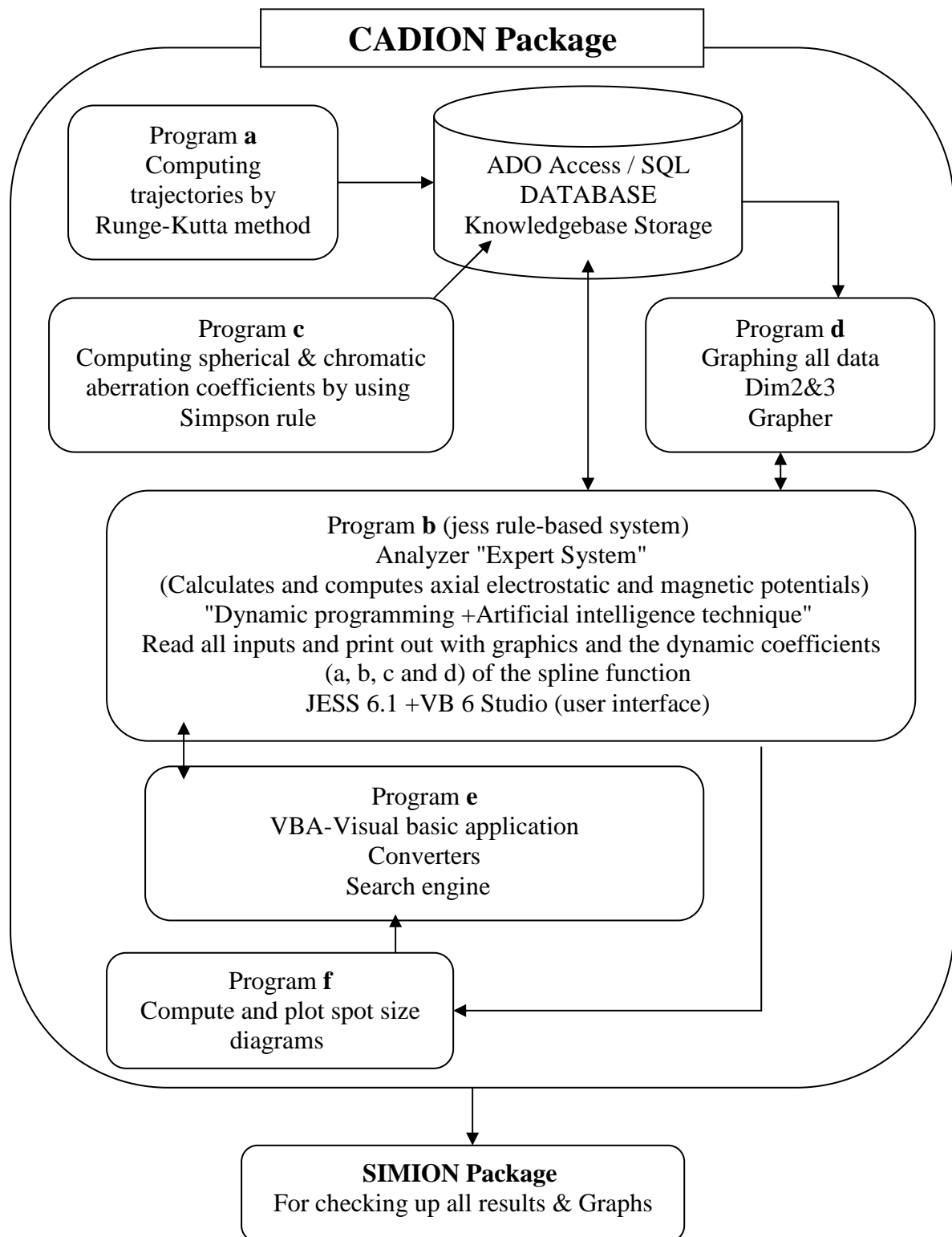


**Figure (3.3)** represents the optimization schematic diagram of the present work software.

### 3.7 Reconstruction of electrodes and pole pieces

Once the axial field distributions of highly favorable optical properties are determined, the next step is to find the electrodes profile that would generate such distributions. An assumption is made that the higher derivatives of the potential function which do not appear anywhere in the expressions of the focal properties should not affect the potential distribution either. The procedure is elementary, it may add an assumption that "the higher derivatives at the boundaries of the regions". Setting the potential equal to  $U$  for an arbitrary point with coordinates  $r$  and  $z$  situated in the  $k$ th region, and then the equation of an equipotential surface is obtained to be as follows [Szilagyi 1984 and 1988]:

$$r^2 = 4(U(z) - U)/U''(z) \dots\dots\dots (3.14)$$

where  $U(z)$  is the cubic function. Both  $U(z)$  and second derivative  $U''(z)$  have different expressions for each region but they are both continuous functions for the entire length of the optical system. By using this simple formula given in equation (3.14), one would be able to reconstruct the equipotential surfaces and thus the electrodes and/or pole pieces that will provide the same functions  $U(z)$ ,  $U'(z)$  and  $U''(z)$ , and thus the same first order properties and third order aberrations as the original theoretical distribution obtained from the optimization technique.

The electrodes (pole pieces) constructions were built from the potential distribution by using the approximated series of the potential equation (eq.3.1). The final electrodes shapes have represented equipotential surfaces according to **ad-hoc** assumption. SIMION simulator is used to find such representations of electrodes (pole pieces). The finite size of the physical system is a limitation to the accuracy of reconstruction because the electrodes must be cut somewhere at

a finite distance from the axis to limit the maximum value of ( $r$ ) to a realistic size, usually half of the total length of the focusing element. Thus parts of the electrodes (or pole piece) are omitted.

### 3.8 Spot Diagrams and Spot size

Having computed the aberration coefficients, it is useful to be able to plot the shape of the aberrated beam at various locations in the image plane, in the form of spot diagrams. Those diagrams are very simple to generate, it could take a bundle of rays uniformly distributed in the aperture plane. The spot size depends on the aberration coefficients of the lens which in turn, depend on the magnification, the potential at the target, and the half acceptance angle  $\alpha$  subtended by the cone of particles at the spot. Then probe disc radius  $r_{ii}$  can be added in quadrature as [Szilagyi 1984 and 1988]:

$$r_{ii}^2 = r_{gi}^2 + (r_{si}/4)^2 + (r_{ci})^2 + (r_{ai})^2 \dots\dots\dots (3.15)$$

where the radii of the Gaussian image ( $r_{gi}$ ), ( $r_{si}$  and  $r_{ci}$ ) are the spherical and chromatic aberration discs radii and ( $r_{ai}$ ) is the Airy disk, respectively. The formulae of each component in equation (3.15) are described as follows:

- $r_{gi} = (I/b_i)^{1/2} / (\pi \alpha) \dots\dots\dots (3.15.a)$
- $r_{si} = M C_{so} \tan^3 (\alpha) \dots\dots\dots (3.15.b)$
- $r_{ci} = M C_{co} \tan (\alpha) \Delta U_o / \{2 [U(z_o) - U_o]\} \dots\dots\dots (3.15.c)$
- $r_{ai} = 0.6 \lambda_i / \sin (\alpha) \dots\dots\dots (3.15.d)$

where the  $I$  is the total current of the Gaussian beam and  $b_i$  is the value of the brightness at the image,  $M$  is the magnification and ( $C_{so}$  and  $C_{co}$ ) are the object-side spherical and chromatic aberration coefficients, respectively. Also,  $\Delta U_o$  is

the total energy spread of the beam and  $\lambda_i$  is the wavelength at the image plane and  $\alpha$  is the half acceptance angle of the ion beam.

Since the ion source was not included in the present investigation aims, CADION package software has been neglected  $[r_{gi}]$  and  $[r_{ai}]$ . Therefore, it uses enhanced spot diagrams that contain angles and path lengths in addition to the intersection coordinates of rays with the image surface. This enables the subroutines to carry out focus-shifting operations without tracing additional rays. Spot diagrams in this code are stored in memory (i.e. jess rule-base [the knowledge base] of our expert system), making computations of image evaluations that may use them very fast. The diameter of the beam transmitted through the system in computing a spot diagram is normally determined by the entrance beam radii.

Therefore, the probe radius to determine the spot size (i.e. equation (3.15)) has been rewritten as follows:

$$r_{ii}^2 = (r_{si}/4)^2 + (r_{ci})^2 \dots\dots\dots (3.16)$$

# *Chapter Four*

## **Results and Discussion**

Both electrostatic and magnetic lenses have been investigated in the present work in two, three and multi-lens system. The axial potential (or field) distributions were optimized by using the combined dynamic programming procedure (DPP) and artificial intelligence technique (AIT), figure (4.1) shows a schematic diagram of our investigation.

The paraxial ray equation was solved numerically by using Runge- Kutta method. The aberration integrals (spherical and chromatic) were solved by using the numerical integration method of Simpson's rule. The optical properties (i.e. the aberration coefficients, focal cardinal points) have been investigated under infinite magnification condition. Also, they were normalized in order to be able to make a meaningful comparison among all results. The present analysis and optimization procedures are considered a nano scale features, which is included by the given results accuracy limitations of the written dynamic program package (i.e. CADION package). These limitations are determined by the following characteristics:

- Numbers precision is fifteen digits (i.e. **15** digits).
- Number of iterations allowed are up to (**32767**) times.
- Largest allowed positive number is  $(1.79769*10^{308})$ .
- Smallest allowed negative number is  $(2.22507*10^{-308})$ .
- Largest allowed negative number is  $(-1*10^{-307})$ .
- Smallest allowed positive number is  $(2.29*10^{-308})$ .

# OUR WORK SCHEME

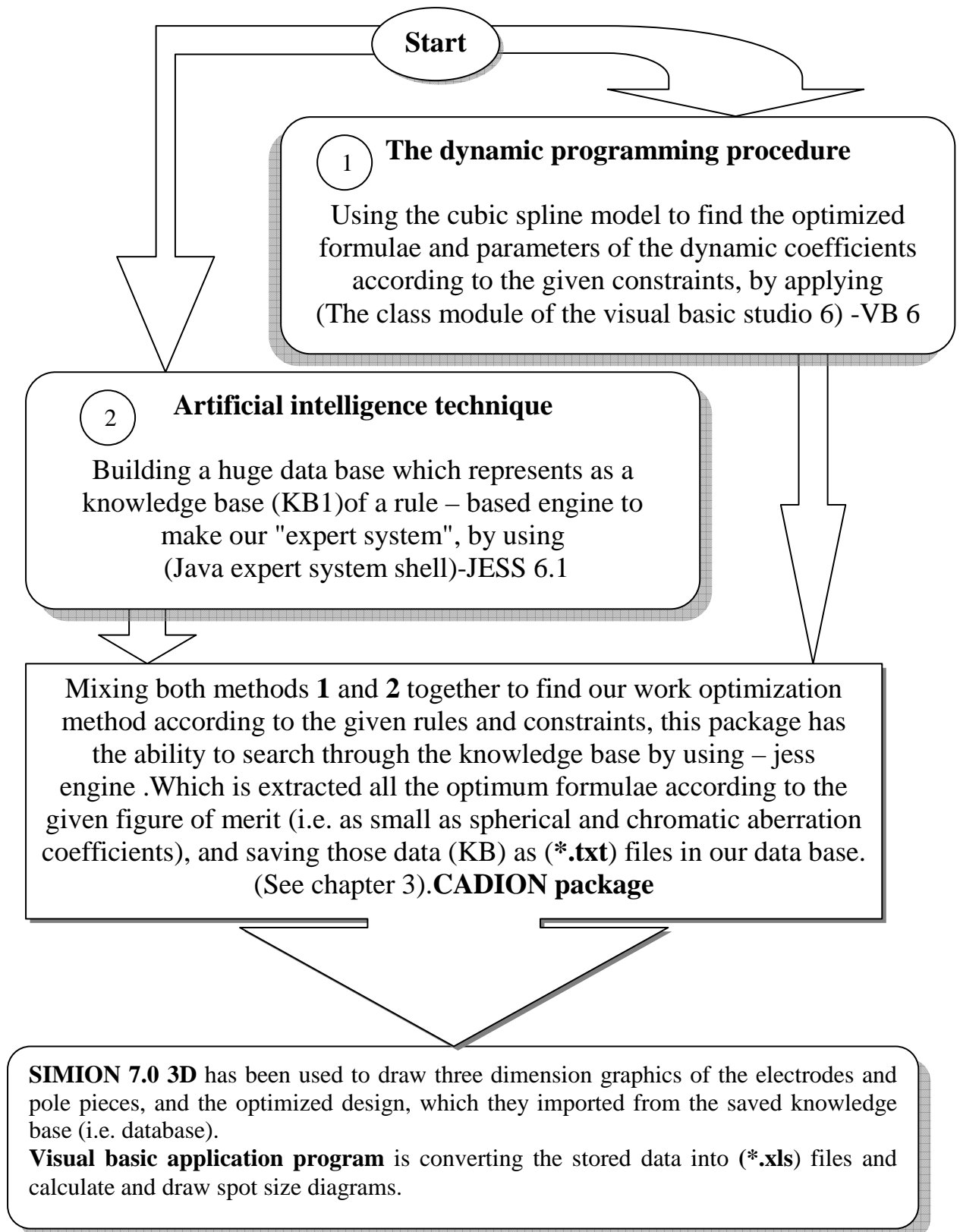


**Figure (4.1)** shows the schematic diagram of our work



## 4.1 Single lens design

Simulations with different parameters have given the spherical and chromatic aberration decreased. The half acceptance angle  $\alpha$  has a value  $= 5 \times 10^{-3}$  rad and the relative accelerating voltage  $\Delta u/u$  for ion beam focused is taken the value  $= 5 \times 10^{-5}$  for very high resolving power instruments [Hawkes 1972].

### 4.1.1 Electrostatic lenses

The axial potential distributions along with first and second derivatives were investigated according to the cubic spline model by using the dynamic programming procedure for twenty intervals. These distributions have been used to make a comparison for getting the minimum optical properties to the optimized axial potential distributions were obtained by using the dynamic programming procedure with the aid of artificial intelligence technique. The results of this procedure are shown in figures (4.2),(4.3),(4.4) and (4.5).

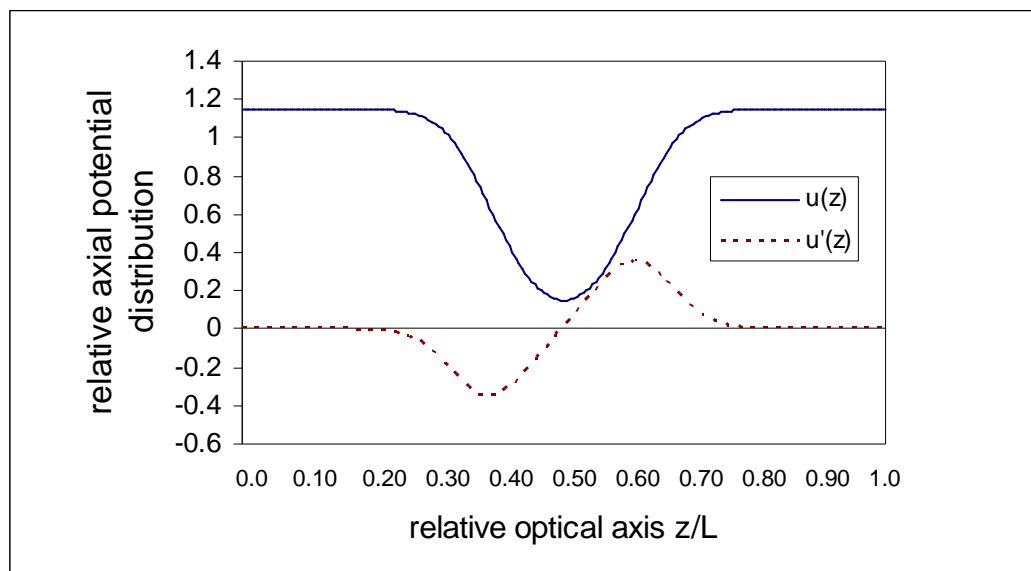


**Figure (4.2)** the relative axial potential distribution and its first and second derivatives  $u(z)$  and  $u'(z)$  for unipotential lens (1) operated in deceleration mode obtained by the dynamic programming procedure.

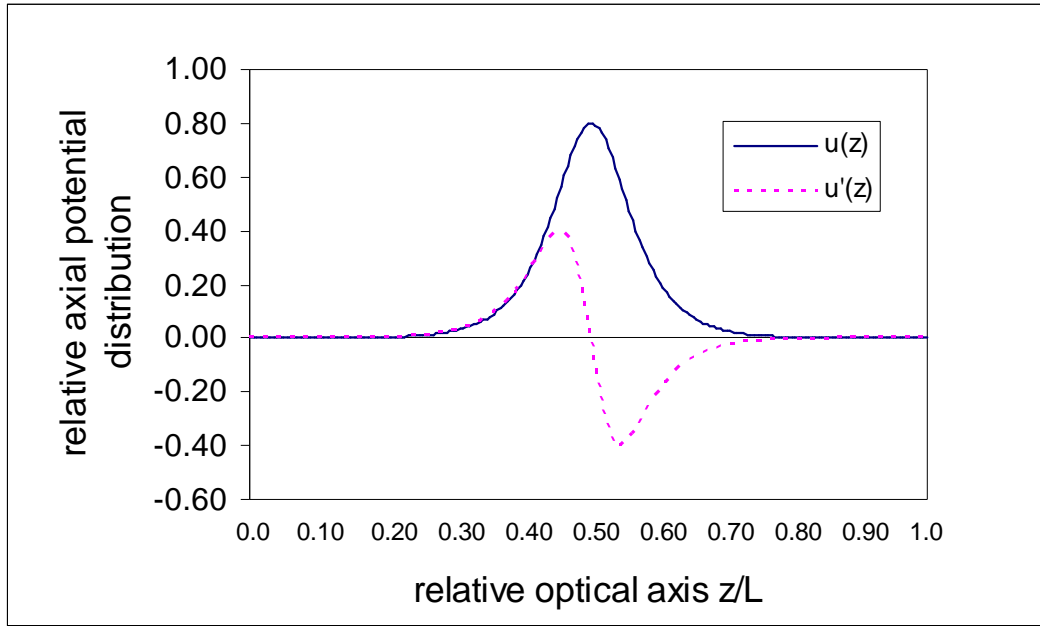


**Figure (4.3)** the axial potential distribution and its first and second derivatives  $u(z)$  and  $u'(z)$  for unipotential lens (2) operated in acceleration mode obtained by the dynamic programming procedure.

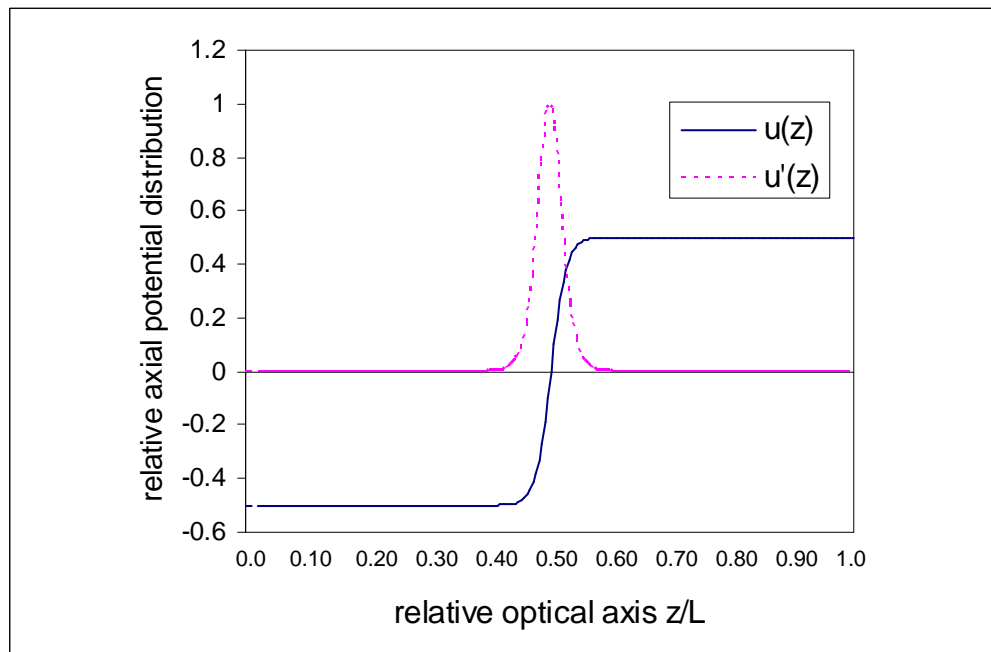


**Figure (4.4)** the axial potential distribution and its first and second derivatives  $u(z)$  and  $u'(z)$  for immersion lens obtained by the dynamic programming procedure.

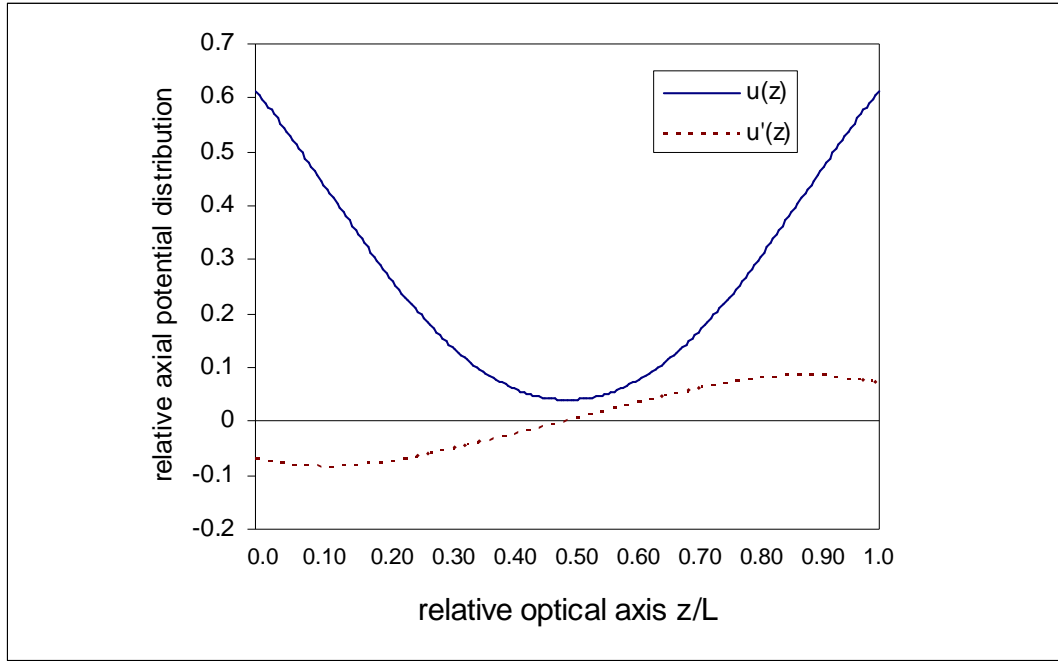


**Figure (4.5)** the axial potential distribution and its first and second derivatives  $u(z)$  and  $u'(z)$  for diaphragm lens obtained by the dynamic programming procedure.

Table (4.1) summarized the dynamic parameters of the axial potential distributions which were investigated by using the dynamic programming procedure according to the cubic spline model for the given electrostatic lenses.

**Table (4.1)** the axial potential distributions cubic spline coefficients of the given electrostatic lenses by using the dynamic programming procedure.

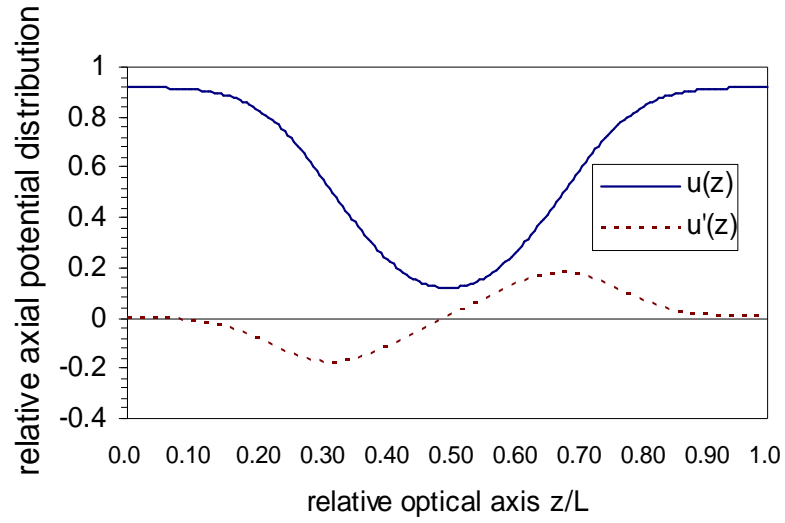
Lens Type	Cubic spline coefficients			
	a	b	c	d
<b>unipotential lens (1)</b>	100	0.1	2.0	15
<b>unipotential lens (2)</b>	0.8	0.001	1.0	0.1
<b>immersion lens</b>	0.5	2.0	1.0	0.0
<b>diaphragm lens</b>	0.8	0.009	2.0	0.04

The four types of the optimum axial potential distributions with its first derivative for the electrostatic lenses have been determined by using the dynamic programming procedure and artificial intelligence technique operated

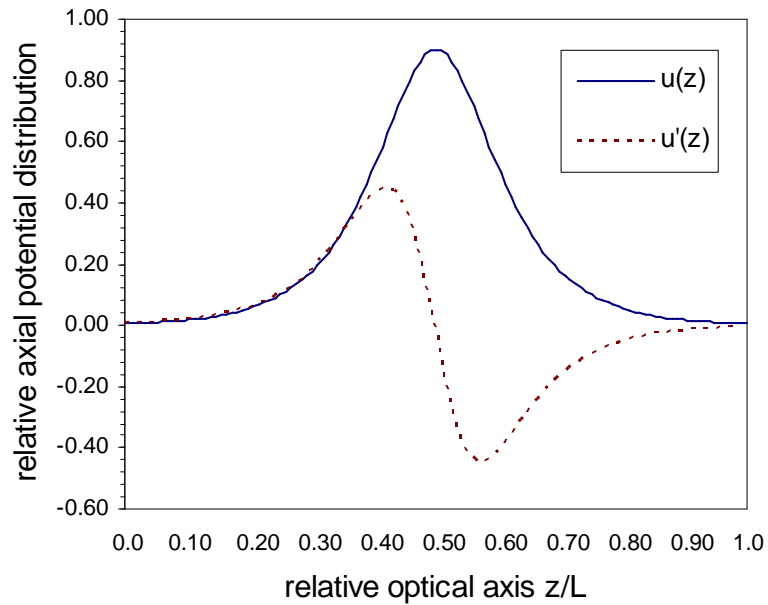
with the acceleration and deceleration modes depending on the given constraints equations (3.10),(3.11) and (3.12) respectively, are shown in figures (4.6, 4.7, 4.8 and 4.9) .The table (4.2) has given the optimized formulae and their dynamic parameters, which has been obtained by the dynamic programming procedure and artificial intelligence technique.

**Table (4.2)** the optimized axial potential distributions with their dynamic parameters of the given electrostatic lenses by using DPP with the aid of AIT.

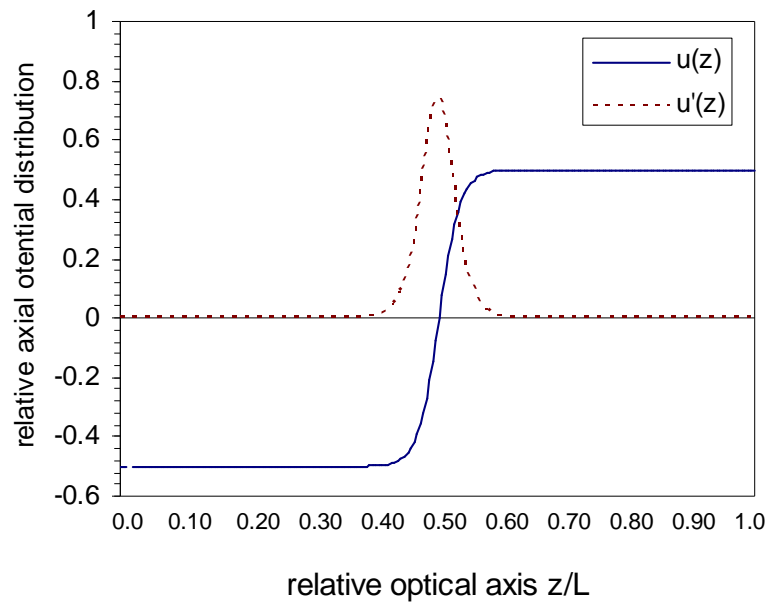
Lens Type	Optimized Axial Potential Distribution Formula	Dynamic Parameters Of Sub-intervals			
		a	b	c	d
unipotential lens (1)	$a \cdot \tanh(b \cdot z^c) + d$	80	0.04	2	12
unipotential lens (2)	$a \cdot \exp(-b \cdot z^c) / \cosh(z-d)$	0.9	3	5	0
immersion lens	$a \cdot \tanh(b \cdot z^c) + d$	0.5	1.5	1	0
diaphragm lens	$a \cdot \tanh(b \cdot z^c) + d$	0.9	0.008	2	0.01



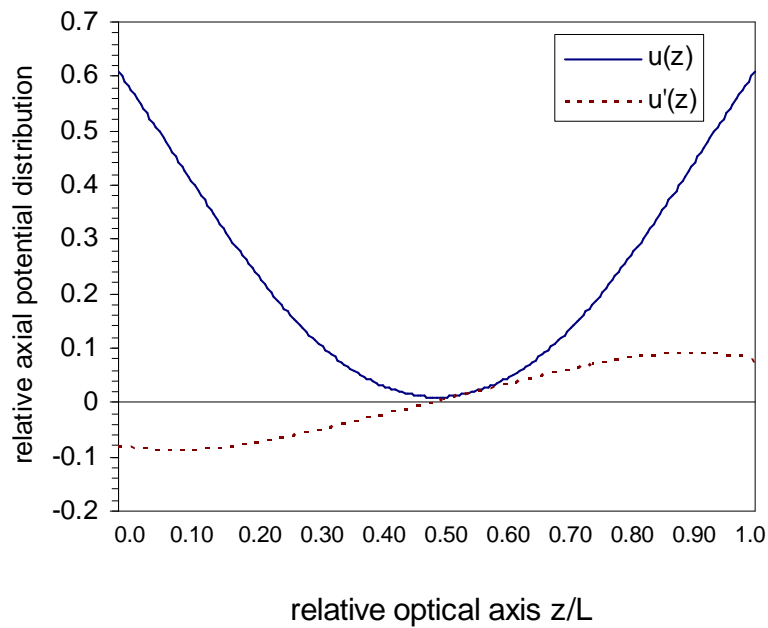
**Figure (4.6)** the optimum axial potential distribution and its first derivative  $u(z)$  and  $u'(z)$  for unipotential lens (1) operated in deceleration mode obtained by the dynamic programming procedure and artificial intelligence technique.



**Figure (4.7)** the optimum axial potential distribution and its first derivative  $u(z)$  and  $u'(z)$  for unipotential lens (2) operated in acceleration mode obtained by the dynamic programming procedure and artificial intelligence technique.

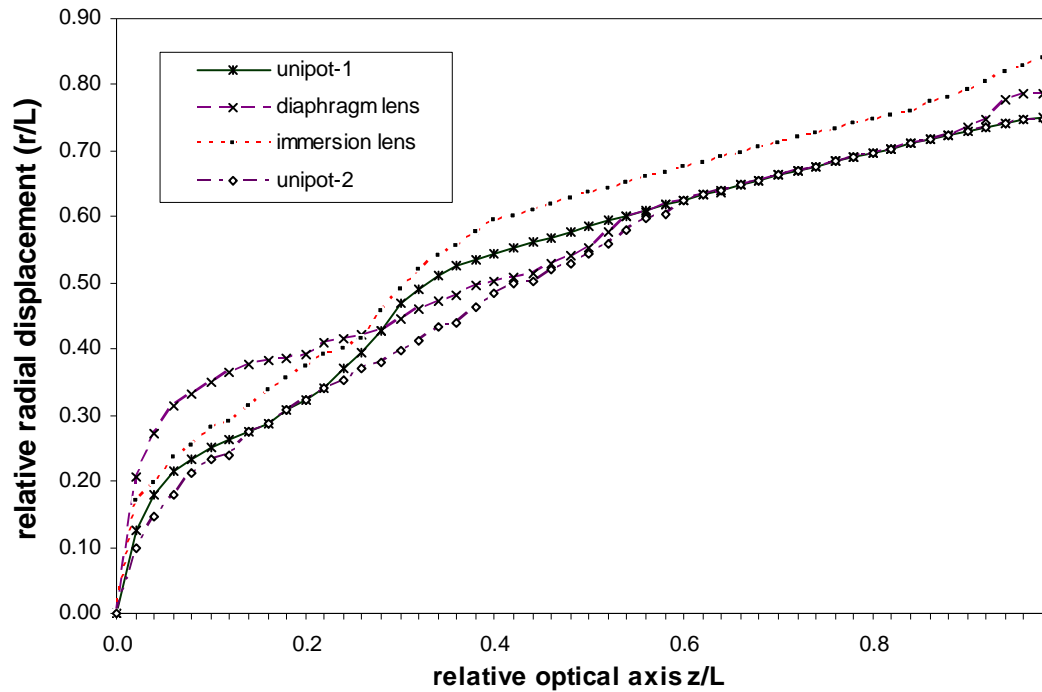


**Figure (4.8)** the optimum axial potential distribution and its first derivative  $u(z)$  and  $u'(z)$  for immersion lens obtained by the dynamic programming procedure and artificial intelligence technique.



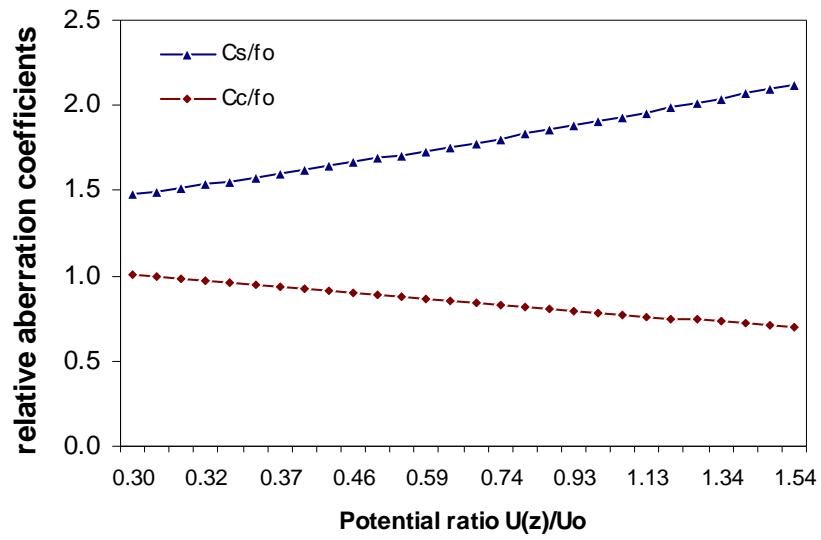
**Figure (4.9)** the optimum axial potential distribution and its first derivative  $u(z)$  and  $u'(z)$  for diaphragm lens obtained by the dynamic programming procedure and artificial intelligence technique.

Figure (4.10) shows the trajectories along the relative optical axis for the optimized electrostatic lenses under infinite magnification condition.



**Figure (4.10)** the ion beam trajectories of electrostatic lenses computed by using dynamic programming and artificial intelligence technique under infinite magnification condition of the four types of lenses.

The following figures (4.11, 4.12, 4.13 and 4.14) show the relative spherical and chromatic aberration coefficients [ $C_s/f_0$  and  $C_c/f_0$ ] against relative values of potential ratio  $U(z)/U_0$  for the optimized electrostatic lenses.



**Figure (4.11)** the relative spherical and chromatic aberration coefficients of the unipotential lens (1) for a potential ratio  $U(z)/U_o$ .

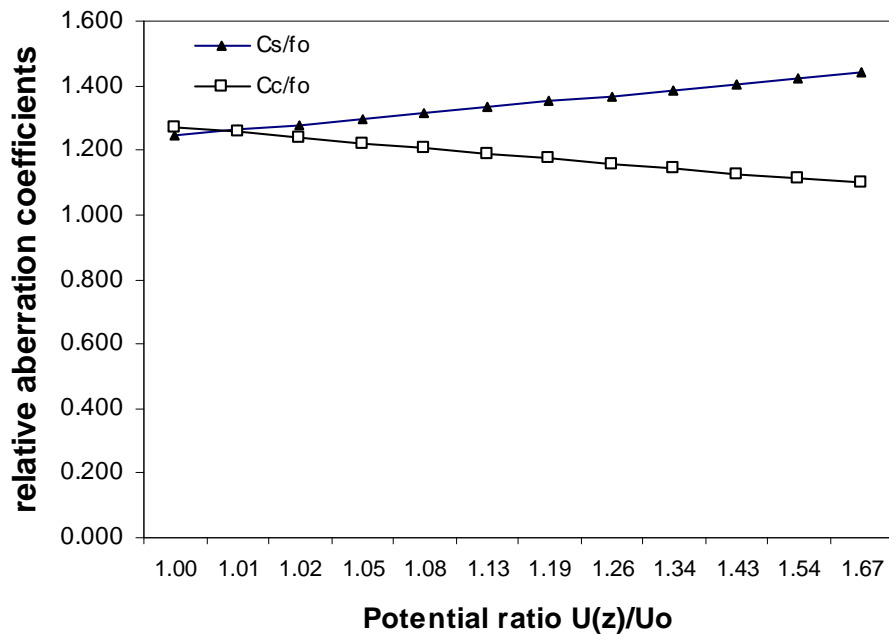


**Figure (4.12)** the relative spherical and chromatic aberration coefficients of the unipotential lens (2) for a potential ratio  $U(z)/U_o$ .



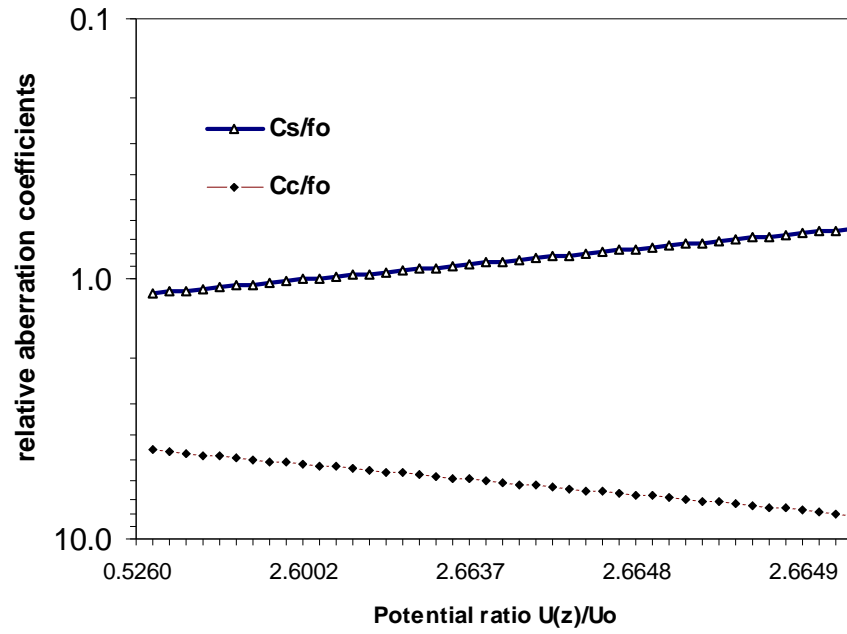


**Figure (4.13)** the relative spherical and chromatic aberration coefficients of the immersion lens for a potential ratio  $U(z)/U_0$ .

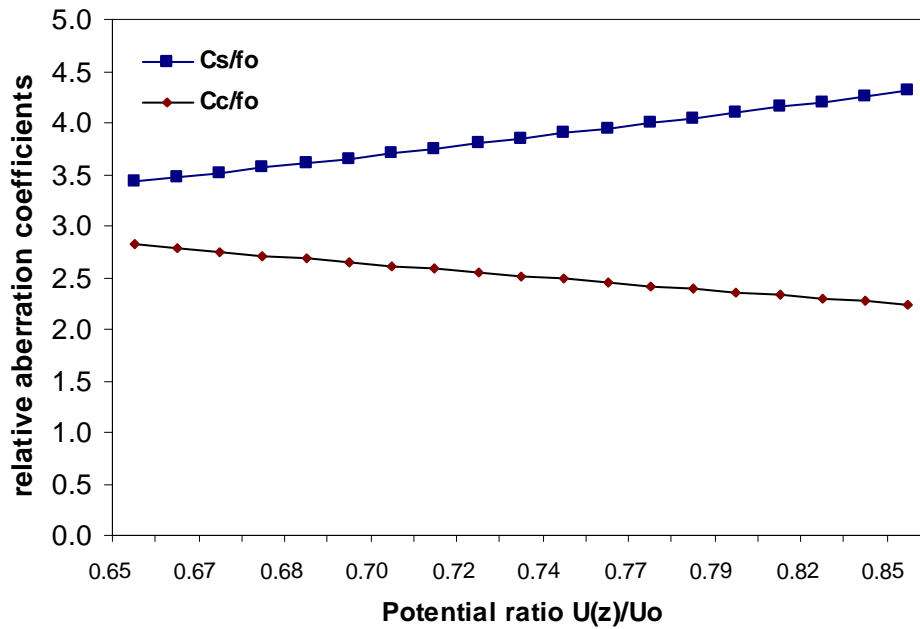


**Figure (4.14)** the relative spherical and chromatic aberration coefficients of the diaphragm lens for a potential ratio  $U(z)/U_0$ .

### 4.1.2 Electrode reconstruction

The electrodes reconstruction processes have been made within the following four types of optimized electrostatic lenses obtained by the dynamic programming procedure with the aid of artificial intelligence technique as follows:-

- Unipotential lens (1) operated in deceleration mode , fig.(4.15)
- Unipotential lens (2 ) operated in acceleration mode ,fig.(4.16)
- Diaphragm lens ,fig.(4.17)

The following figures (4.15), (4.16) and (4.17) show three-electrode lens of the optimized axial potential distributions in two dimension profiles. SIMION 7.0 simulator has plotted the configurations of such graphs in three dimensions. Figures (4.18), (4.19) and (4.20) give those electrodes of the optimized lenses (unipotential lens (1), unipotential lens (2) and diaphragm lens), respectively.

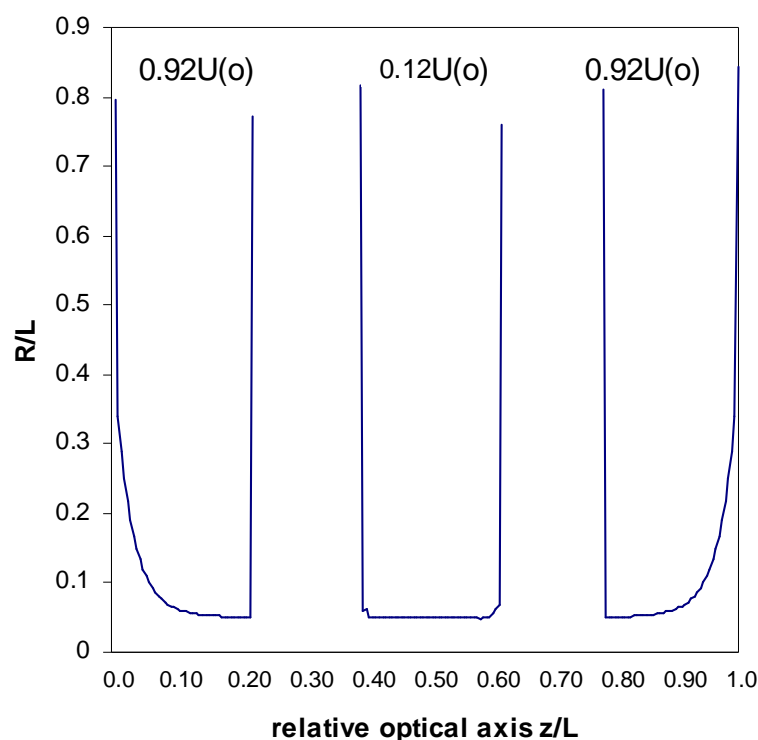


**Figure (4.15)** the electrodes profile for a three-electrode unipotential lens (1) at energies  $0.92U(o)$ ,  $0.12U(o)$  and  $0.92U(o)$  respectively.

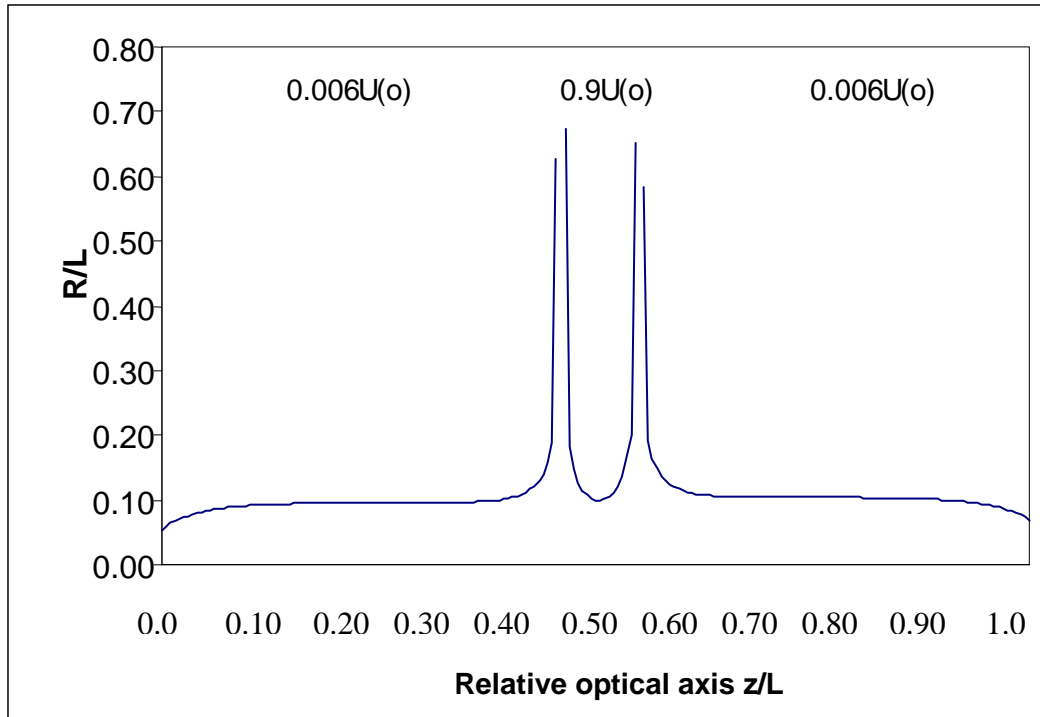


**Figure (4.16)** the electrodes profile for a three-electrode unipotential lens (2) at energies  $0.006U(o)$ ,  $0.9U(o)$  and  $0.006U(o)$  respectively.

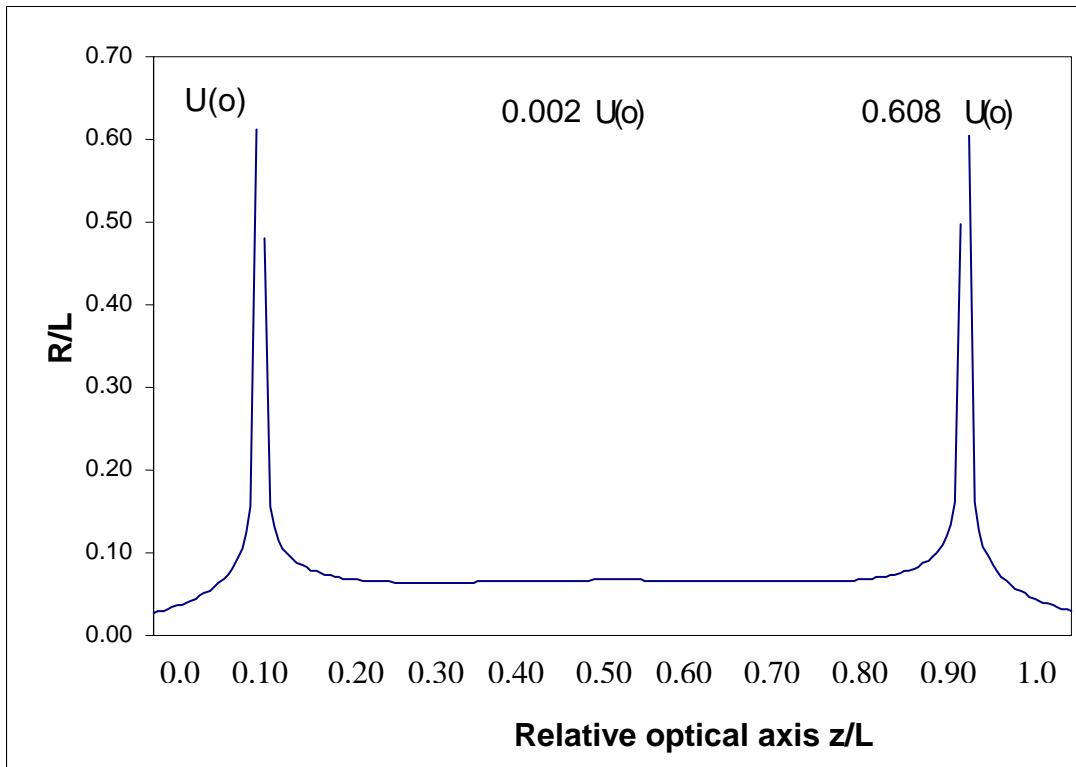


**Figure (4.17)** the electrodes profile for a three-electrode diaphragm lens at energies  $U(o)$ ,  $0.002U(o)$  and  $0.608U(o)$  respectively.

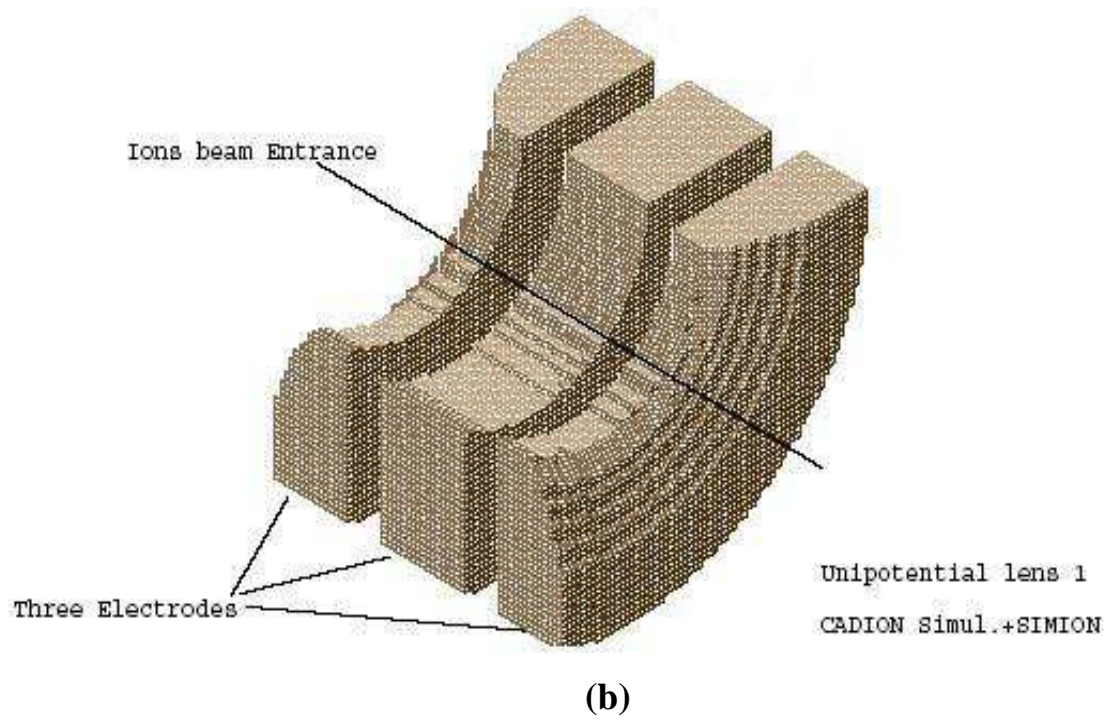
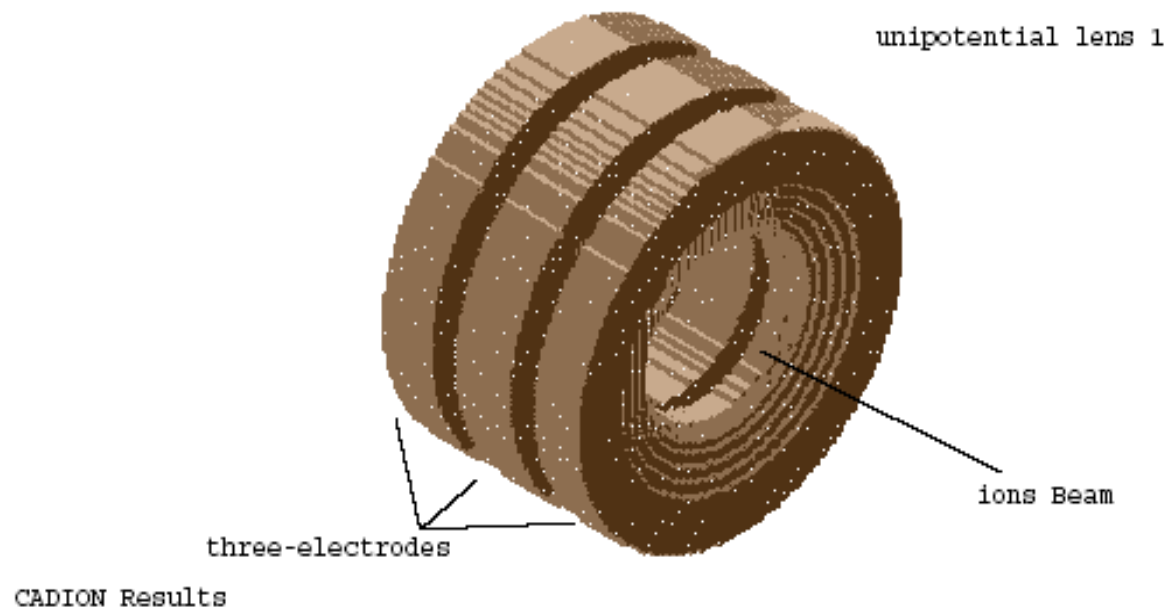


**Figure (4.18)** three-electrode profile for unipotential lens (1) by using SIMION 7[(a) total profile and (b)cross section].

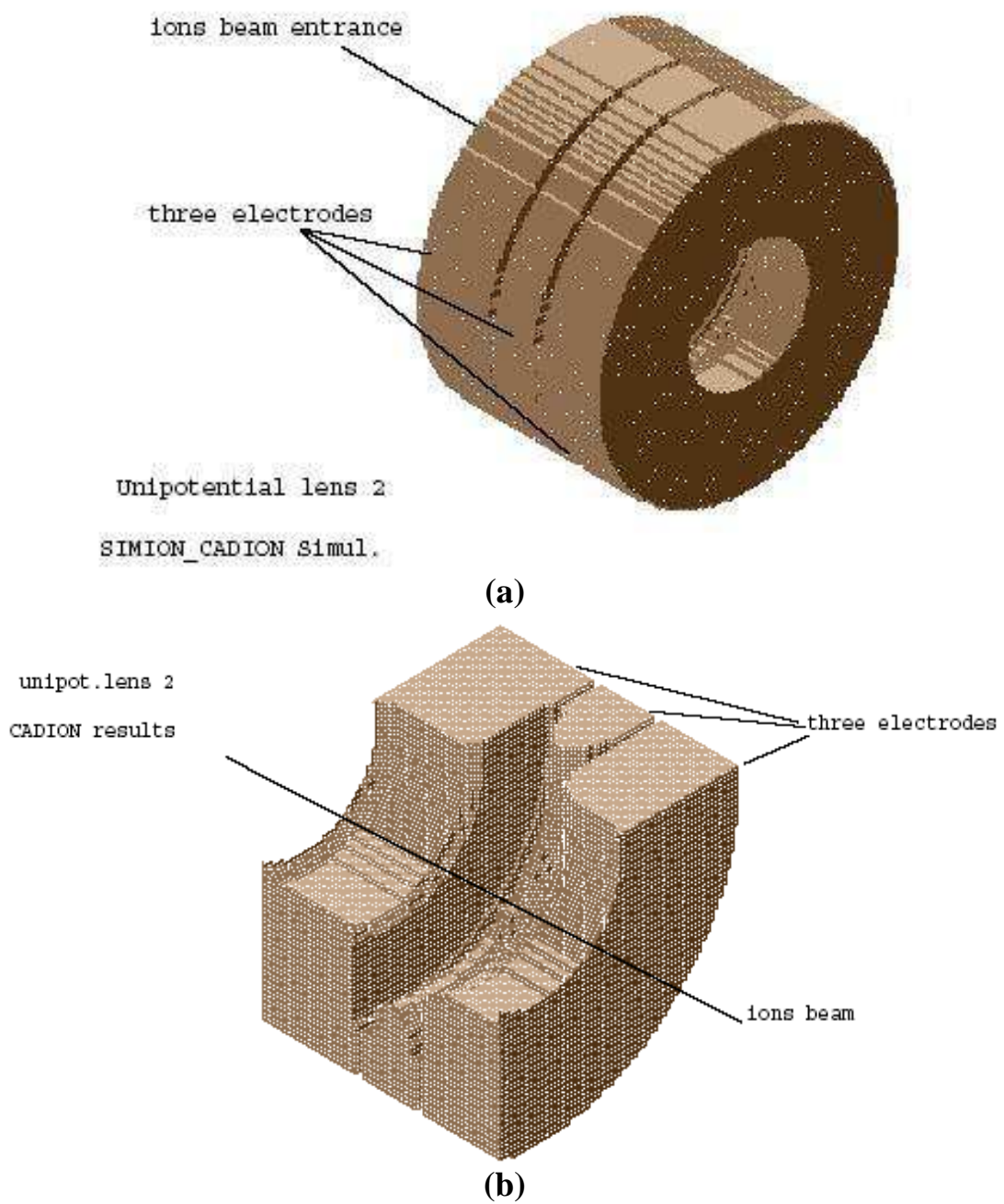


**Figure (4.19)** three-electrode profile for unipotential lens (2) by using SIMION 7[(a) total profile and (b)cross section].

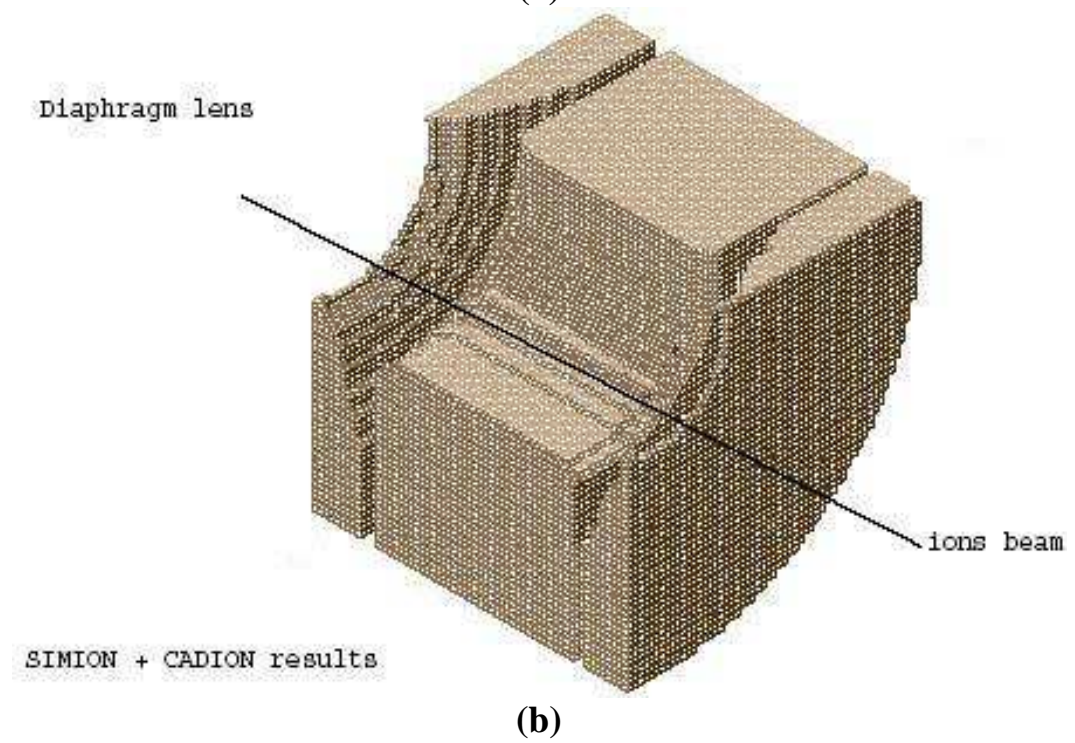
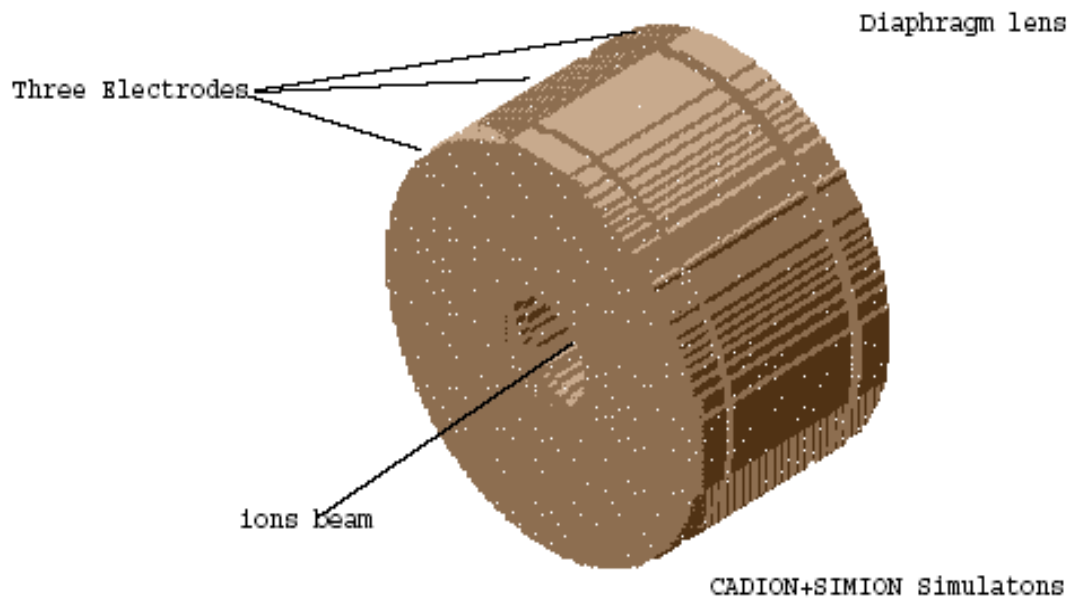


**Figure (4.20)** three-electrode profile for diaphragm lens by using SIMION 7[(a) total profile and (b)cross section].

The immersion lens with an optimized axial potential distribution as in figure (4.8) would get two electrodes taken the potential at the range amount of about  $U(o)$  and  $0.5 U(o)$  respectively. Figures (4.21) and (4.22) show our the immersion two electrodes lens profile (i.e. two dimensions profile) ,as well as three dimensions graphic electrodes shape has been plotted by using SIMION 7.

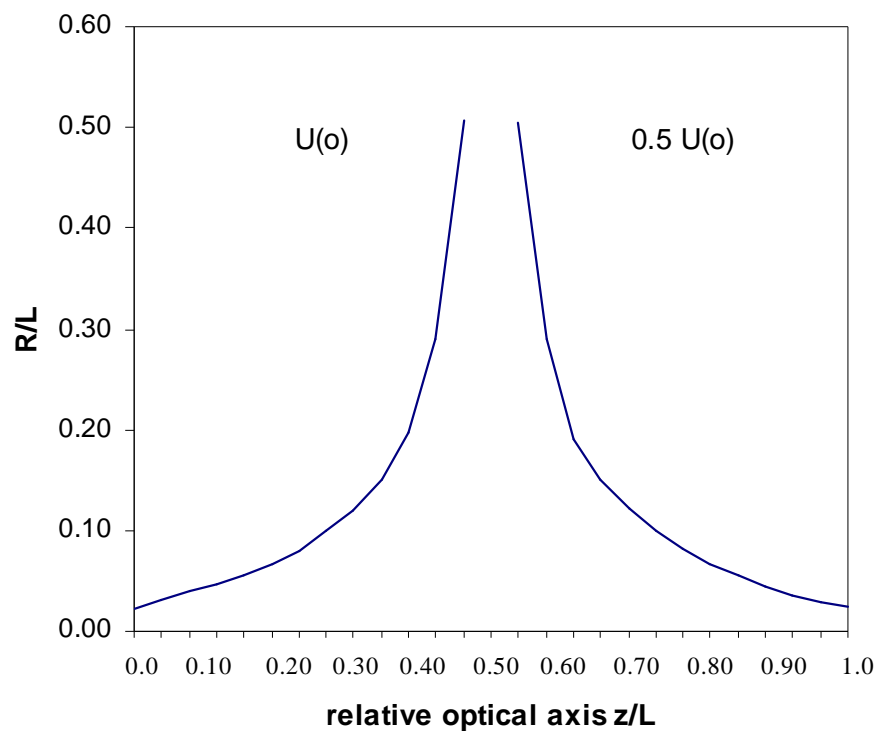


**Figure (4.21)** the electrodes profile for a two-electrode immersion lens at energies  $U(o)$  and  $0.5U(o)$  respectively.



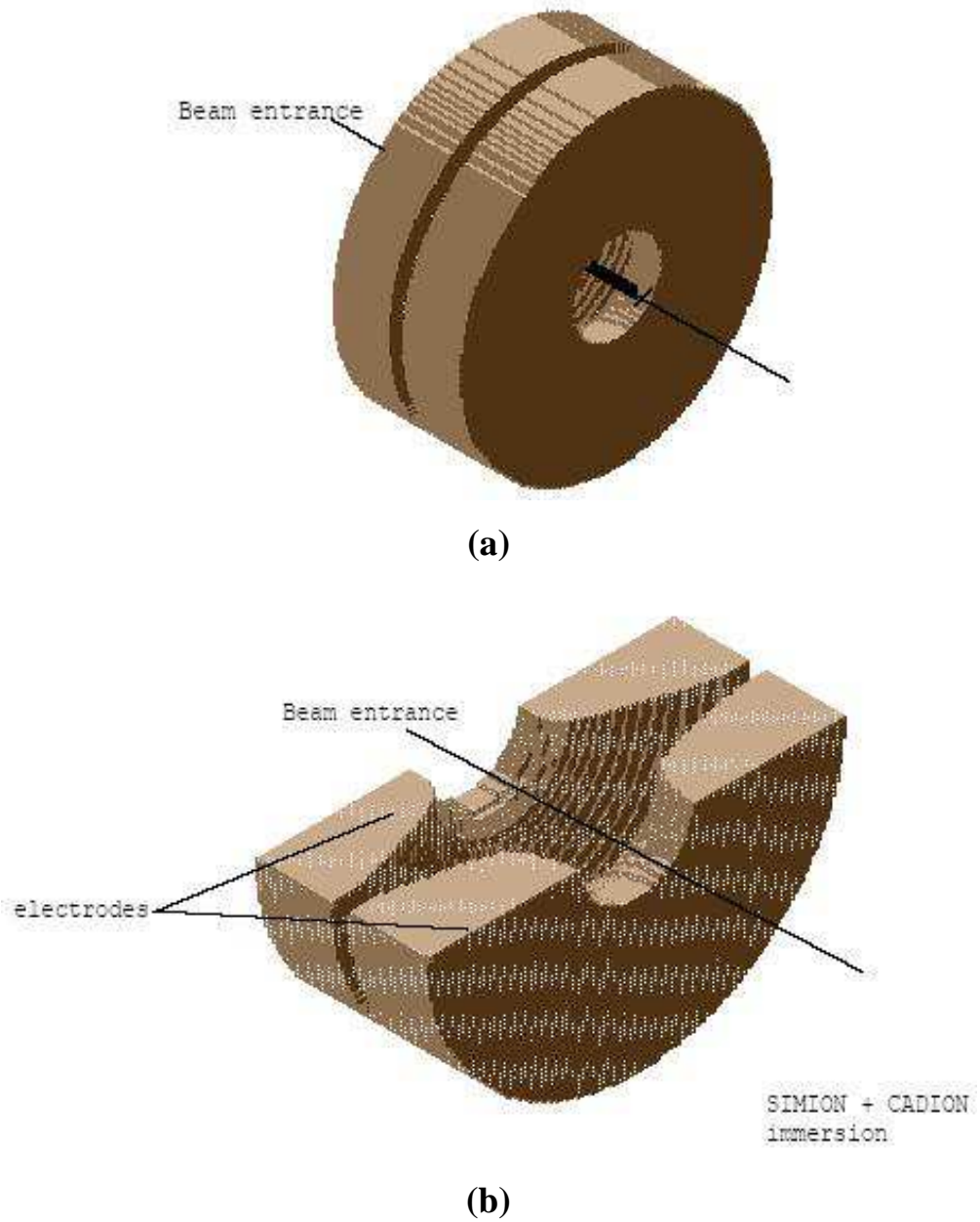


**Figure (4.22)** two-electrode profile for immersion lens by using SIMION 7[(a) total profile and (b)cross section].



### 4.1.3 Magnetic lens design

In present work only one case of a magnetic lens has been designed. The optical properties (i.e. the relative spherical and chromatic aberration coefficients) are characterized by the dimensionless parameter ( $\mathbf{k}^2\mathbf{d}^2$ ), where  $\mathbf{k}^2$  as in paraxial ray equation (2.4) and  $\mathbf{d}$  is the field half-width, in which is determined by the shape of the pole pieces and by the degree of saturation. The axial flux density distribution was optimized like Grivet-Lenz model for magnetic lenses, which it can be used for the description of unsaturated lenses.

The optimized formula of the axial magnetic field distribution (i.e. the axial flux density distribution  $\mathbf{B}(\mathbf{z})$ ) was obtained by using the dynamic programming procedure with the aid of artificial intelligence technique included in CADION package. Figure (4.23) and table (4.3) are shown the optimized field distribution with its first derivative and its optimized formula respectively. The maximum value has been taken in our work for the axial flux density distribution  $\mathbf{B}_{\max}$  is equal to (6.0) mTesla. For future work optimization will be done to get a formula depending on the magnetic permeability  $\mu$  in ferromagnetic materials as a function of the optical axis and radial.

**Table (4.3)** the optimized magnetic lens formula with its dynamic parameters by using DPP and AIT.

Lens Type	Optimized Flux density Distribution Formula	Dynamic Parameters			
		a	b	c	d
magnetic lens (1)	$\mathbf{a}*\text{sech}(\mathbf{z}^{\wedge}\mathbf{c}/\mathbf{b})+\mathbf{d}$	$\mathbf{B}_{\max}$	2.0	1.0	0

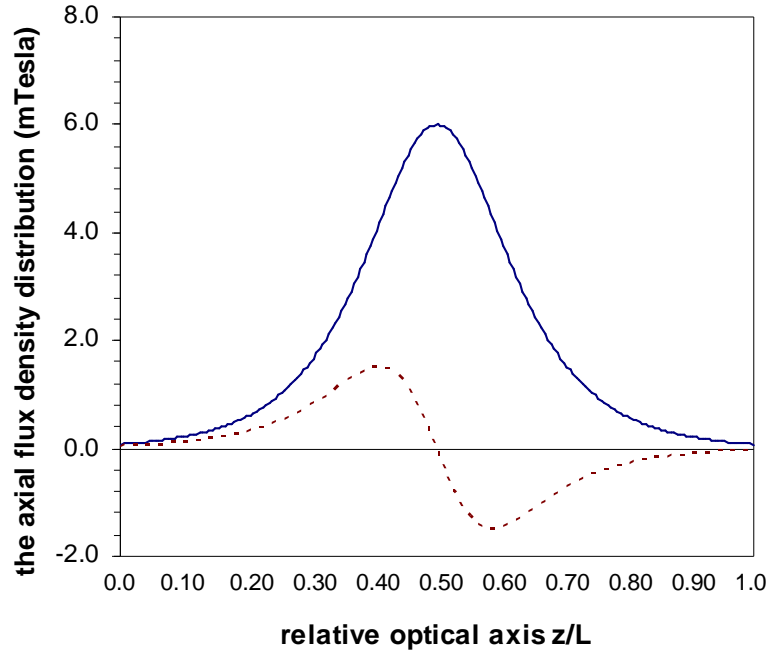


**Figure (4.23)** the optimum axial magnetic flux density distribution  $B(z)$  with its first derivative for the given magnetic lens (1) obtained by the dynamic programming procedure and artificial intelligence technique.

Figure (4.24) shows the trajectory along the relative optical axis for the optimized magnetic field obtained in table (4.3). Figure (4.25) shows the relative spherical and chromatic aberration coefficients  $C_s/f_0$  and  $C_c/f_0$  - respectively, as a function as the dimensionless parameter  $k^2 d^2$  which related to the half-width  $d$  for the optimized magnetic field. Table (4.4) gives the values of the relative aberration coefficients and the dimensionless parameter  $k^2 d^2$ .

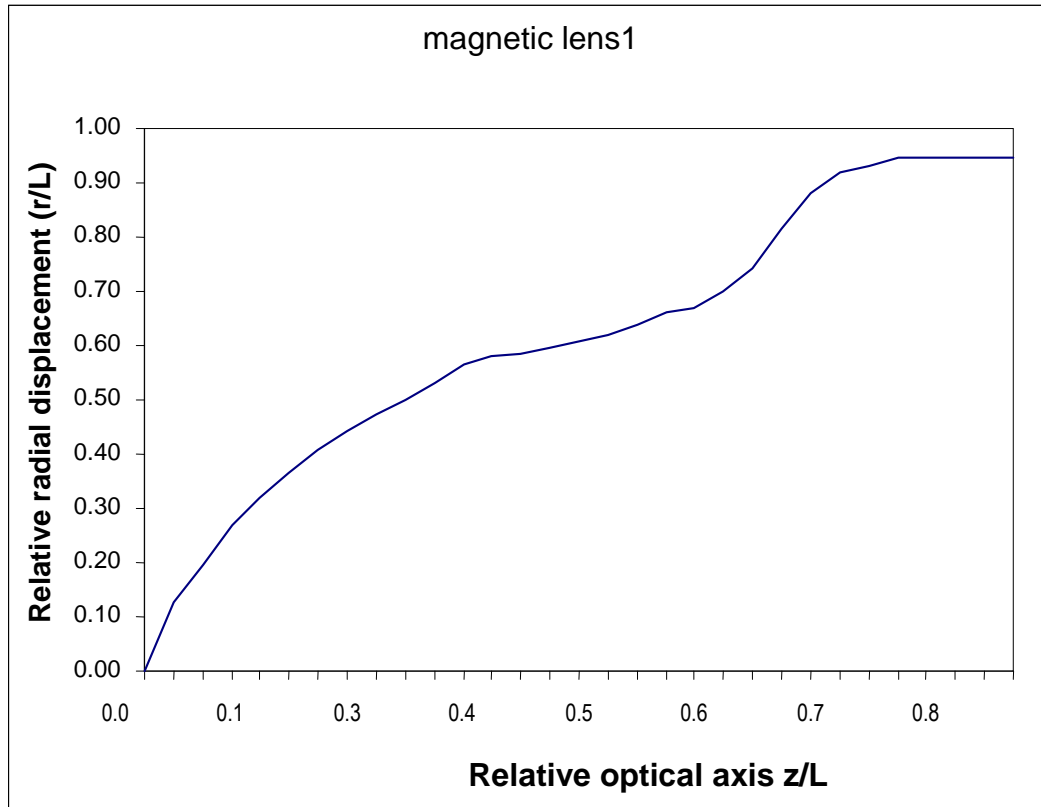


**Figure (4.24)** the ion beam trajectories of magnetic lens (1) under infinite magnification condition.

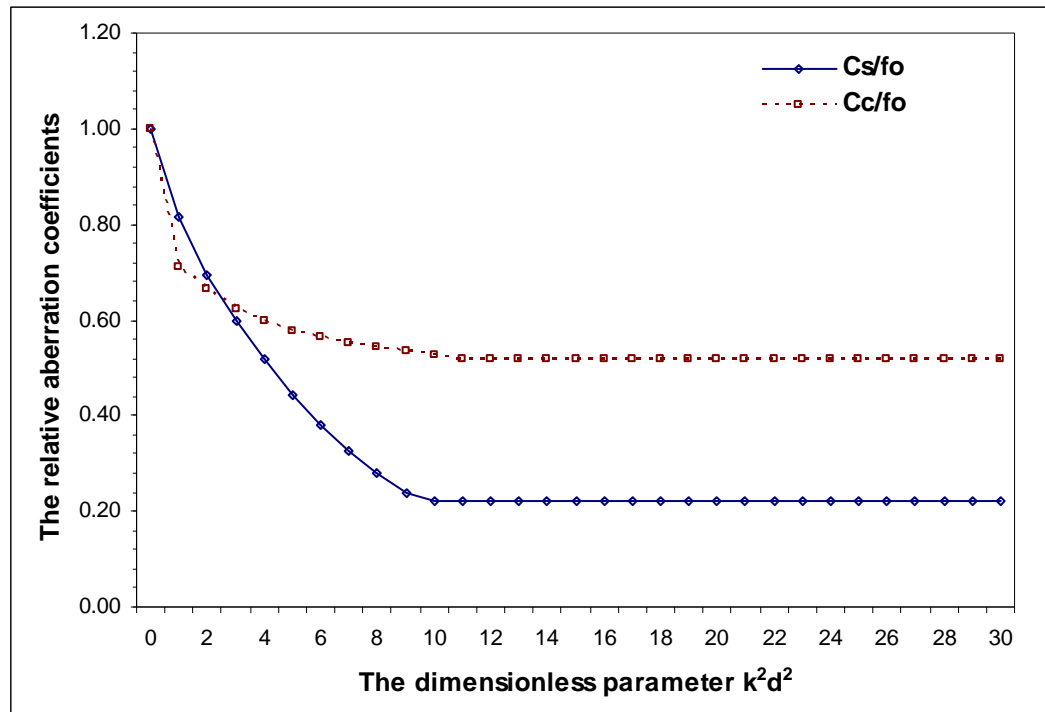


**Figure (4.25)** the relative spherical and chromatic aberration coefficients of the optimized magnetic lens (1) related to the dimensionless parameter  $k^2d^2$ .

**Table (4.4)** the relative spherical and chromatic aberration coefficients of the optimized magnetic lens (1) and the dimensionless parameter  $k^2d^2$ .

$C_s / f_o$	$C_c / f_o$	$k^2d^2$
1.00	1.00	0.00
0.82	0.71	1.00
0.69	0.67	2.00
0.60	0.62	3.00
0.52	0.60	4.00
0.44	0.58	5.00
0.38	0.57	6.00
0.33	0.55	7.00
0.28	0.55	8.00
0.24	0.54	9.00
0.22	0.53	10.00
0.22	0.52	11.00
0.22	0.52	12.00
0.22	0.52	13.00
0.22	0.52	14.00
0.22	0.52	15.00
0.22	0.52	16.00
0.22	0.52	17.00
0.22	0.52	18.00
0.22	0.52	19.00
0.22	0.52	20.00
0.22	0.52	21.00
0.22	0.52	22.00
0.22	0.52	23.00
0.22	0.52	24.00
0.22	0.52	25.00
0.22	0.52	26.00
0.22	0.52	27.00
0.22	0.52	28.00
0.22	0.52	29.00
0.22	0.52	30.00

#### 4.1.4 Pole pieces reconstruction

The pole pieces reconstruction has taken the same analyzed procedure by using SIMION 7. The following figures (4.26) and (4.27) show the profiles of the pole pieces of the optimized magnetic field in two and three dimensions respectively.

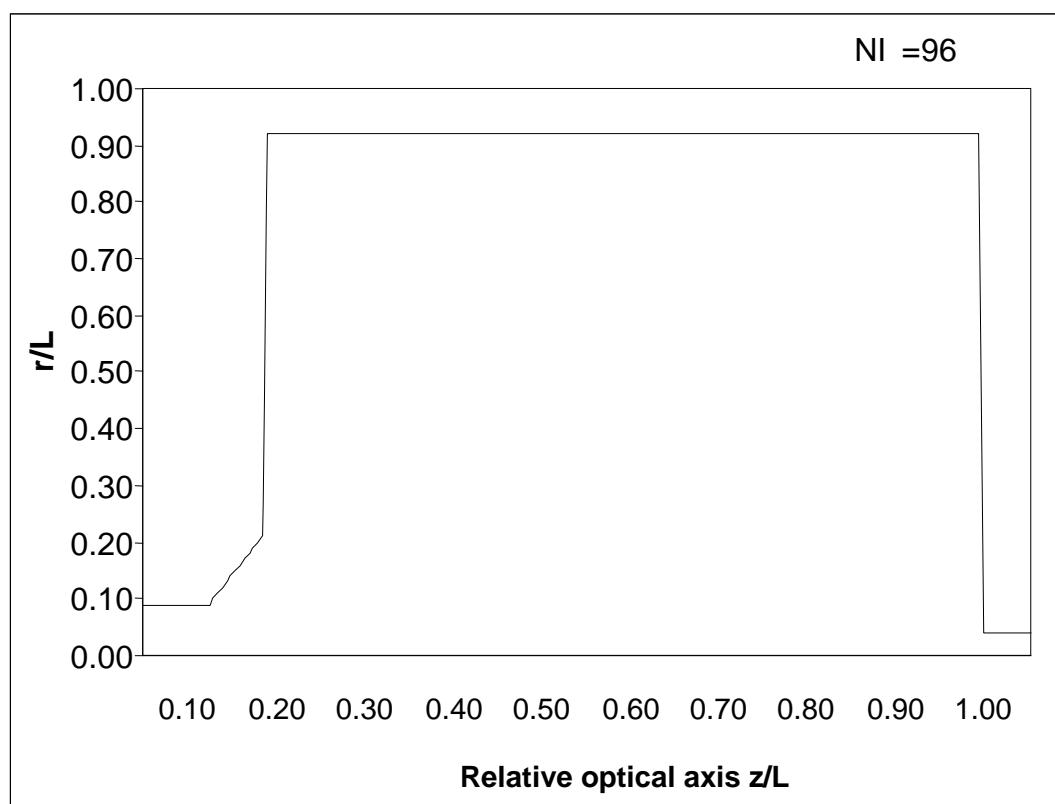


**Figure (4.26)** the two dimension profile of a pole piece for a magnetic lens (1) with **NI = 96** ampere-turns.

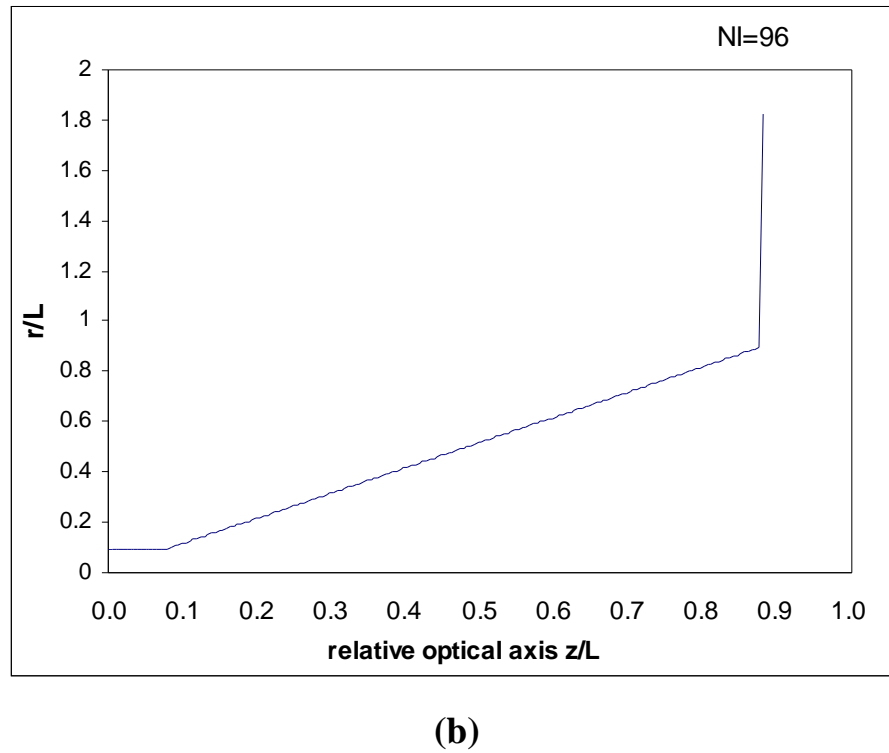
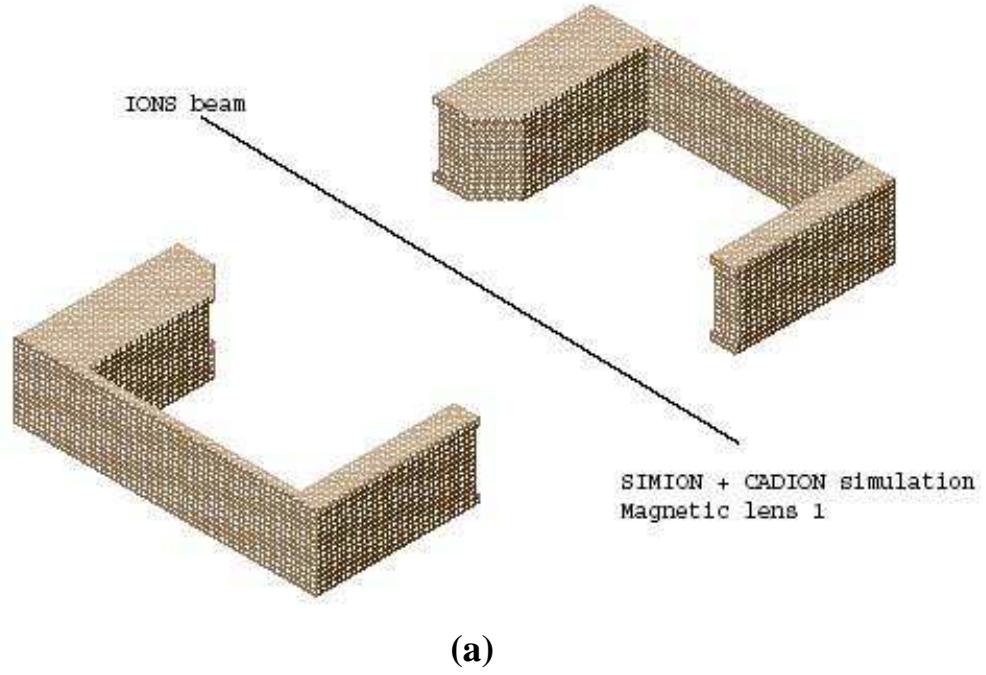


**Figure (4.27)** (a) three dimensions graph of the pole piece of a magnetic lens (1). (b) The optimized pole piece profile of a magnetic lens (1).

To make a comparison of the optimum magnetic lens (1), figure (4.28) shows the axial magnetic flux density distribution  $B(z)$  with its first derivative for the

Glaser's model (i.e. magnetic lens (2)).Table (4.5) gives the magnetic lens (2) formula with its dynamic parameters obtained by using CADION package.

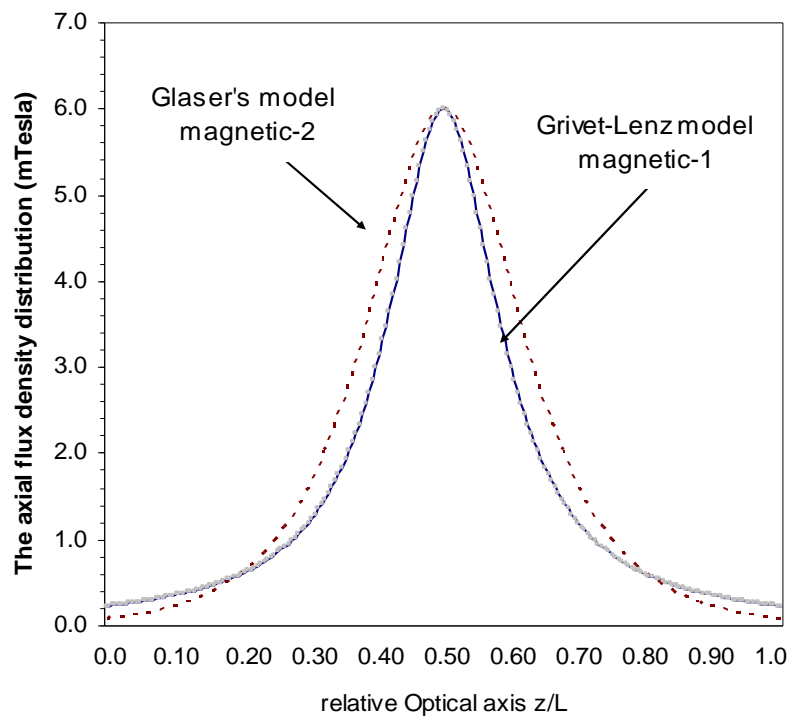


**Figure (4.28)** the magnetic flux density distributions  $B(z)$  for both magnetic lens (1) and (2).

**Table (4.5)** the magnetic field (2) formula with its dynamic parameters by using CADION package.

Lens Type	Flux density Distribution Formula	Dynamic Parameters			
		a	b	c	d
magnetic lens (2)	$a/[1+((z/b)^c)+d]$	$B_{\max}$	2.0	2.0	0

To summarize the optimized results obtained in the single-lens design for the aberration discs diameters ( $d_s$  –spherical aberration disc diameter,  $d_c$  – chromatic aberration disc diameter and  $d_t$ – total aberration disc diameter), table (4.6) gives the values in micro scale ( $\mu\text{m}$ ) under the infinite magnification condition. In which they were calculated depending on equations (2.14, 2.19 and 2.20 respectively) by choosing the minimum values (i.e. figure of merit) of the given relative spherical and chromatic aberration coefficients ( $Cs/f_o$  and  $Cc/f_o$ ) of the optimized lenses.

**Table (4.6)** the minimum optical properties in a single-lens under infinite magnification conditions.

<b>Lens Types</b>	<b>relative aberration coefficients</b>		<b>aberration discs diameter (<math>\mu\text{m}</math>)</b>		
	$Cs/f_o$	$Cc/f_o$	<b>spherical <math>d_s</math></b>	<b>chromatic <math>d_c</math></b>	<b>total <math>d_t</math></b>
Unipotential -1	1.50	0.70	0.19	0.18	0.26
Unipotential- 2	1.25	1.10	0.16	0.28	0.32
Immersion	0.60	4.56	0.08	1.14	1.14
Diaphragm	3.40	2.24	0.43	0.56	0.70
Magnetic lens -1	0.22	0.52	0.03	0.13	0.133



## 4.2 Two-lens system

The two-lens system is constructed from the optimized electrostatic lenses that have been used the dynamic programming procedure and artificial intelligence technique. Furthermore has to be done for improving the ion beam collimated design to achieve smaller spot size.

However, if the first lens is operated under zero magnification and the second lens is operated under infinite magnification, one would have a telescopic lens system with a beam cross over between the two electrostatic lenses. It should be noted that when operating the first lens under infinite magnification and the second lens under zero magnification the combined lenses act as a demagnifying system, which has been considered in our investigation. The axial potential distribution is determined with their first and second derivatives of a given two - lens system forming two collimated beams as follows:

1. Unipotential lens (1) [**einzel**] lens is operated under infinite magnification condition – immersion lens is operated under zero magnification condition.
2. Diaphragm lens is operated under infinite magnification condition – immersion lens is operated under zero magnification condition.

Figures (4.29 and 4.30) show the ion beam trajectory for a given two- lens systems (i.e. 1 and 2) with its collimated beam between focusing elements obtained by using dynamic programming procedure with the aid of artificial intelligence technique. The gap between the two fields is a field free region which is traversed by the ion beam as straight lines. The ion beam leaves the left hand side field and enters the right hand side field along a path parallel to

the optical axis. An axial extension for the field free region is important to prevent an interaction between the two fields and loss of energy associated with the charged particles which both would affect the optical properties of the whole system.

### Collimated ion beam of a two lens system 1

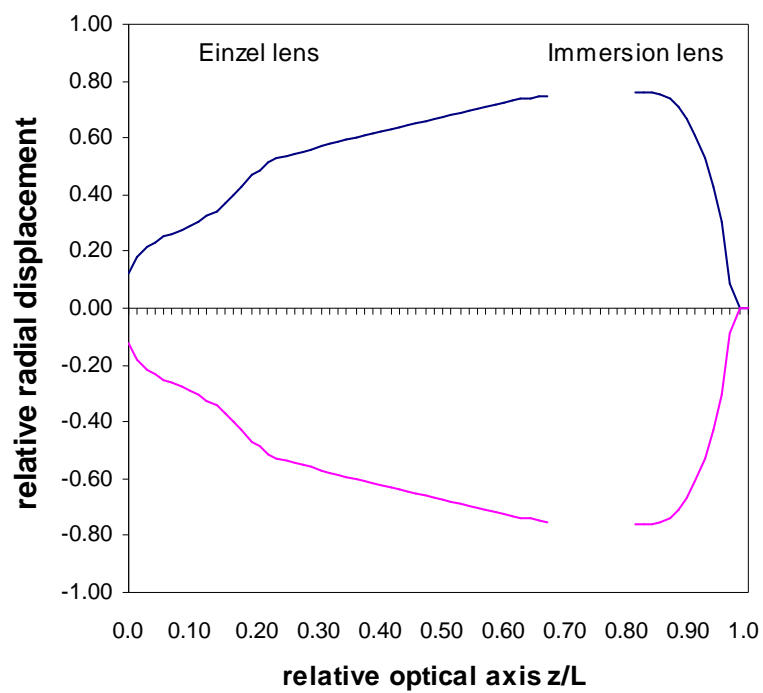


**Figure (4.29)** the ion beam trajectory for a two-lens system (1).

## Collimated ion beam of a two lens system 2

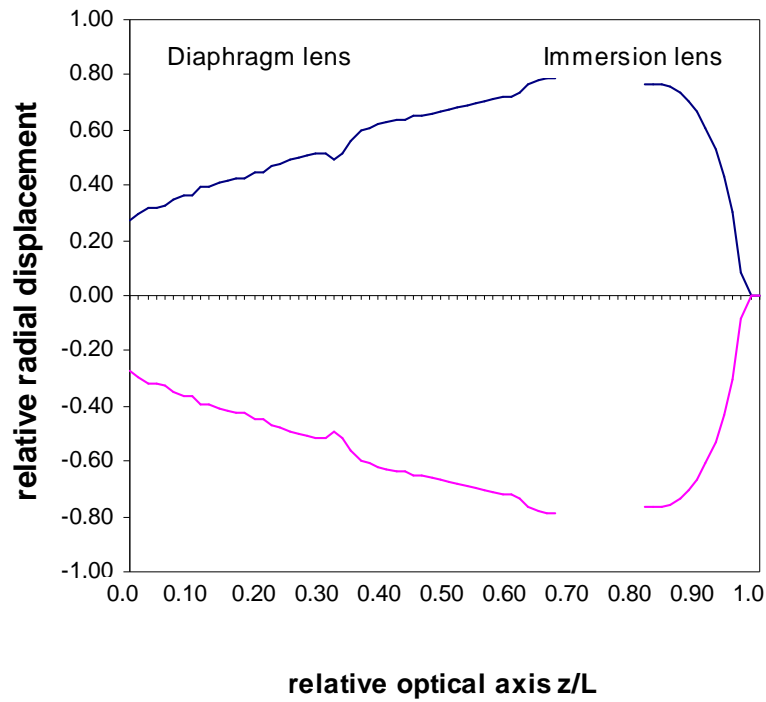


**Figure (4.30)** the ion beam trajectory for a two-lens system (2).

The given ion beam columns have been optimized and analyzed by using the dynamic programming procedure and artificial intelligence technique included in CADION package. Figures (4.31 and 4.32) show the electrodes configuration plotted in three dimensions by using SIMION 7 simulator of the two ion beam columns, respectively.

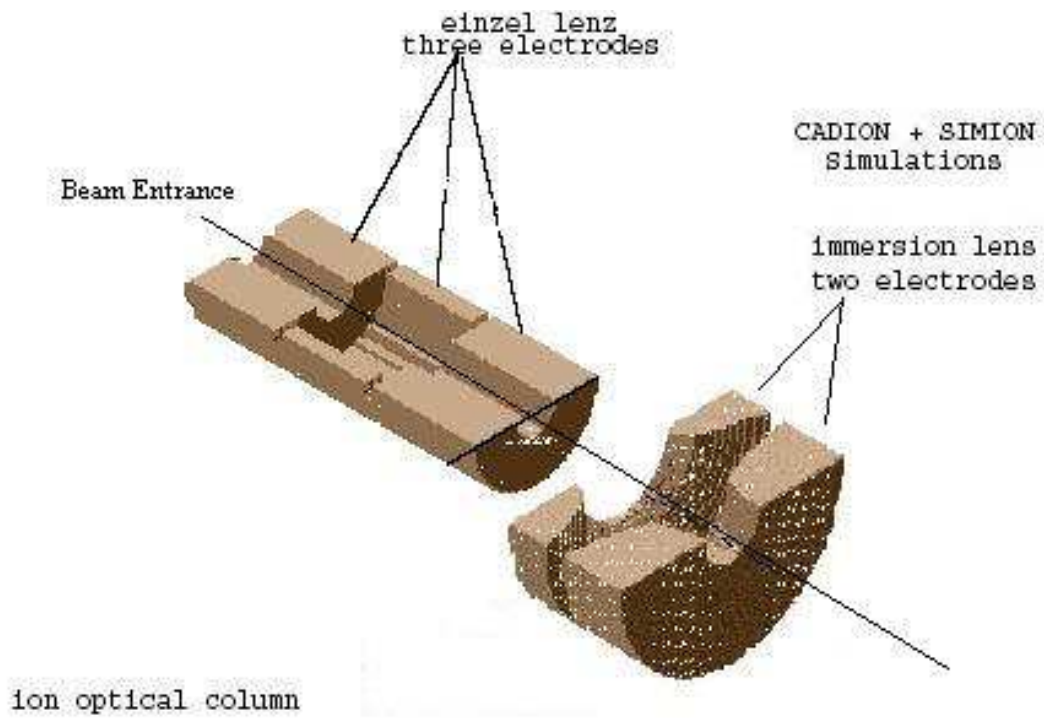


**Figure (4.31)** the electrodes configuration for a two-lens system (1) with collimated beam between focusing elements.

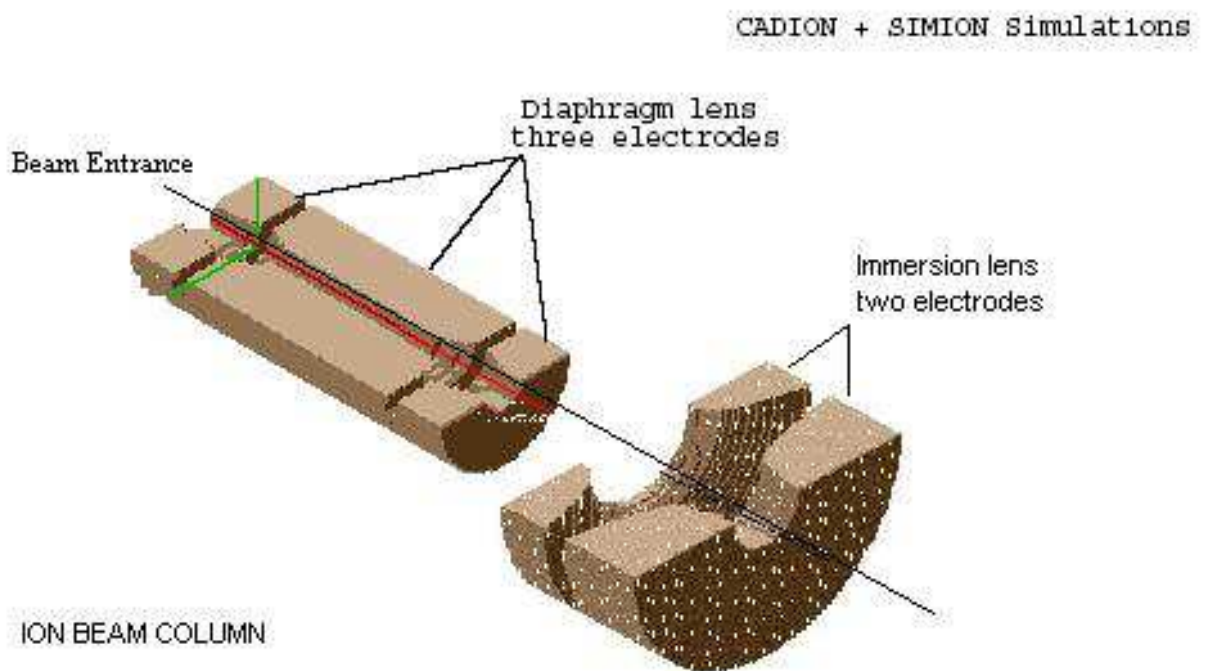


**Figure (4.32)** the electrodes configuration for a two-lens system (2) with collimated beam between focusing elements.

The relative optical properties of these two systems (i.e. system (1) and (2)) are given in tables (4.7 and 4.8), respectively. The relative aberration coefficients are taken in terms of the image-side focal length of the second lens, by which it's the overall image-side focal length of the system. The spherical, chromatic and total aberration discs ( $\mathbf{d}_{si}$ ,  $\mathbf{d}_{ci}$  and  $\mathbf{d}_{ti}$ ) are calculated with the aid of equations (2.26, 2.27 and 2.28), respectively.

**Table (4.7)** the relative optical properties for a two-lens system (1) with collimated beam between focusing elements.

<b>DEMAGNIFICATION CONDITION FOR TWO LENSES SYSTEM -1</b>			
<b>relative optical properties</b>	<b>einzel lens</b>	<b>immersion lens</b>	<b>The system</b>
<b>magnification</b>	<b>infinite</b>	<b>zero</b>	<b>-0.553</b>
$U_i/U_o$	1.545	2.70	2.70
$f_i/L$	infinite	1.082	1.082
$f_o/L$	1.48	infinite	1.48
$C_{si}/f_i$	---	6.22	---
$C_{so}/f_o$	1.50	---	5.30
$C_{ci}/f_i$	---	0.541	---
$C_{co}/f_o$	0.70	---	3.30
$\mathbf{d}_{si}(\mu\mathbf{m})$	---	0.08	1.702
$\mathbf{d}_{so}(\mu\mathbf{m})$	0.19	---	---
$\mathbf{d}_{ci}(\mu\mathbf{m})$	---	1.14	1.365
$\mathbf{d}_{co}(\mu\mathbf{m})$	0.18	---	---
$\mathbf{d}_{ti}(\mu\mathbf{m})$	---	1.142	1.703
$\mathbf{d}_{to}(\mu\mathbf{m})$	0.26	---	---

**Table (4.8)** the relative optical properties for a two-lens system (2) with collimated beam between focusing elements.

<b>DEMAGNIFICATION CONDITION FOR TWO LENSES SYSTEM -2</b>			
<b>relative optical properties</b>	<b>diaphragm lens</b>	<b>immersion lens</b>	<b>The system</b>
<b>magnification</b>	<b>infinite</b>	<b>zero</b>	<b>-0.98</b>
$U_i/U_o$	0.846	2.70	2.70
$f_i/L$	infinite	1.082	1.082
$f_o/L$	0.618	infinite	0.618
$C_{si}/f_i$	---	6.22	---
$C_{so}/f_o$	3.40	---	5.33
$C_{ci}/f_i$	---	0.541	---
$C_{co}/f_o$	2.24	---	5.51
$d_{si}(\mu m)$	---	0.08	1.31
$d_{so}(\mu m)$	0.43	---	---
$d_{ci}(\mu m)$	---	1.14	0.763
$d_{co}(\mu m)$	0.56	---	---
$d_{ti}(\mu m)$	---	1.142	0.764
$d_{to}(\mu m)$	0.70	---	---

The aberration discs diameters over the beam angles  $\alpha$  (5, 10,30,50,75 and 100) **mrad** of the given two-lens system are shown in figure (4.33) ,which is given the variations of contours over the beam angles of such an optical column. While; the percentage distribution of the aberration disc densities along the given optical column of the same beam angles range are shown in figure (4.34).

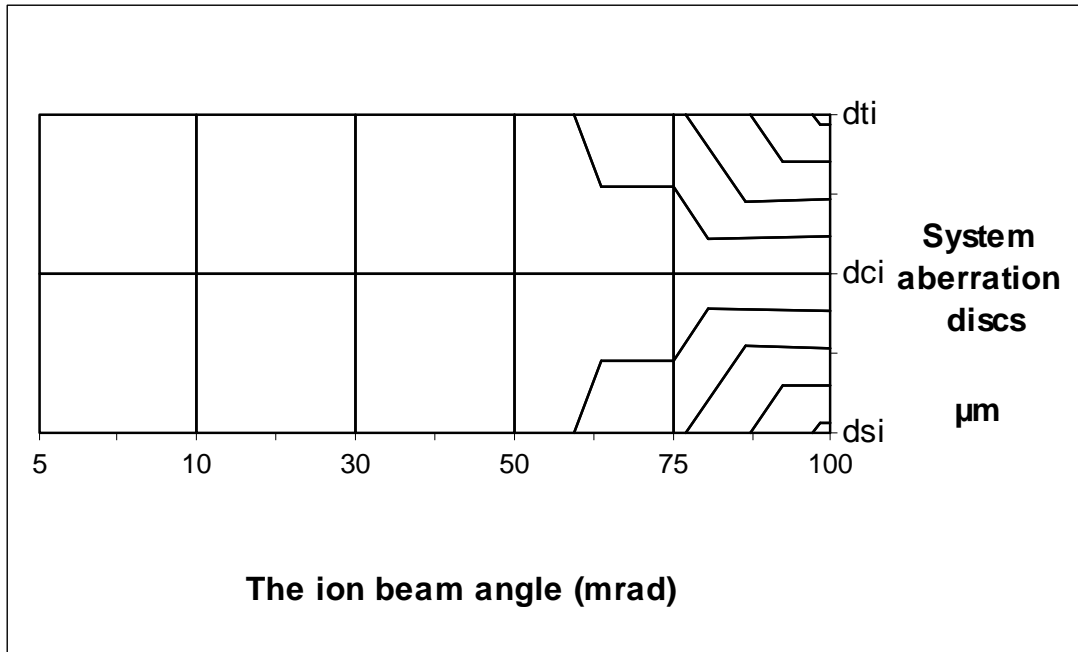


**Figure (4.33)** two-lens system aberration discs contours versus the beam angle  $\alpha$ .

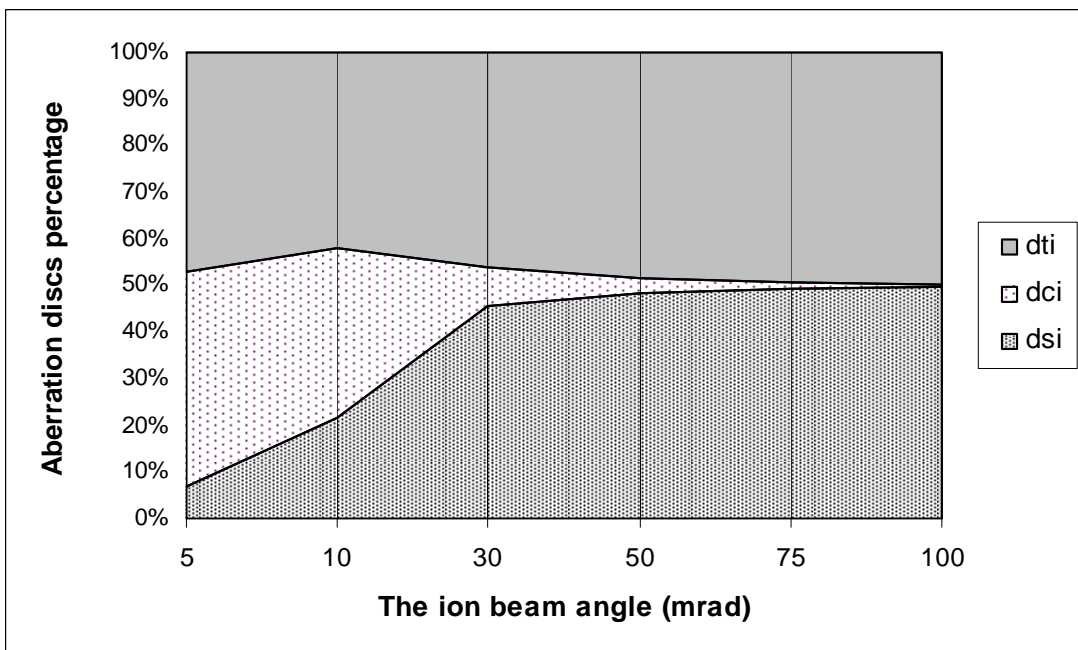


**Figure (4.34)** the two-lens system aberration disc densities percentage distribution versus the beam angle  $\alpha$ .

## 4.3 Three-lens system

Demagnification of the beam size in the image plane is one of the most requirements of focused ion beam, which should be associated with low aberrations. The ion beam systems consisting of three lenses with a beam crossover take the following setup.

### 4.3.1 Column setup

The axial potential distribution is determined with their first and second derivatives of a given two-lens system for ion collimated beam, which is forming three lenses with a beam crossover as follows:

1. Unipotential lens (1) [**einzel**] lens operates under infinite magnification condition – immersion lens operates under zero magnification condition- Diaphragm lens operates under finite magnification condition.
2. Diaphragm lens operates under infinite magnification condition – immersion lens operates under zero magnification condition- Diaphragm lens operates under finite magnification condition.

Likewise, the two-lens system selectivity the third lens or the right hand side of the given columns operates under finite magnification condition, as they are shown in figures (4.35) and (4.36), respectively.



### Collimated ion beam of three lens system 1

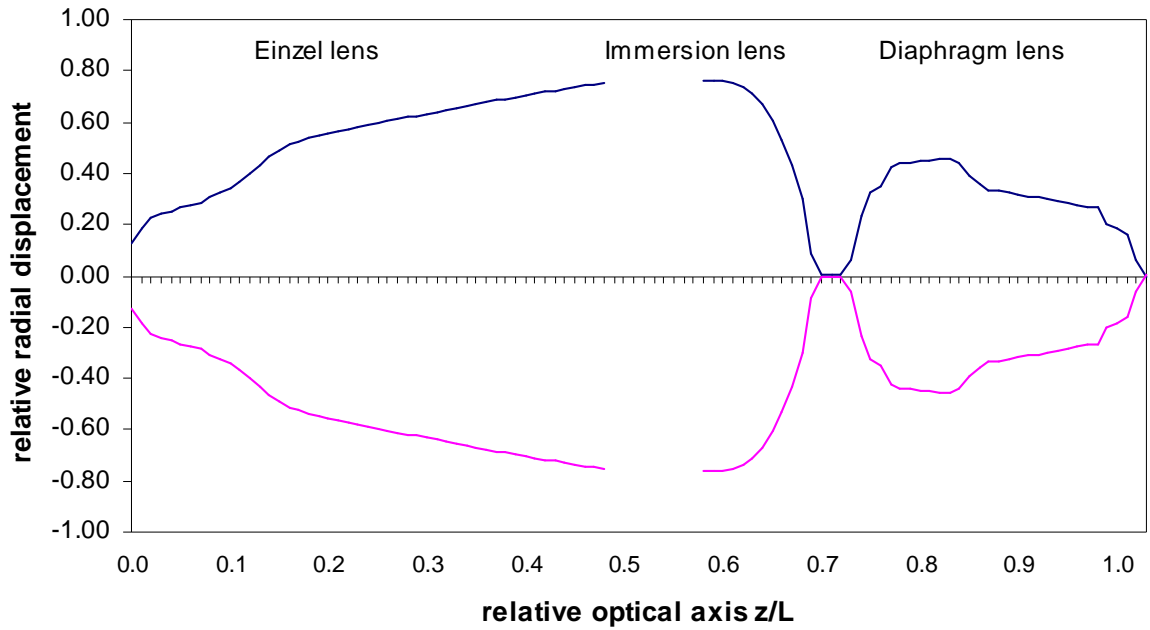


Figure (4.35) the ion beam trajectory for a three-lens system (1).

### Collimated ion beam of three lens system 2

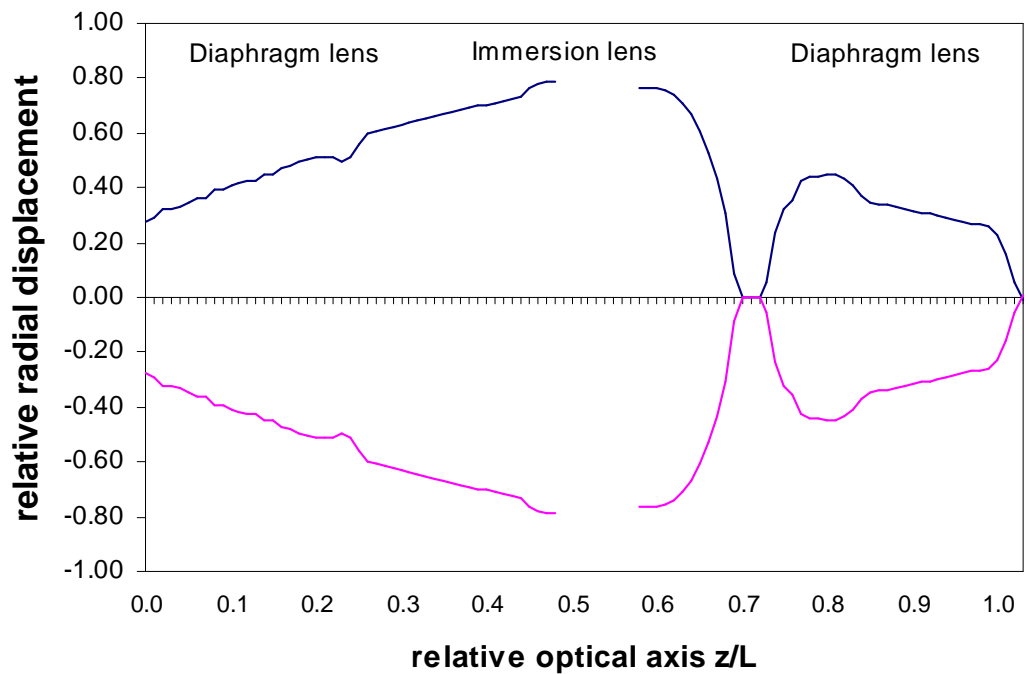


Figure (4.36) the ion beam trajectory for a three-lens system (2).

The relative optical properties of the given three - lens systems are listed in tables (4.9) and (4.10), also those properties have been obtained using the equations (2.26, 2.27 and 2.28), which they were used to calculate the spherical, chromatic and total aberration discs ( $\mathbf{d_{si}}$ ,  $\mathbf{d_{ci}}$  and  $\mathbf{d_{ti}}$ ). The relative aberration coefficients are taken in terms of the image-side focal length of the second lens, by which it's the overall image-side focal length of the system.

**Table (4.9)** the relative optical properties for a three-lens system (1).

<b>DEMAGNIFICATION CONDITION FOR THREE LENSES SYSTEM - 1</b>				
<b>relative optical properties</b>	<b>einzel lens</b>	<b>immersion lens</b>	<b>diaphragm lens</b>	<b>The system</b>
<b>magnification</b>	<b>infinite</b>	<b>zero</b>	<b>-0.999</b>	<b>-0.403</b>
$\mathbf{U_i/U_o}$	1.545	2.70	1.545	---
$\mathbf{f_i/L}$	infinite	1.082	0.244	0.244
$\mathbf{f_o/L}$	1.48	infinite	0.244	0.50
$\mathbf{C_{si}/f_i}$	---	6.22	5.67	---
$\mathbf{C_{so}/f_o}$	1.50	---	---	5.04
$\mathbf{C_{ci}/f_i}$	---	0.541	0.63	---
$\mathbf{C_{co}/f_o}$	0.70	---	---	4.32
$\mathbf{d_{si}(\mu m)}$	---	0.08	1.80	8.788
$\mathbf{d_{so}(\mu m)}$	0.19	---	---	---
$\mathbf{d_{ci}(\mu m)}$	---	1.14	8.910	9.393
$\mathbf{d_{co}(\mu m)}$	0.18	---	---	---
$\mathbf{d_{ti}(\mu m)}$	---	1.142	8.912	9.396
$\mathbf{d_{to}(\mu m)}$	0.26	---	---	---

**Table (4.10)** the relative optical properties for a three-lens system (2).

<b>DEMAGNIFICATION CONDITION FOR THREE LENSES SYSTEM - 2</b>				
<b>relative optical properties</b>	<b>diaphragm lens</b>	<b>immersion lens</b>	<b>diaphragm lens</b>	<b>The system</b>
<b>magnification</b>	<b>infinite</b>	<b>zero</b>	<b>-0.999</b>	<b>-0.400</b>
$U_i/U_o$	0.846	2.70	0.846	---
$f_i/L$	infinite	1.082	0.244	0.244
$f_o/L$	0.618	infinite	0.244	0.51
$C_{si}/f_i$	---	6.22	5.67	---
$C_{so}/f_o$	3.40	---	---	4.927
$C_{ci}/f_i$	---	0.541	0.63	---
$C_{co}/f_o$	2.24	---	---	1.036
$d_{si}(\mu m)$	---	0.08	1.80	2.247
$d_{so}(\mu m)$	0.43	---	---	---
$d_{ci}(\mu m)$	---	1.14	8.910	1.774
$d_{co}(\mu m)$	0.56	---	---	---
$d_{ti}(\mu m)$	---	1.142	8.912	1.78
$d_{to}(\mu m)$	0.70	---	---	---

### 4.3.2 Beam spot size measurement

According to the principles and methods in section 2.8, and using equation (3.16), using the software (i.e. CADION package) the spot size has been calculated. Figure (4.37) shows the spot size calculations for a range of beam angles [5, 10,30,50,75, and 100] **mrad** of the given ion beam three-lens systems. From these results one can distinguish the nano scale optimization which is very useful for FIB designing.

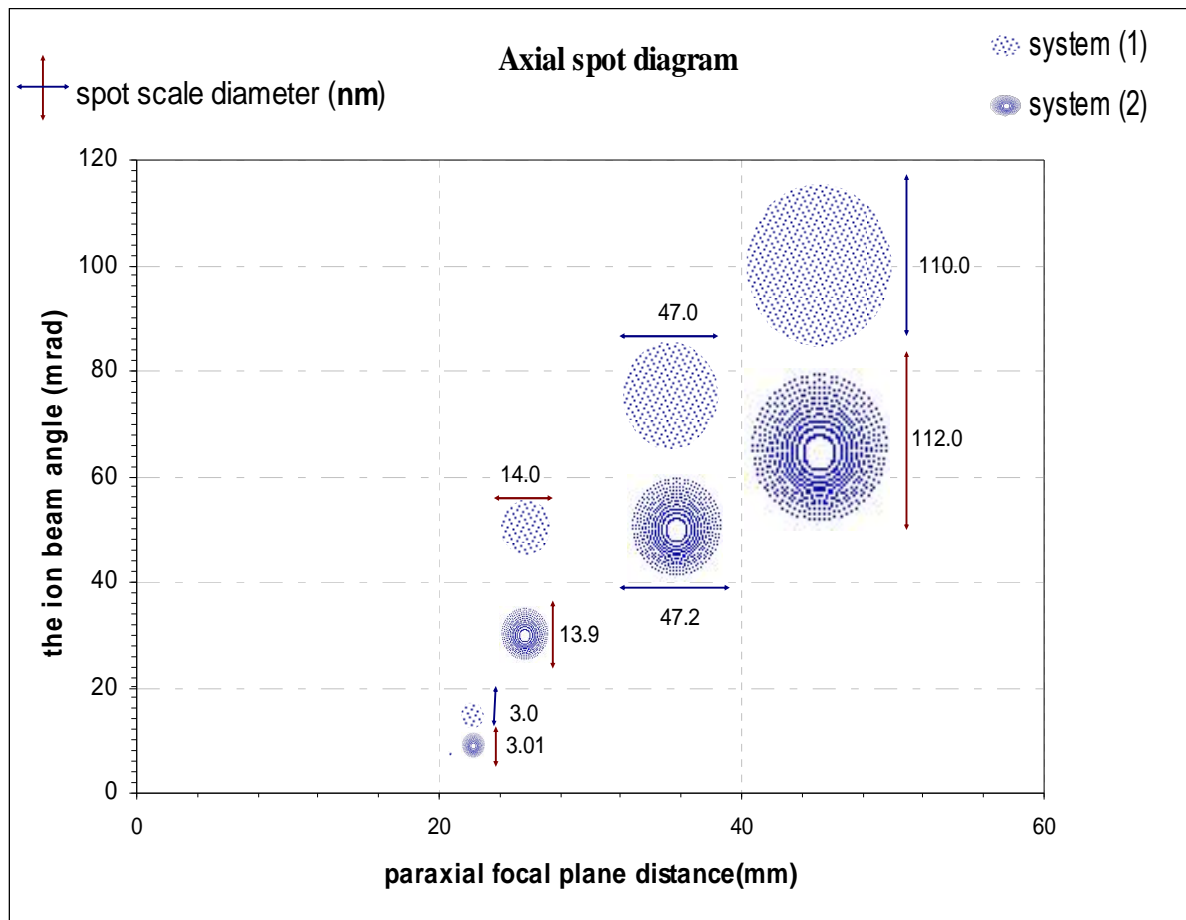


**Figure (4.37)** the axial spot size measurements versus the beam angle for three-lens systems (1& 2).

However over the same range of ion beam angles (5, 10, 30, 50, 75 and 100) **mrad**, one see that the spot size measurements are given the distribution of the ions concentration through the image side. As it seen from the figure (4.37) the spot size would get smaller with small beam angles, consequently the reduction of aperture defects may take the right process. Figure (4.38) shows the variation of the ions distribution of that concentration for different ion beam angles.

Also, it has shown at beam angle 100 mrad the spot size is (110 nm) and (112 nm), while at the beam angle of high resolved system are taken the values (3.0 nm) and (3.01 nm), respectively. This might be a good indication to get the optimum reduction for the aberrations inside the given systems.

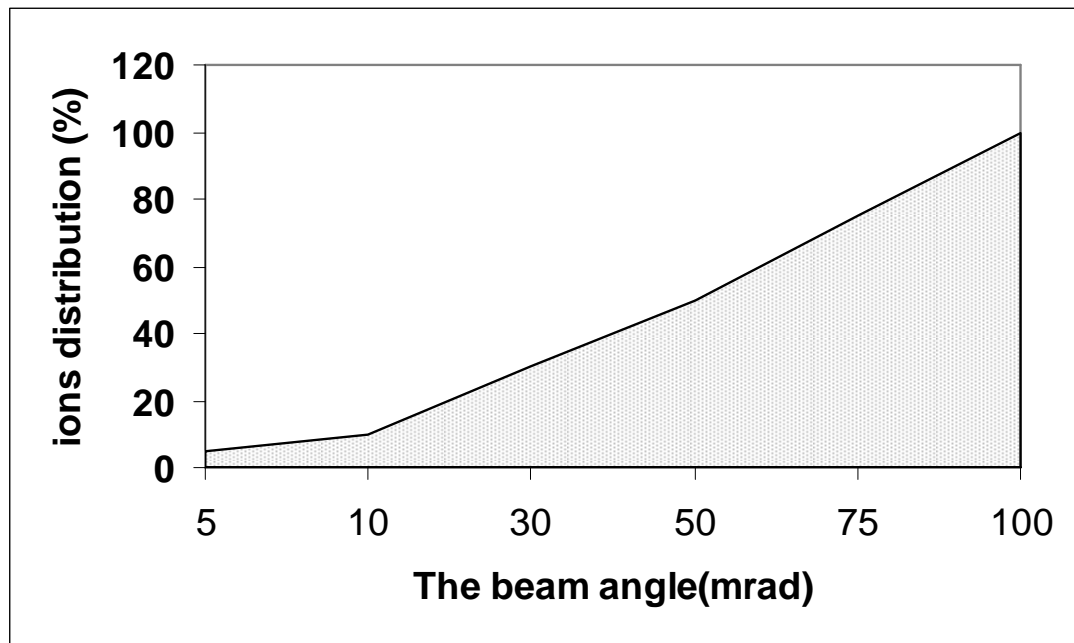


**Figure (4.38)** Ions distributions in percentage versus the beam angle for a three-lens systems (1& 2).

## 4.4 Multi-lens system

A multi-lens system may have an acceptable form over a range of three collimated beam systems (1, 2 and 3), which are determined by using the optimized formulae as follows:

1. Unipotential lens (1) [**einzel**] lens operates under infinite magnification condition – magnetic lens (1) operates under zero magnification condition.
2. Diaphragm lens operates under infinite magnification condition – magnetic lens (1) operates under zero magnification condition.
3. Immersion lens operates under infinite magnification condition – magnetic lens (1) operates under zero magnification condition.

Figures (4.39, 4.40 and 4.41) show the ion beam trajectory for the multi-lens systems (i.e. 1,2 and 3) with its collimated beam between focusing elements obtained by using dynamic programming procedure with the aid of artificial intelligence technique. Our software (i.e. CADION package) has an ability to perform multi-lens designs with minimized aberrations.

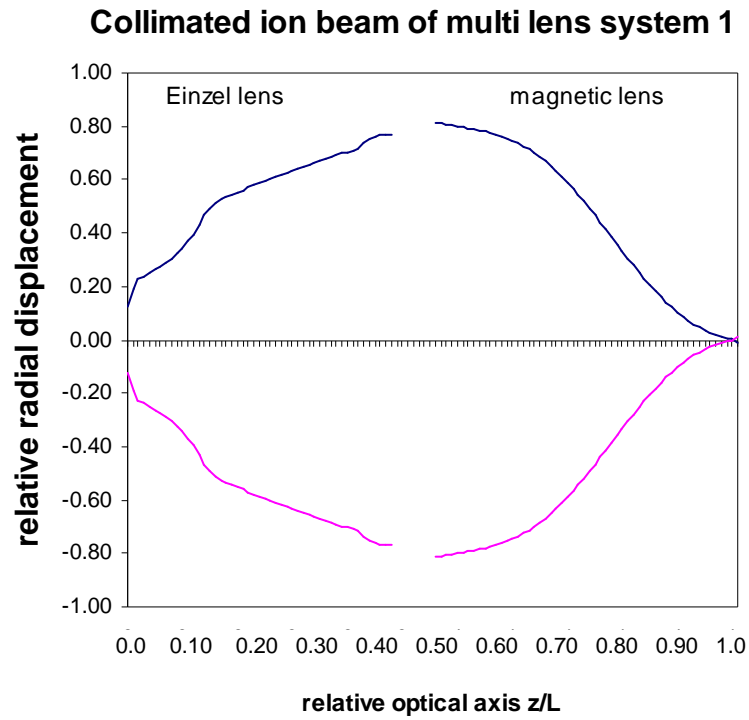


**Figure (4.39)** the ion beam trajectory for a multi-lens system (1).

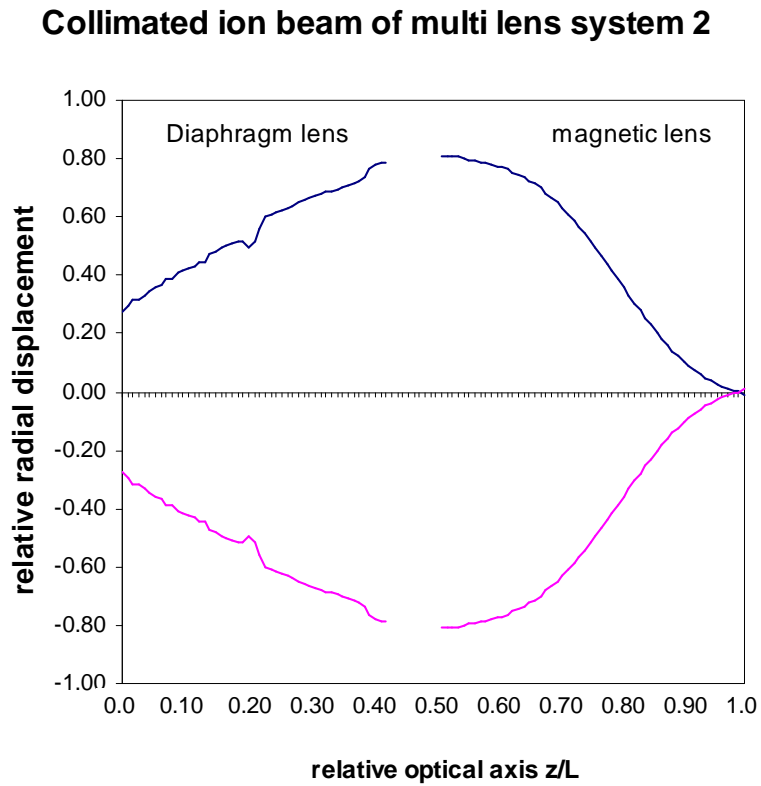


**Figure (4.40)** the ion beam trajectory for a multi-lens system (2).

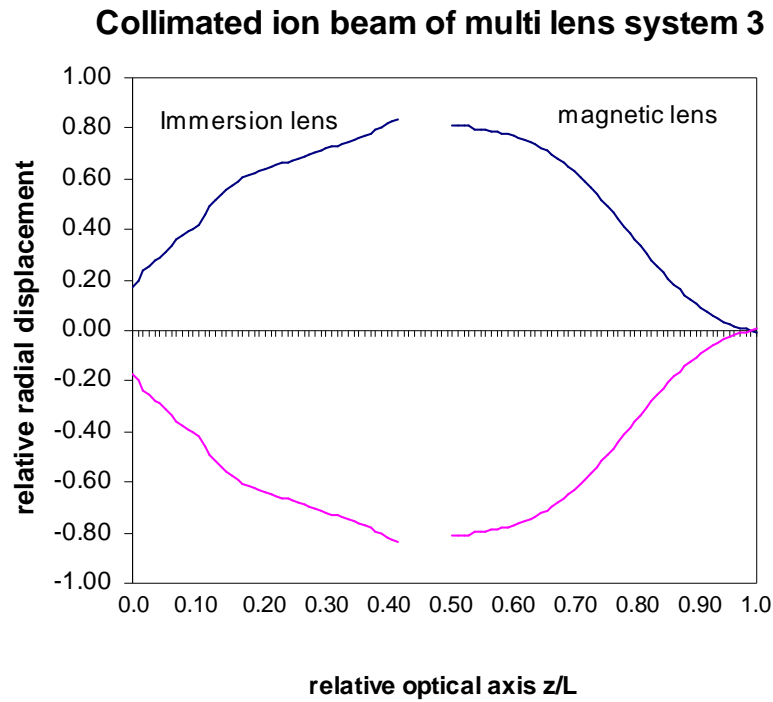


**Figure (4.41)** the ion beam trajectory for a multi-lens system (3).

The following tables (4.11), (4.12) and (4.13) are given the relative optical properties of the multi-lens systems (1, 2 and 3), respectively. However, relative aberration coefficients are taken in terms of the image-side focal length of the second lens, by which it's the overall image-side focal length of the system. Also, the spherical, chromatic and total aberration discs ( $\mathbf{d}_{si}$ ,  $\mathbf{d}_{ci}$  and  $\mathbf{d}_{ti}$ ) are calculated with the aid of equations (2.26, 2.27 and 2.28), respectively.



**Table (4.11)** the relative optical properties for a multi-lens system (1) with collimated beam between focusing elements.

<b>DEMAGNIFICATION CONDITION FOR MULTI-LENS SYSTEM -1</b>			
<b>relative optical properties</b>	<b>einzel lens</b>	<b>magnetic lens (1)</b>	<b>The system</b>
<b>magnification</b>	<b>infinite</b>	<b>zero</b>	<b>-0.763</b>
$U_i/U_o$	1.545	1.66	1.66
$f_i/L$	infinite	2.01	2.01
$f_o/L$	1.48	infinite	1.48
$C_{si}/f_i$	---	0.52	---
$C_{so}/f_o$	1.50	---	6.316
$C_{ci}/f_i$	---	0.22	---
$C_{co}/f_o$	0.70	---	1.077
$d_{si}(\mu m)$	---	0.03	0.07
$d_{so}(\mu m)$	0.19	---	---
$d_{ci}(\mu m)$	---	0.14	0.106
$d_{co}(\mu m)$	0.18	---	---
$d_{ti}(\mu m)$	---	0.141	0.107
$d_{to}(\mu m)$	0.26	---	---

**Table (4.12)** the relative optical properties for a multi-lens system (2) with collimated beam between focusing elements.

<b>DEMAGNIFICATION CONDITION FOR MULTI- LENS SYSTEM -2</b>			
<b>relative optical properties</b>	<b>diaphragm lens</b>	<b>magnetic lens (1)</b>	<b>The system</b>
<b>magnification</b>	<b>infinite</b>	<b>zero</b>	<b>-0.433</b>
$U_i/U_o$	0.846	1.66	1.66
$f_i/L$	infinite	2.01	2.01
$f_o/L$	0.618	infinite	0.618
$C_{si}/f_i$	---	0.52	---
$C_{so}/f_o$	3.40	---	4.94
$C_{ci}/f_i$	---	0.22	---
$C_{co}/f_o$	2.24	---	1.41
$d_{si}(\mu m)$	---	0.03	0.054
$d_{so}(\mu m)$	0.43	---	---
$d_{ci}(\mu m)$	---	0.14	0.0768
$d_{co}(\mu m)$	0.56	---	---
$d_{ti}(\mu m)$	---	0.141	0.0772
$d_{to}(\mu m)$	0.70	---	---

**Table (4.13)** the relative optical properties for a multi-lens system (3) with collimated beam between focusing elements.

<b>DEMAGNIFICATION CONDITION FOR MULTI- LENS SYSTEM -3</b>			
<b>relative optical properties</b>	<b>immersion lens</b>	<b>magnetic lens (1)</b>	<b>The system</b>
<b>magnification</b>	<b>infinite</b>	<b>zero</b>	<b>-0.541</b>
$U_i/U_o$	0.53	1.66	1.66
$f_i/L$	infinite	2.01	2.01
$f_o/L$	2.10	infinite	2.10
$C_{si}/f_i$	---	0.52	---
$C_{so}/f_o$	0.60	---	0.76
$C_{ci}/f_i$	---	0.22	---
$C_{co}/f_o$	4.56	---	3.55
$d_{si}(\mu m)$	---	0.03	0.049
$d_{so}(\mu m)$	0.08	---	---
$d_{ci}(\mu m)$	---	0.14	0.0701
$d_{co}(\mu m)$	1.140	---	---
$d_{ti}(\mu m)$	---	0.141	0.0703
$d_{to}(\mu m)$	1.142	---	---

#### 4.5 A suggested estimations in charged particles optics

According to the principals and formulae in chapter 2, section 2.3 and optical properties representations, a suggested mathematical approach has been used in this investigation. Nevertheless, the most significant optical properties have to be examined by multi tests and iteration methods .For the first sought to the lenses were designed according to the optimized potentials, most of their spherical and chromatic aberration coefficients have values near to reach Planck's constant. However, these values are much more closely to the nano

scale considerations. In charged – particle optics as well as in classical optics, the aperture aberration (spherical aberration or stop aperture) is by far the most important, because it limits the resolution of electron microscopes and the smallness of the probes of microanalysers. These aberrations are characterized by the values of the deviations  $\Delta \mathbf{x}$  and  $\Delta \mathbf{y}$  from the point of the image formed by the paraxial beam [Septier 1966].

The radius of the stop aperture ( $r_a$ ) is proportional to the tangent of the aperture angle  $\alpha$  (half acceptance angle). Since  $\alpha$  is very small (i.e.  $\tan(\alpha) \sim \alpha$  in radians). Thus, it would get the disc formula as [El-Kareh and El-Kareh 1970];

$$\mathbf{d}_s = \mathbf{Cs} \alpha^3 \dots\dots\dots (4.1)$$

where  $\mathbf{d}_s$  and  $\mathbf{Cs}$  are the diameter spherical aberration disc and its coefficient, respectively. Also, the spherical aberration coefficient of the focusing device depends primarily on the diameter of the aperture. On the other hand, the spherical aberration will cause blurring in the formed image if the angle  $\alpha$  is not very small. Mainly, the present work results have given this value the proper indication of uncertainty relationship like. To evaluate the aberration disc for a very small angle  $\alpha$ , it makes the easiest way for getting such indications. Thus, changing in measuring the position of the incident and reflected rays will appear in the spherical aberration coefficient  $\mathbf{Cs}$ .

In micro scale systems this might take place many times, and the effect of smallness the angle  $\alpha$  it could be neglected. So that the equation (4.1) may be rewritten as a definition of the spherical aberration coefficient  $\mathbf{Cs}$  according to **eikonal method** as follows [Hawkes and Kasper 1989]:

$$\mathbf{Cs} = \Delta \mathbf{d}_s (\text{space}) / \alpha^3 \dots\dots\dots (4.2)$$

The sign of the spherical aberration is always positive such that rays remote from the axis focus more strongly than rays close to it. It has shown that in the absence of space charges in the region through which the trajectories pass, the formula of the aberration can be expressed as the sum of squared terms, so that the sign cannot be changed, in particular the aberration cannot be made zero [Szilagyi 1988]. As a micro scale point of view, the spherical aberration disc is a function of space for various trajectories of the charged particle.

On the other hand, the chromatic aberration results from the dependence of the optical parameters of the charged – particle lenses on the energy of the beam being focused. Depending on the whole formulae of chapter 2 upon the definitions of chromatic aberration disc diameter  $\mathbf{d_c}$ , then the disc can be written as:

$$\mathbf{d_c} = 2 \mathbf{C_c} \alpha \Delta p/p \dots\dots\dots (4.3)$$

where  $\mathbf{d_c}$ ,  $\mathbf{C_c}$  is the diameter chromatic aberration disc and its coefficient respectively. Since the present work deals with the non-relativistic case; the disc may get the new definition [Lawson 1977]:

$$\mathbf{d_c} = \mathbf{C_c} \alpha (\Delta u / u) \dots\dots\dots (4.4)$$

where U is the potential energy through which the charged – particles have been accelerated to reach the momentum p, and  $\Delta U$  refers to half the total energy spread in the beam. It can be seen from the above equation that  $\mathbf{d_c}$  is proportional to the initial slope of the outermost ray and the relative energy spread ( $\Delta u / u$ ).

From equations (4.1) through (4.4) one notes that at low values of the acceptance angle the performance of the optical system is limited by its chromatic aberration, where at larger apertures spherical aberration becomes the

dominant limiting factor [Szilagy and Szepe 1988]. In the sub micro scale the chromatic aberration disc  $d_c$  has appeared like a function of momentum in a space along optical axis- $z$ . This will give us a strong indication for the non-commutative approaches, since the energy spread  $(\Delta u/u)$  has relative expression within estimated fields or potentials in the optical systems. Equation (4.4) becomes more fitted to the case in sub micro systems, and the chromatic aberration coefficient  $C_c$  may be considered as in **eikonal method** [Hawkes and Kasper 1989] as follows:

$$C_c = \Delta d_c (\text{momentum}) / \alpha (\Delta u / u) \dots\dots\dots (4.5)$$

Once the limitations of non commutative operations have been fixed , the uncertainty principle relationship like for the aberrations ( spherical and chromatic)discs may take place .In terms of the above indications , most of present work results (i.e. the spherical and chromatic aberration coefficients) may have explained strongly enough .

A consideration of the aberration theorem as a part of the uncertainty principle has raised the similarity for finding charged – particles along optical path. Hence, the probability of finding those particles with a specific amount of energy, diffracted from the edges of the target (object) in an optical system. Therefore, the quantization of electrostatic lenses have dominantly worked at micro or nano scale only. The aspects of verification according to the strong principle of the uncertainty relationship like have done.

It may be raised in different models (lenses) but not for all kinds. The present work tables are giving the most estimated results, as new configurations of doing the fuzziness systems like [Stelzer and Grill 2000].Our work could

lead to get suggested aspects and hypothesis in the charged particle optics, also it may give a raise to consider most of the results as suggested estimations for entering the non classical technology. Obviously, the values of the aberration coefficients and discs are showing a significant behavior of the uncertainty relationship like. According to the uncertainty principle (chapter 2), and equation (2.9) this approach will lead to new idea , which has been considered for improving the design of mesoscopic optical lenses and it may take such manipulation as:

$$[\Delta \mathbf{d}_s \text{ (space)} / \alpha^3]. [\Delta \mathbf{d}_c \text{ (momentum)} / \alpha (\Delta \mathbf{u} / \mathbf{u})] = i \hbar \delta_{ij} \dots\dots\dots (4.6)$$

where  $[\Delta \mathbf{d}_s \text{ (space)} / \alpha^3]$  represents the position of the charged particles along the optical path, and  $[\Delta \mathbf{d}_c \text{ (momentum)} / \alpha (\Delta \mathbf{u} / \mathbf{u})]$  represents the momentum of the charged particles accelerated through the optical column. This formula (i.e. equation (4.6)) leads to get a new aspect in optical systems, and it could be rewritten as:

$$[\mathbf{d}_s. \mathbf{d}_c] / [\alpha^4 (\Delta \mathbf{u} / \mathbf{u})] = i \hbar \delta_{ij} \dots\dots\dots (4.7)$$

One can see from the equation (4.7), that a small angle  $\alpha$  total amount of aberration discs has become very large. The only exception is about the range of energy spread  $(\Delta u/u)$ ; this is a well-known formula for the micro scale conditions. It would be the success of non commutative approach for both aberration discs (spherical and chromatic) as well.

# *Chapter Five*

## **Conclusions and Suggestions for Future Work**

### **5.1 Conclusions**

The present investigation has clearly used optimization methods by mixing the dynamic programming procedure and the artificial intelligence technique, to find a simulator, packed in one program.

Our work achievements have been summarized as follows:

- The single-lens design electrodes and optimized formulae for obtaining axial potential for four types of electrostatic lenses and a magnetic lens as in tables (4.2) and (4.3).
- Get minimum optical properties of relative aberration coefficients, and then calculate the aberration disc diameters as summarized in table (4.6).
- Setting up an optical column as follows:
  - Two-lens system as in figures (4.29) and (4.30).
  - Three-lens system as in figures (4.35) and (4.36).
  - Multi-lens system as in figures (4.39), (4.40) and (4.41).
- Nano scale measurements of spot size diameter, focusing ions in the image plane have values are very useful for getting FIB designing (figure (4.37)). Over a range of ion beam angles (5, 10, 30, 50, 75 and 100) **mrad**, the results were summarized as follows:
  - System (1)-have values [3.0, 14.0, 47.0 and 110.0] **nm**.
  - System (2) - have values [3.01, 13.9, 47.2 and 112.0] **nm**.
- Suggesting mathematical manipulations for the aberration coefficients basing on the uncertainty principle hypothesis.



- Artificial intelligence has promise for building FIB in charged particle optics.

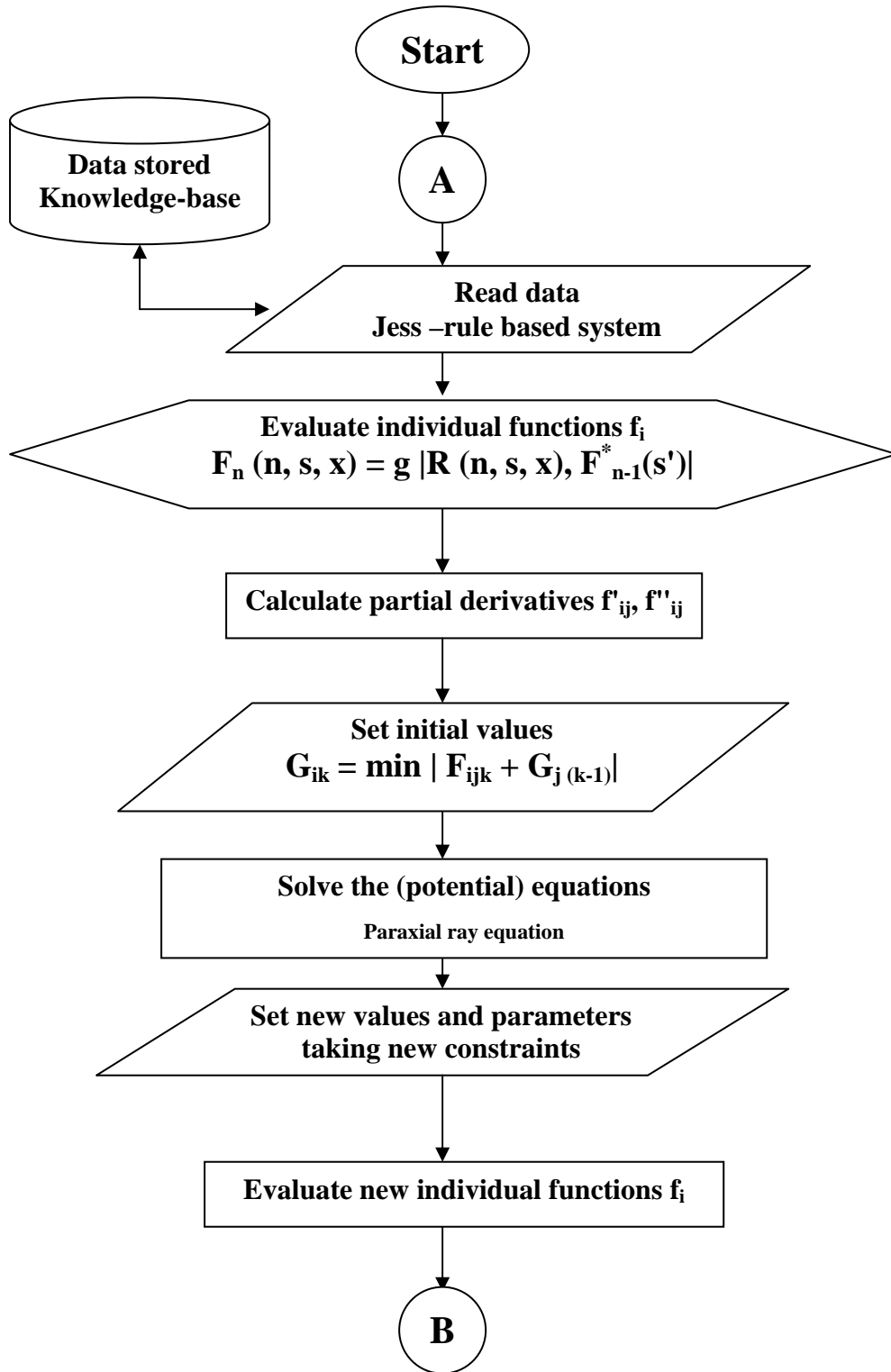
## 5.2 Suggestions for Future work

Plenty of projects and investigations may be suggested for further work upon the designing , optimizing , analyzing and reconstructed new lens systems (electrostatic and/or magnetic) holding for nano optical ion and electron lens column. Such suggestions are listed as follows:

1. Considering the effect of the magnetic permeability  $\mu$  as a dominant factor in magnetic lens systems.
2. Investigating the design of the optical column and lens systems where the relativistic charged particle velocities and the space charge effects are taken into account.
3. Design a quantum-lens system.
4. Design a quadrapole's deflectors and mirrors.

## Appendix

The program CADION Analyzer is the main significant optimizer" expert system"; the steps are configured as included in the following flowchart:



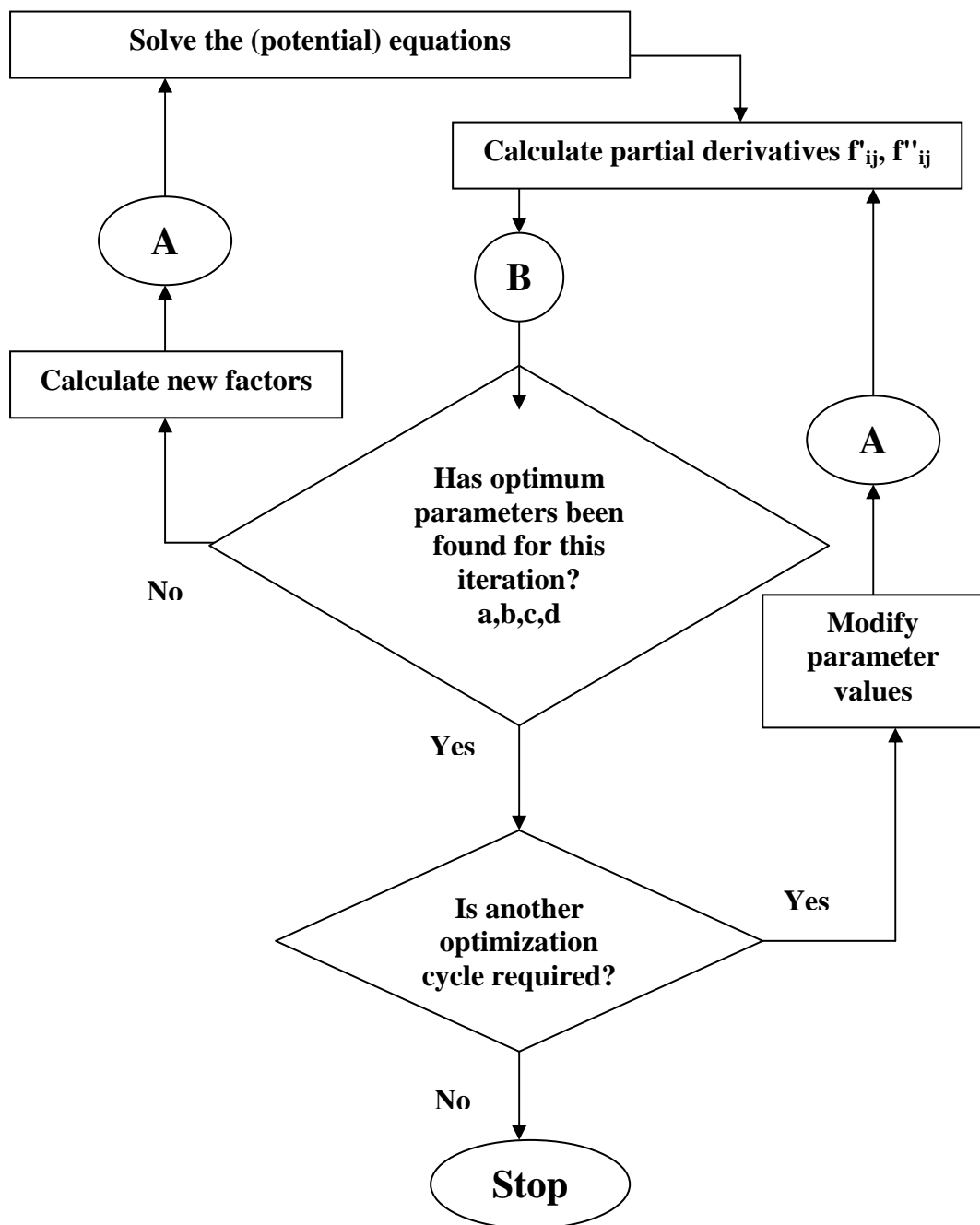


**Figure (A)** shows CADION analyzer "expert system" flowchart.

## References

Ahmad, A.K., 1993

Computerized investigation on the optimum design and properties of the electrostatic lenses

Ph.D. Thesis, Al-Nahrain University

Baghdad, Iraq.

Ahmad, A.K., Sabah M.J. and Ahmed A.Al-Tabbakh, 2002

Computer aided design of an electrostatic FIB system

Indian J.Phys. **76B (6), 711-714**

Amos R.J., Evans G.A., Ghazikhanian J., Smith R., and Storey C., 1988

Optimization of the properties of a microfocused ion beam system

J.Phys.E.Sci.Instrum., **21, 86-91**

Burden R.L., Faires J.D., and Reynolds A.C., 1981

Numerical analysis and optimization, second edition

Prindel , Weber and Schmidt , Boston

Choi Y.-K., Lindert N., Xuan P., Tang S., Ha D., Anderson E., King T.-J., Bokor

J. and Hu C., 2001

Sub-20nm CMOS FinFET technologies,

International Electron Devices Meeting Technical Digest, **421-424**

Chapra S., Canale R., 1998

Numerical Methods for Engineers, 3rd Ed.

McGraw-Hill, New York, **331-422**

El-Kareh A.B. and El-Kareh J.C.J., 1970

Electron Beams, Lenses and Optics

Academic Press New York and London

Friedman E. J., 2003

(Jess) The Rule Engine for the Java Platform

Computing Systems Sandia National Laboratories Livermore

CA USA, Version **6.1,4**

Forbes G.W., 1988

Computing spot size

J.Opt.Soc.Am. **A5, 1943-1956**

Grosof B. N., Gandhe M. D. and Finin T. W., 2002

SweetJess: Translating DamlRuleML to Jess

MIT Sloan School of Management

Cambridge, USA, **MA 02142**

Glaser W., 1952

Grundlagen der Elektronenoptik

Springer, Wien

Harriott H. R., March 2001

Limits of Lithography

Proceeding of the IEEE, **vol. 89, No. 3, 366**

Harriott H. R., 2001.

Semiconductor Industry Association (SIA)

The International Technology Roadmap for Semiconductors

Huang X., Lee W.-C., Kuo, Hisamoto C. D., Chang L., Kedzierski J., Anderson E., Takeuchi H., Choi Y.-K., Asano K., Subramanian V., King T.-J., Bokor J. and Hu C., 2001.

Sub-50 nm p-channel FinFET,"*IEEE Transactions on Electron Devices* **Vol. 48, No. 5, 880-886**

Hawkes P. W. 1989

Advances in Electronics and electron physics

Academic press, London, Supplements, no.13.

Hawkes P.W. and Kasper E., 1989

Principle of Electron Optics, vol.1

Academic press, London

Harting E., and Read F.H., 1976

Electrostatic Lenses

Elsevier: Oxford and New York

Hawkes P.W., 1972

Electron Optics and Electron Microscopy

Taylor and Francis: London, **27-82**

Kedzierski J., Xuan P., Anderson E. H., Bokor J., King T.-J. and Hu C., 2000

Complementary silicide source/drain thin-body MOSFETs

For the 20nm gate length regime

International Electron Devices Meeting Technical Digest, **57-60**

Kaesmaier R. and Loschner H., 2000  
Overview of the Ion Projection Lithography European MEDEA and  
International Program  
PIE Conference on Microlithography  
Santa Clara, California, USA

Kiss L., 1989  
Electrostatic lens potential with small relativistic spherical aberration  
Rev.Sci.instrum., **60**, **907-909**

Kurihara K., 1985  
A focused ion beam system for submicron lithography  
J.Vac.Sci.Technol., **B3**, **41-44**

Kuester J.L. and Mize J.H., 1973  
Optimization technique with FORTRAN  
McGraw-Hill book company, London

Lencova B. and Wisselink G., 2001  
MLD (Magnetic Lens Design)  
Particle Optics Group, TU Delft and SPOC, Brno

Lencova B., 1997  
Electrostatic Lenses,  
Handbook of Charged Particle Optics  
Edited by J.Orloff, **177-222**

Lawson J.D., 1977

The Physics of Charged Particle Beams

Clarendon Press, Oxford, **13-117**

Menken M., 2002

Jess Tutorial

Vrije Universiteit, Amsterdam, the Netherlands

Melngailis J., Mondelli A. A., Berry III I. L., and Mohondro R., 1998

A review of ion projection lithography

J. Vac. Sci. Techno., **B 16, 927**

Moore G., 1995

Progress in digital integrated electronics

Proc. IEEE Int. Electron Devices Meeting, Dig. Tech. Papers, **11**

Melngailis J., 1987

Focused ion beam technology and applications

J. Vac. Sci. echnol, **B5, 469**

Martinez G. and Sancho M., 1983

Four cylinder electrostatic lens I: Potential distribution and focal properties

J.Phys.E.Sci.Instrum, **16, 625-635**

Michiel A. van der Stam, Barth J.E., Kruit P., 1993

Design of a multimode transport lens with optimization program

SOEM

Delft Univ. of Technology, Netherlands, **45-56**



Martinez G. and Sancho M., 1995

Accurate calculation of geometrical aberrations in electrostatic lenses

Nucl.Instr. and Meth.in Phys.Res. , **A363, 198-204**

Martinez G. and Dymnikov A.D., 1997

Optimal electrostatic axisymmetric microprobe focusing system

Nucl.Instr. and Meth.in Phys.Res. , **B130, 74-79**

Munro E., 1975

A set of computer programs for calculating the properties of the electron lenses

Department of Engineering Report CUED/B-ElectTR45, University of Cambridge, UK

Orloff J., 1993

High-resolution focused ion beams

Rev. Sci. Instrum, **64(5), 1105**

Preuss P., 2002

Next generation Semiconductors may relay on ion beam lithography

Berkeley LAB, Nanoscale ion beam lithography

Science beat **1-3**

California USA

Press W., 1996

Numerical recipes in FORTRAN 90

The art of scientific computing, 2nd Ed.

Pierce J.R., 1949 and 1954  
Theory and Design of Electron Beams  
Van Nostrand, Princeton

Romijn J. and van der Drift E., 1988  
Chapter two of thesis J. Romijn  
Metallic Structures with Reduced Dimensions,  
TUDelft Physica, **B152, 14 - 21**

Raymond H., 1993  
Using optimum magnification as a figure of merit to evaluate the  
Performance of focused-ion-beam columns  
Micrion Corp., Peabody, MA, USA. , **112-119**

Rollett T., Garmestani H., 2003  
Advanced Characterization and Microstructural Analysis Microscopy  
Materials Science and Engineering  
Georgia Institute of Technology, USA

Stelzer E.H.K., and Grill S., 2000  
The uncertainty principle applied to estimate the focal spot dimensions  
Optics Communications, **173, 51-56**

Stelzer E.H.K., 1999  
Certain quality with the uncertainty principle  
Ernst Abbe Lecture, Light Microscopy Group  
European molecular biology laboratory  
Meyerhofstraße 1, D-69117Heidleberg  
Germany

Sales T.R.M, 1998

The axial lateral gain factors are related by a Heisenberg – like relationship  
Phys. Rev. Lett. , **81**, **3844**

Steve C. J., Alan W. G., David Y. Wang, and Dilworth D. C., 1993

Combination of global-optimization and expert-systems techniques in optical design

Breault Research Organization, Tucson, AZ, and

Optical Systems Design, Inc., East Boothbay, ME, USA. , **192-196**

Sinclair D.C. and McLaughlin P.O., 1989

Systems with vignette pupils

Proc. SPIE **1049**, **55**

Szilagyi M., 1988

Electron and Ion Optics

Plenum Press, N.Y., **5**, **8-16**

Szilagyi M. and Szep J., 1988

Optimum design of electrostatic lenses

J.Vac.Sci.Technol., **B6**, **953-957**

Szilagyi M., 1983

Improvement of electrostatic lenses for ion beam lithography

J.Vac.Sci.Technol., **B1**, **1137-1140**

Szilagyi M., 1984

Reconstruction of electron and pole pieces from optimized axial field  
distribution of electron and ion optical systems

Appl.Phys.Lett. **45**, **499-501**

Szilagyi M., 1985

Electron optical synthesis and optimization

Proc. IEEE, **73**, **412-418**

Septier A., 1966

The struggle to overcome spherical aberration in electron optics

Adv.Optic.Electron Microscopy vol.1

Ed.R.Barer and V.E. Cosslett

Academic Press, London and New York, **204-274**

Shannon C.E. and Weaver W., 1949

The Mathematical Theory of Communication

University of Illinois Press, Urbana Ill., **67**

Tsumagari T., Kimata Y., Ohiwa H., and Noda T., 1988

An optimum design of focused ion beam system with a beam crossover

Jpn. J.Appl.Phys. , **27**, **L1567-L1578**

Tang T.T. and Sheng C.Y., 1987

Design of electrostatic optical system for ion beam lithography

J.Vac.Sci.Technol., **5**, **165-168**

Xiaogang C., Zhijiang W., Da-Jian L., and Guoliang Sun, 1993

Small expert system used in lens design

Institute of Optics and Electronics, China, **197-201**

Yariv A., 1982

An Introduction to Theory and Applications of Quantum Mechanics

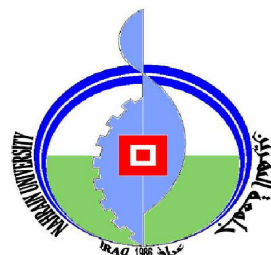
John Wiley & Sons, N.Y., **27, 31, 33**

Republic of Iraq

Ministry of Higher Education and Scientific Research

Al-Nahrain University

College of Science



# Computer - Aided - Design Of Focused Ion Beam For a Lithography System

*A thesis*

*Submitted to the College of Science of  
Al-Nahrain University  
in Partial Fulfillment of the Requirements for  
the Degree of Doctor of Philosophy  
in  
Physics*

By

Fadhil A. Ali

(B.Sc. in Physics) 1992

(M.Sc. in Physics) 1995

**April 2006 A.D.**

**Rabee-alawal 1427 A.H.**

Dedicated to my parents



جمهورية العراق  
وزارة التعليم العالي و البحث العلمى  
جامعة النهرين  
كلية العلوم

# تصميم حاسوبي لحزمة آيونية مركزة للمنظومة الليثوغرافية

أطروحة

مقدمة الى كلية العلوم فى جامعة النهرين  
كجزء من متطلبات نيل درجة دكتوراه فلسفة  
فى الفيزياء

من قبل

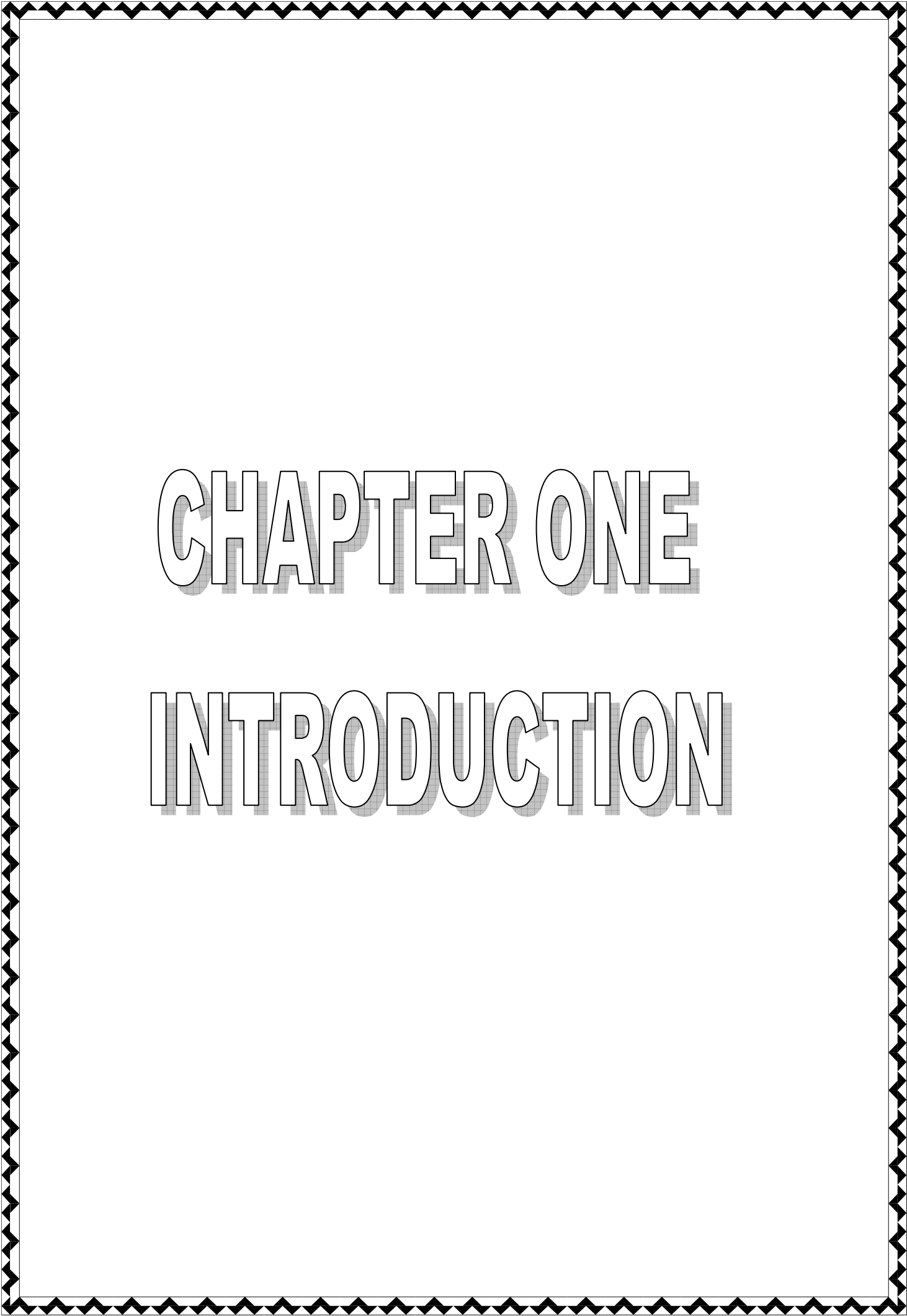
فاضل عبدالعباس على

( بكالوريوس علوم فيزياء ) ١٩٩٢  
( ماجستير علوم فيزياء ) ١٩٩٥

ربيع الأول ١٤٢٧ هجرى

نيسان ٢٠٠٦ ميلادى





# CHAPTER ONE

## INTRODUCTION

# CHAPTER TWO

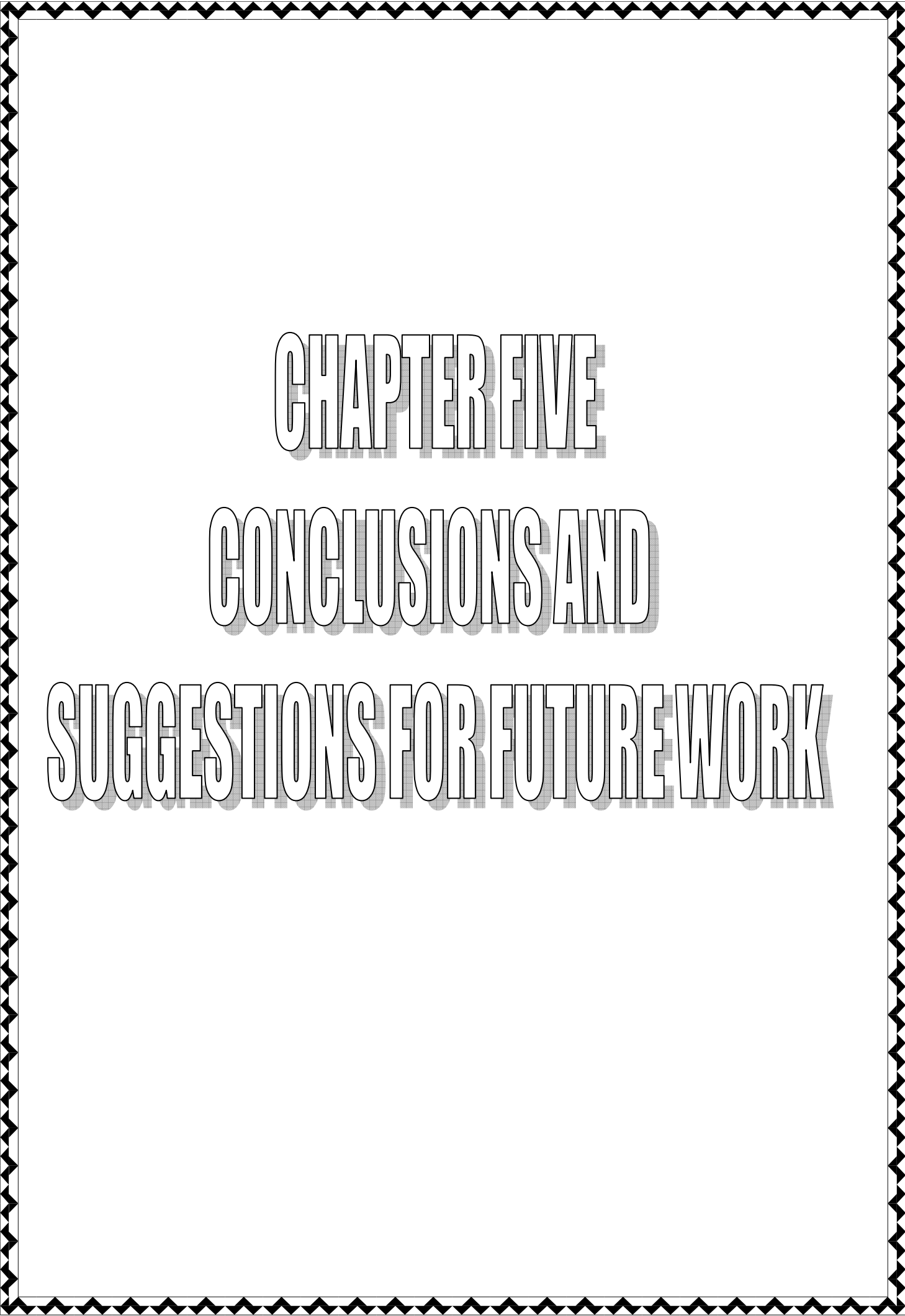
# THEORETICAL CONSIDERATIONS

# CHAPTER THREE

# COMPUTATIONS AND ANALYSIS

# CHAPTER FOUR

# RESULTS AND DISCUSSION



CHAPTER FIVE

CONCLUSIONS AND

SUGGESTIONS FOR FUTURE WORK

# APPENDICIES

## المخلص

تم بناء تصميم متكامل بمساعدة الحاسوب و باستخدام الطرق الأمثلية لمنظومة بصرية أيونية ، و ذلك بدمج طريقة البرمجة الديناميكية مع طريقة تقنية الذكاء الاصطناعي. فقد تم الحصول على معاملات الزيوغ النسبية الكروية و اللونية إستنادا الى معامل الهيئة للمنظومات البصرية المثلى ، و حسب الآتى :

- أ. تصميم عدسة مفردة ( كهربائية و مغناطيسية).
- ب. تصميم منظومة بصرية مكونة من عدستين كهربائيتين.
- ت. تصميم منظومة بصرية مكونة من ثلاث عدسات كهربائيات.
- ث. تصميم منظومة بصرية مختلطة العدسات (كهربائية و مغناطيسية).

كذلك تم تصميم أربعة أنواع من العدسات الكهروستاتيكية مع نموذج لعدسة مغناطيسية لأصغر زيوغ بصرية ( المرتبة البصرية الأولى و الثالثة ) ، حيث تم إعادة بناء الأقطاب الكهربائية و المغناطيسية ثم رسمها لبعدين و ثلاث أبعاد ببرنامج المحاكاة (7)SIMION ، و بالإعتماد على قاعدة البيانات المخزونة (قاعدة المعرفة). هذه العدسات هى كما يأتى:

- عدسة أحادية الجهد (١) فى نمط التباطىء .
- عدسة أحادية الجهد (٢) فى نمط التعجيل .
- عدسة مغمورة.
- عدسة الحاجز.
- عدسة مغناطيسية (١).

تم تصميم و كتابة الحزمة البرمجية بلغة الجافا منظومة الخبير (JESS) و البيسك المرئى النسخة السادسة (VB 6) إستوديو ، و ذلك للتحليل و الحصول على حسابات الأمثلية الكاملة للمنظومة البصرية الأيونية.حيث تم تسمية تلك الحزمة CADION .

أيضا تم إستخدام توزيع الجهد المحورى الأمثل لكلا المجالين الكهروستاتيكي و المغناطيسى ، بالإعتماد على الشروط المحددة لبناء و تركيب العمود البصرى المكون من عدستين وثلاث عدسات و مختلط العدسات.

تم حساب حجم البقعة لقياسات النانومتر و تم الحصول على قيم تقترب الى (٣,٠) نانومتر المسـتخدمة فى تطبيقات تقنية النانومتر. و كذلك تم إقتراح تعاريف و مفردات لبصريات الجسيمات المشحونة بإعتبار بعض النتائج محققة لعلاقة شبيهة بمداً اللادقة.